N° Ordre : ……

UNIVERSITE DE MOHAMED BOUDHIAF- M'SILA
FACULTE DES MATHEMATIQUES ET DE L'INFOMATIQUE INFORMATICS
Département d'informatique

THESE

Présentée pour l'obtention du diplôme de Doctorat 3ème Cycle
Spécialité : Informatique
Option : Systèmes d'informations avancées.

Par:

Somia LEKEHALI

THEME

APPROCHE EVOLUTIONAIRE BASE AUTOMATE CELLULAIRE POUR LA SEGMENTATION DES IMAGES MEDICALES

Soutenue publiquement Le : / /2019, devant le jury composé de :

B. BOUDERAH	Prof. Universté de Mohamed Boudiaf, M'sila	**Président**
A. MOUSSAOUI	Prof. Universté de Ferhat Abbas, Setif	**Rapporteur**
M. SAIDI	Dr. Universté de Ferhat Abbas, Setif -1	**Examinateur**
C. LAMICHE	Dr. Universté de Mohamed Boudiaf, M'sila	**Examinateur**
A. HEMMAK	Dr. Universté de Mohamed Boudiaf, M'sila	**Examinateur**
D. ZOUACHE	Dr. Universté de Bordj Bou Arreridj	**Examinateur**

Promotion 2018 /2019

Reference: ……

UNIVERSITY OF MOHAMED BOUDHIAF- M'SILA
FACULTY OF MATHEMATICS AND INFORMATICS
Department of Computer Science

Thesis

Submitted in partial fulfilment of the requirements for the degree of *DOCTORATE 3rd Cycle* in Computer Science
Option: Advanced Information Systems

By:

Somia LEKEHALI

SUBJECT

An Evolutionary Approach Based Cellular Automata for Medical Image Edge Detection

Presented publicly: / /2019, to the jury:

B. BOUDERAH	Prof. University Mohamed Boudiaf of M'sila	President
A. MOUSSAOUI	Prof. University Ferhat Abbas of Setif	Reporter
M. SAIDI	Dr. University Ferhat Abbas of Setif -1	Examiner
C. LAMICHE	Dr. University Mohamed Boudiaf of M'sila	Examiner
A. HEMMAK	Dr. University Mohamed Boudiaf of M'sila	Examiner
D. ZOUACHE	Dr. University of Bordj Bou Arreridj	Examiner

Academic year 2018 /2019

Acknowledgements

I would like to express my deepest gratitude to my advisor, ***Pr. Abdelouahab MOUSSAOUI*** for his ultimate support. He has been patiently giving me guidance, encouragement and support. Thanks to him, I got much experience in the domain that I investigated and discovered for the first time.

I would like to thank the president of the jury ***Pr. Brahim Bouderah*** and the rest of members of the jury: ***Dr***. ***Mohamed Saidi***, **Dr.** ***Chaabane Lamiche,*** **Dr.** ***Alloua Hemma*****k** and **Dr. Djaafar Zouache** for giving the honor of accepting judging and evaluation of this work.

Last but not least, I would like to thank my parents, my husband and all my family and friends for all their love and support.

ملخـــــص

يعتبــر تقسيم الصور خطوة هامة وحساسة لمختلف التطبيقات الطبية وتطبيقات الحاسوب المساعدة على التشخيص. استخراج وتحديد البنيات المتعددة والمختلفة في الصورة مطلوب كمرحلة اولية وقاعدية للتطبيقات الطبية المتقدمة. في تطبيقات اكتشاف واستخراج الحواف التقليدية التصور القاعدي للعملية هو حساب المشتق الأول او الثاني لشدة تدرجات اللون الرمادي للصورة، مما قد يواجه عقبات وقدرات محدودة عند وجود بنيات مختلفة. الهدف من هذه الاطروحة هو تطوير وانشاء طريقة قوية، دقيقة وناجعة لكشف الحواف في صور الرنين المغناطيسي للدماغ. نقترح في هده الاطروحة اجراء جديد لاستخراج بنيات صور الرنين المغناطيسي للدماغ مستعملين نظرية المعلومة الكمية للنمط المحلي الثنائي. وقد استغللنا هدا الاخير في تنفيذ ثلاث تطبيقات أخرى متقدمة تخص استكشاف الحواف. أولا استخدمنا النموذج المقترح في تخفيف الضوضاء من نوع (ملح وفلفل) لصور الرنين المغناطيسي لخوارزمية كاني-دريش. في الطريقة الثانية استخدمنا النموذج المقترح بمساعده الالية الخلوية لاستخراج الحواف في صور الرنين المغناطيسي. اما بالنسبة للتطبيق الثالث والأخير في هد الاطروحة فقد قدمنا خوارزمية استمثال بحث البطاريق في استخراج حواف الأورام الدماغية ودائما باستعمال النموذج المقترح. توضح مختلف الاختبارات المتنوعة والواسعة للكل ان النتائج كانت مقنعة ومتفوقة على الطرق المقارن بها الخاصة في كل تطبيق.

الكلمات المفتاحية: تجزئة الصورة، كشف الحواف، النمط الثنائي المحلي، التصنيف المحلي، المعلومات الكمية، التصوير بالرنين المغناطيسي، خفض الضوضاء، الالية الخلوية، خوارزمية التطور.

Abstract

Segmentation isa crucial step for different medical image applications and computer-aided diagnosis (CAD). Delimitation of the various structures present in images is needed as a pre-processing stage for advanced medical images applications. In conventional edge detectors, the basic concept is to calculate the first or thesecond-order of derivative of image intensities, which is limited when the images are textured. The objective of this thesis is to develop a new approach for accurate, robust and computationally efficient brain MRI images edge detection. In this thesis, we propose a novel procedure to extract the textures from brain MR images, which use the quantum information aspect for the local binary pattern (LBP) descriptor. Then, we investigate this model for three applications: a salt and pepper noise reduction for the Canny-deriche algorithm, as second application a cellular automaton (CA) based algorithm in combination with the new texture descriptor for edge detection task and finally, the model combined with Penguin search optimization algorithm (PeSOA) for brain tumor edge detection. The different experimental results demonstrate that each of these proposed approaches produces good results, in comparison to the appropriate methods devoted to each application.

Keywords: Image segmentation, Edge detection, Local Classifier, Quantum Information, Magnetic Resonance Imaging (MRI), Noise Reduction, Cellular Automaton (CA), evolutionary algorithm

Résumé

La segmentation est une étape primordiale pour des applications différentes d'imagerie médicale et de diagnostic assisté par ordinateur (CAO). La délimitation des différentes structures présentes dans les images est nécessaire comme étape de prétraitement pour les applications d'images médicales avancées. Dans les détecteurs de contours classiques, le concept de base est de calculer la dérivée première ou secondaire des intensités d'une image, dont elle est limitée quand l'image est texturée. L'objectif de cette thèse est de développer une nouvelle approche pour une détection exacte, robuste et efficace des contours dans les images IRM cérébrales. Dans cette thèse, d'abord, nous proposons une nouvelle méthode pour extraire les textures des images de résonance magnétique cérébrale, cette méthode utilise l'information quantique pour le descripteur de modèle binaire local (LBP). Ensuite, nous présentons ce modèle pour trois applications : une réduction du bruit de sel et de poivre pour l'algorithme de Canny-deriche, comme deuxième application un algorithme basé sur un automate cellulaire (CA) combiné avec le nouveau descripteur de texture pour la détection de contours et enfin, comme troisième application le modèle combiné avec l'optimisation d algoe recherche des pingouins (PeSOA) pour la détection de contours de tumeur cérébrale. Les différents résultats expérimentaux démontrent que chacune des approches proposées donne de bons résultats, en comparaison avec les méthodes appropriées consacrées à chaque application.

Mots clé : Segmentation de l'image, détection des contours, modèle binaire local (LBP), classificateur local, information quantique, imagerie par résonance magnétique (IRM), réduction du bruit, automate cellulaire (CA), Algorithme évolutionnaire.

Contents

List of Figures

List of Tables

General introduction

Medical imaging plays a crucial role in clinical diagnosis and scientific research. It can explore the human body and visualize its anatomy without the need for medical surgeries.

The past decade has seen considerable growth in the development of medical imaging techniques and has revolutionized the medical industry. Many tools have been developed, we mention the first producing of 2D representations of the body: X-ray, Ultra-Sound and more. Recently, 3D volumes assets of 2D images of the body. These imaging modalities, such as Computed Tomography (CT) or Magnetic Resonance Imaging (MRI), allow taking 3D images of the body in a noninvasive way. Thus, medical images became increasingly important for medical practice. These images indeed contribute to many medical tasks such as diagnosis, follow-up of patients and evaluation of treatments. In this thesis, we are interested in MR imaging technique.

Magnetic Resonance Imaging (MRI) is a medical imaging process, based on the phenomenon known as Nuclear Magnetic Resonance (NMR), which is gaining widespread acceptance for a large variety of medical explorations. It is one of the most commonly used techniques in radiology to visualize the body soft tissues with great contrast, including the brain.

Segmentation is one of the most important operations for any automatic image processing. It is necessary as a preliminary stage for several medical image analysis. It can be defined as the extraction of the boundaries of an object of interest from the image. In other sense, it can be viewed as a labelling problem, where image pixels are assigned either to the object or to the background. Segmentation has great importance in MR images because it provides qualitative and quantitative information about the image.

Medical images often exhibit poor image quality, such as low contrast, decoy structures, and the complex shape and appearance of some anatomical structures, which makes segmentation in medical imaging a difficult and challenging problem. A number of researchers have found ways of categorizing segmentation approaches according to their appearance. Several algorithms have been developed to address these problems and enhance such segmentation. These algorithms fall into two categories: region-based methods and boundary-based methods.

Region-based segmentation methods group pixels with similar properties together to produce regions that represent meaningful objects or areas in the images. Boundary-based segmentation involves identifying the boundaries of adjacent regions in an image by detecting edges and isolated points. Region-based segmentation methods are simple to implement. However, most of them require the integration of information prior in the searched areas.

The classical boundary-based algorithms use abrupt change and discontinuities of intensity. Most of these methods calculate the first-order or the second-order derivative of a pixel value as a measure of the edge's magnitude and orientation.

In real-world applications, each of these classical methods still has challenging limitations and drawbacks depending on different variables in the medical images, such as several objects with similar intensities, noise, and even the edge structures. In MR images, intensity inhomogeneities can be attributed to imperfections in the RF coils or some problems associated with the acquisition sequences which makes the edge detection with classical methods more than challenging task.

To enhance medical image edge detection, we have investigated the use of another image feature, namely, texture. In MRI images, the texture is the most important characteristic for distinguishing between different brain tissues. Several texture analysis operators for extracting texture features are described. The self-invariant feature transform (SIFT) with low-level and high-level descriptors is used to differentiate the tissues present in breast images, a Gaussian Markov random field has also been used for texture recognition and the Gabor filtering method has shown good results in comparative studies of texture analysis.

Recently, particular attention has been paid to the Local Binary Pattern. LBP is a robust, fast, and simple texture analysis operator, it is developed to meet the requirements of real-world applications. In this thesis, we investigate the texture as a new characteristic instead of the intensity derivation for the edge detection task in brain MR images.

The objective of this thesis covers four tasks or contributions: First, is to propose the Quantum Local Binary Pattern (QuLBP) as a new variant involving quantum information aspect. The QuLBP model is proposed for characterizing the MR images and lays a role as a local classifier. Moreover, three main applications that investigate the QuLBP model are presented. The first application combines the proposed model as an edge filter with Canny-deriche edge detection for salt and pepper noise resistance, the second application performs an edge detection task using a CA as the next process to obtain the edges of images, as third and last application, it uses as the first time the PeSOA for the edge detection task. The algorithm was changed to deal with brain tumor edge detection in combination with the cellular automata. Compared to traditional edge detection operators, the QuLBP efficiently and accurately obtained edges for several datasets.

The thesis is composed of four themed chapters.

In the first chapter, we introduce different brain anatomy and its structure. To deal with such organ, different medical imaging techniques are presented for diagnosis of various tissue abnormalities, detection of the tumor. Different aspects of MRI are introduced.

The second chapter reviews the most common medical image segmentation methods that are devoted to brain MR images. For each method, we describe its fundamental concept then the recent techniques with high citation are cited as examples in this review.

The third chapter begins by laying out the theoretical dimensions of the research. We start with the texture analysis definition, then, we present the basic concept of LBP. This chapter contains the first contribution which is the proposed QuLBP and the second one which is the salt and pepper noise reduction for Canny-Deriche algorithm. Different evaluations experiments are done to validate both of applications.

In the third chapter, we develop other two contributions based on the QuLBP model devoted to edge detection in brain MR images. The CA edge detection, the PeSOA-CA edge detector.

We conclude the chapter by providing the experimental results, the different dataset and the metrics that used to accomplish this phase.

Finally, the conclusion gives the thesis summary and critique of the findings. Areas for further research are identified.

Own publications

The first work was presented in the Biomedical Engineering International Conference (BIOMEIC'14), Tlemcen, Algeria, it included the first approach proposed for detecting edges using conventional LBP. The second work which is an enhancement of the first one is proposing the quantum information to improve the LBP. The paper was a participation in the Second International Symposium on Informatics and its Applications (ISIA 2016). We have improved this method and create the QuLBP for two contributions, this work was published in (LEKEHALI & MOUSSAOUI, 2019) . As the fourth contribution in this paper, we investigate the PeSOA with LBP for brain tumor edge detection.

Chapter 1

Brain MR Imaging

Contents

1.1 Introduction

The brain has a very complex anatomical structure of the human body. It not only contains the nervous center that controls every other organ of the body but also includes other organs embedded in it. Nature has provided maximum security by housing the brain inside a tough bone structure called the skull. This complicates the study of the brain, its function and makes any diagnosis more complex. The complexity of the brain gives rise to complicated disease and lack of diagnosis at the proper time can be fatal. Any abnormalities within the brain will change its normal structure and behavior. Automatic detection of abnormalities using MRI is quite useful in several diagnostic and therapeutic applications; computed tomography and

MRI are two imaging modalities that are useful to researchers and medical practitioners to study the brain by looking at it non-invasively.

In this chapter, First, we introduce the brain anatomy and the brain MR imaging choosing the MRI, then we give more details for MR imaging modality.

1.2 Brain anatomy

The brain is an extraordinary organ that controls the human body. The average weight of an adult human brain is about 1800 g. The brain is composed of thee gross divisions (Figure 1.1): cerebrum, the brainstem and cerebellum (see Figure 1.1.) (Yves, Jean-Pierre et Vera 2006)

- **Cerebrum**: the largest part and the most complex of the brain, it is composed of the right and left hemispheres. It performs higher functions like interpreting touch, vision and hearing, as well as speech, reasoning, emotions, learning, and fine control of movement.

  The brain is made up like the rest of the central nervous system, of gray matter (body of neurons and synapses is located under the cerebrum. Its function is to coordinate muscle movements, maintain posture, and balance) and of white matter. The brain is bathed in a liquid playing the shock absorber called cerebrospinal fluid (CSF).

- **The brainstem**: It is comprised of the midbrain, pons, and medulla. It connects the spinal cord to the brain. It controls vital functions like blood pressure, breathing activity and heartbeat cardiac as well as controlling eye movements and facial expressions.

- **Cerebellum**: is located under the cerebrum. Its function is to coordinate muscle movements, maintain posture, and balance

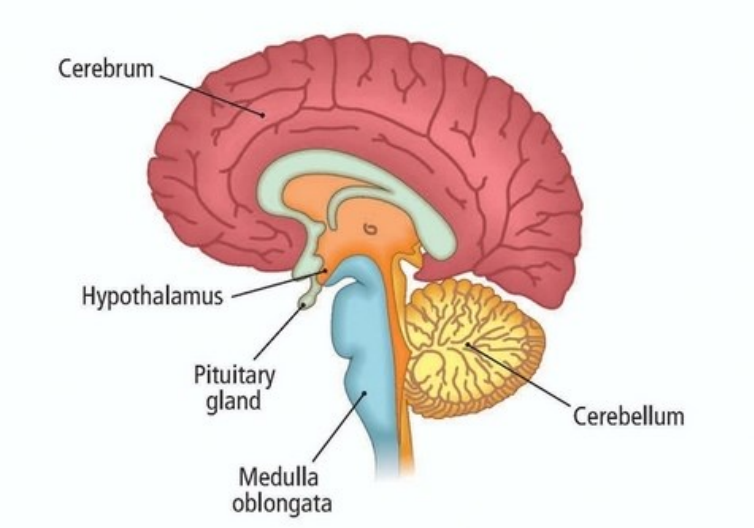

Figure 1.1 The brain

1.2.1 Principle of Brain tissues

- **The white matter (WM)**: corresponds to the myelinated axons that are located in the outer regions of the brain and spinal cord. It has a whitish and bright color. The myelinated axons assemble into bundles to establish connections between groups in the of neurons which coordinate the different brain regions (Figure 1.2).

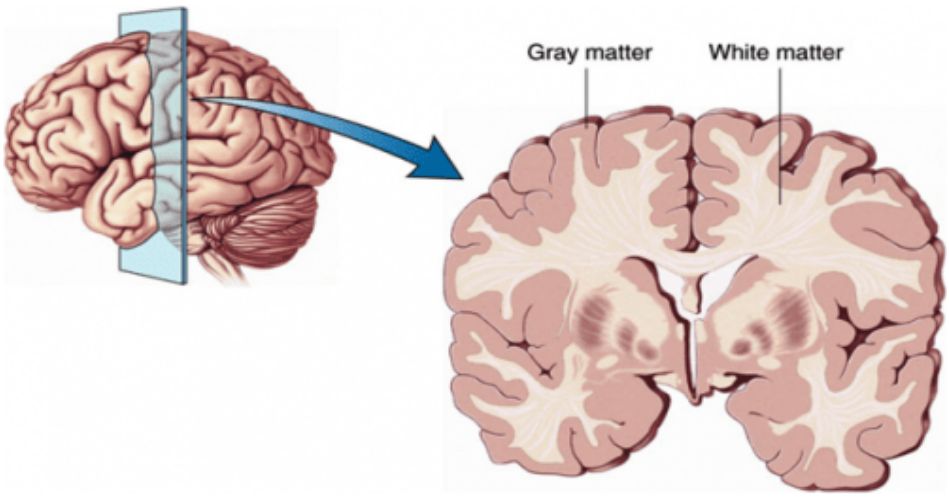

Figure 1.2 Brain tissues s

- **Gray matter (GM):** is responsible for processing and regulating information, it corresponds to unmyelinated axons. It is presented by the cortex and some of the

subcortical structures: cerebellum, thalamus, basal ganglia besides the spinal cord. It has a darker

- **Cerebral spinal fluid (CSP):** is a substance that surrounds the brain and fills the cerebral ventricles. It protects the nervous system, serves protection against the infections and provides an important role in the transport of hormones between different brain regions.

1.2.2 Medical imaging

Medical imaging methods have known a great revolution in medicine. Medical imaging provides different modalities to create various images for the human body, allowing to scientists and clinicians the understanding, modelling diagnosis and treatment for diseases.

There are several medical imaging technics, we can cite: X-ray radiography: to find orthopaedic damage, tumors, pneumonia, foreign objects, etc.., CT (Computed Tomography): to produce cross-sectional images of the body. MRI (Magnetic Resonance Imaging): can diagnose or monitor treatments for a variety of medical conditions such as abnormalities of the brain and spinal cord Tumors, cysts, and other abnormalities in various parts of the body Injuries or abnormalities of the joints Certain types of heart problems diseases of the liver and other abdominal organs, ultrasound: ultrasound Doppler(to visualize blood flow through a blood vessel), Echocardiogram (to view the heart) Fetal ultrasound (to view the fetus in pregnancy) etc.

1.2.3 Brain medical imaging

Over the past decade, brain medical imaging or neuroimaging knew enormous progress to develop different technics to understand better the human brain and see what is inside without the need for neurosurgery. Among these technics, we can cite the Electroencephalography (EEG) to measure the neurophysiological activity of the brain. It produces electroencephalogram (EEG) to detect the different abnormalities of cerebral activity such as epilepsy in its different cases. Functional magnetic resonance imaging (fMRI) is another brain activity measurement. Its basic is to detect the changing in blood oxygenation and flow that occur in response to neural activity. fMRI is used to produce an activation map, visualizing the involved part in a particular brain mental process.

CT scanning is commonly used in building up brain pictures. This technique is based on the differential absorption of X-rays revealing the gross features the brain. Positron Emission Tomography (PET) maps the brain functional processes. It uses trace amounts of short-lived radioactive material. Near-infrared spectroscopy (NIRS) is another brain activity measurement depends on the measuring of the blood oxygenation and Magnetoencephalography (MEG) is used to measure the magnetic field produced by the brain electrical activity.

1.3 Magnetic resonance Imaging

Magnetic Resonance Imaging (MRI), is a medical imaging technique that revolutionized the study of the brain. It is considered as one of the most flexible methods among other medical imaging modalities but also the most complex. MRI allows the best characterization of the tissues with high resolution and good contrast, at a level of details that can be hardly reached using other 3D images modalities; thus, it is the modality the more suitable for observing the tissues and structures of the brain. MRI uses strong magnetic fields and radio waves to produce 2D and 3D detailed images with thin resolution (~ 1mm) and from 1 min to 20 min for acquisition times (Erasmus, et al. 2004), (Dubois, Cohen et Zeineh. 2000). It is based on the nuclear magnetic resonance phenomena (NMR term created by Issac Rabi, Nobel prize in physics,1944). The first MR image created was published by Paul Christian Lauterbur (P. C. Lauterbur Mar 1973), in 1973.

There are two major classificationss for brain MR imaging:

- **Anatomical or structural MRI:** allows to obtain information on the structure, shape, content of brain tissues and blood-brain barrier (BBB).

- **Functional MRI (fMRI):** it studies of brain activity and less interesting to the anatomic of the brain. FMRI is most often related to the field of cognitive science and neuroscience research.

1.3.1 MR basics

The MR image creation uses the magnetic resonance phenomenon that is present in Hydrogen protons in the human body placed in magnetic field B_0. These particles can selectively absorb and re-emit electromagnetic energy. The resonance is the process of energy absorption, and

The process in which the excess of energy is released as radio frequency waves is called relaxation. This wave can be detected by an antenna, and the received signal can be used to construct an image (MRI), to perform a spectrometric analysis (MRS), or a combination of both. From a general point of view, the process is shown in Figure 1.4. Magnetic Resonance Imaging for clinical diagnosis utilizes the MR of the hydrogen nucleus (protons). Other nuclei, such as Na^{23} have been studied to be used in neuroimaging, but they are not yet commonly utilized.

1.3.2 Image acquisition

For obtaining body information tissues through MR, A strong magnetic field $\sim B$ aligned the magnetization $\sim M$ the body tissue's (Figure 1.3(a)). The sum of magnetic moment of all nuclei presents the magnetization $\sim M$. The magnetic moment of the nuclei $\sim\mu$ has two possible states: Up (low energy) and DOWN (high energy). The magnetic moments precess around the direction of $\sim B$ (Figure 1.3(b)) with a frequency of precession or resonance f_p. Boltzman distribution makes the spin UP and DOWN in thermodynamic equilibrium.

-Resonance: is a phenomenon happens when the nuclei absorb electromagnetic energy of the particular frequency f_p . The nucleus in state UP absorbs energy when the electromagnetic signal with appropriate frequency is emitted and moves to state DOWN. And this change accompanied a tissue magnetization $\sim M$ change electromagnetic momentum moves.

The energy emitted by the electromagnetic pulse of frequency *fp* affects the displacement angle of the electromagnetic momentum. When the direction of the tissue magnetization is orthogonal to the external magnetic field(Figure 1.4), the number of nuclei in UP and DOWN states are equal. Moreover, after the emission of a radio frequency pulse, all the magnetic moments of the nuclei $\sim\mu$ are in phase. (Galdames, 2012)

-Relaxation: is a phenomenon happens when the radio frequency signals stops. The tissue in stage returns to its initial state. When Boltzmann equilibrium is reached the relaxation stops. The return of magnetization to its initial state generates transformations in the magnetic field

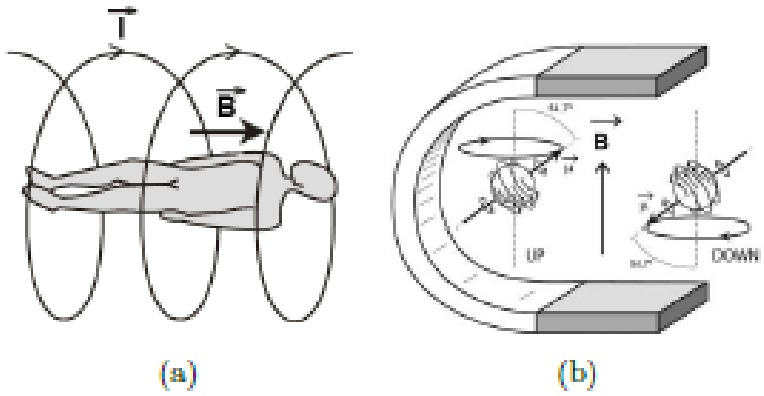

Figure 1.3 a. Magnetic field, b. created by an helix-shaped conductor (solenoid) through which direct current flows (Galdames, 2012)

The return of the magnetization to its initial state produces changes in the magnetic field that can be detected with antennas, inducing a signal known as the Free Induction Decay (FID) The relaxation process depends on many factors, such as the molecule in which are the nuclei, the material (tissue) in which the molecule is immersed, or the external magnetic field. Five different variables measure in the relaxation are used to construct images: spin density, T1 and T2 relaxation times; and flow and spectral shifts. By changing the parameters on the scanner, it is possible to weight the effect of one of these parameters over others. This effect is used to create contrast between different types of body tissue or between other properties. In addition to the traditional anatomical images, images with physiological or biochemical information can be acquired. Moreover, the new systems are faster, allowing to acquire dynamic images.

Sequence parameters:

The sequence parameters are the parameters that the operator axes on the console to generate the corresponding MRI sequence.

Echo time: the echo time (TE) refers to the time between the application of the RF radio frequency excitation pulse and the top of the induced signal in the coil. It is measured in milliseconds.

Repetition time: the repetition time (TR) is the time of the application from an excitation pulse to the application of the next pulse. It determines the amount of longitudinal

magnetization that recovers between each pulse. He is measures in milliseconds. The TR, like the TE, is a contrast ratio.

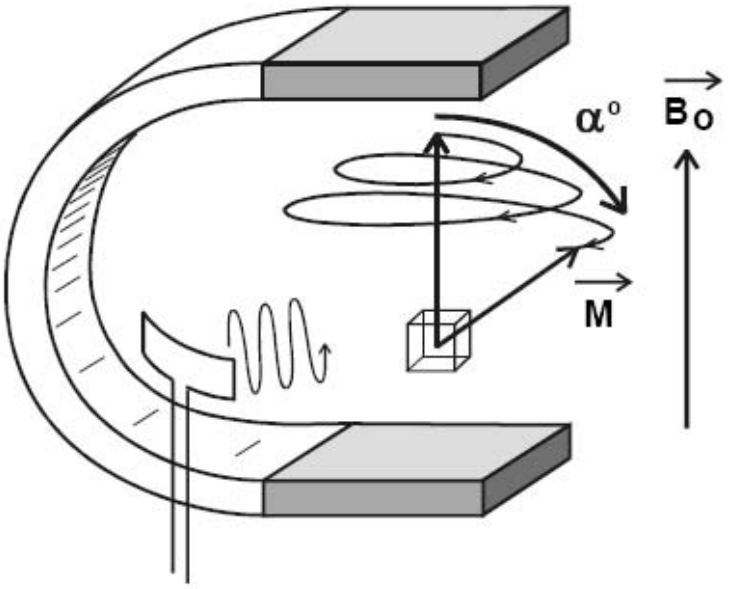

Figure 1.4 Movement of the magnetization vector ~M when the nuclei of a volume absorb energy in the resonance induced by the radio frequency signal of frequency fp.

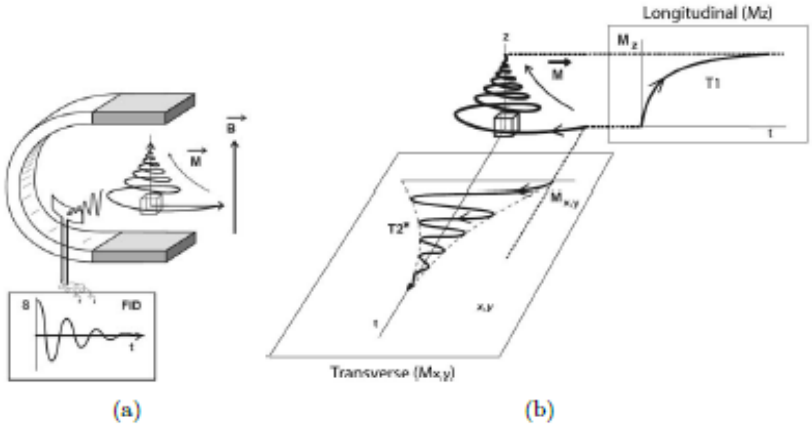

Figure 1.5 (a) Detection of the changes in the electromagnetic field when the magnetization vector ~M returns to its initial position in the relaxation process(Gili,2007).

1.3.2.1 MRI sequences

It is a common practice in automatic analysis to use a combination of several MR sequences to achieve more valuable and accurate results. In this work, three different MR sequences. The most used types of MR images are explained below.

Spin density weighted MRI:

They are also referred to as weighted proton density (PD). The value of the magnetization is proportional to the density of hydrogen nuclei. For a long TR and a TE, in short, we obtain a sequence weighted in DP proton density. The fabrics are ordered by increasing grayscale in MB, MG and LCR.

T_1-weighted MRI:

T1 weighted image: for a short TR and a short TE, the image obtained is weighted in T1. The tissues are ordered by increasing grey levels in CSF, GM and WM.

Each MRI sequence contains specific information, so the choice between ifferent sequences depend on the structure to be studied.

T_2-weighted MRI:

T2 weighted image: for a long TR and a long TE, we obtain an image weighted in T2. The fabrics are ordered by increasing grayscales in MB, MG and CSF.

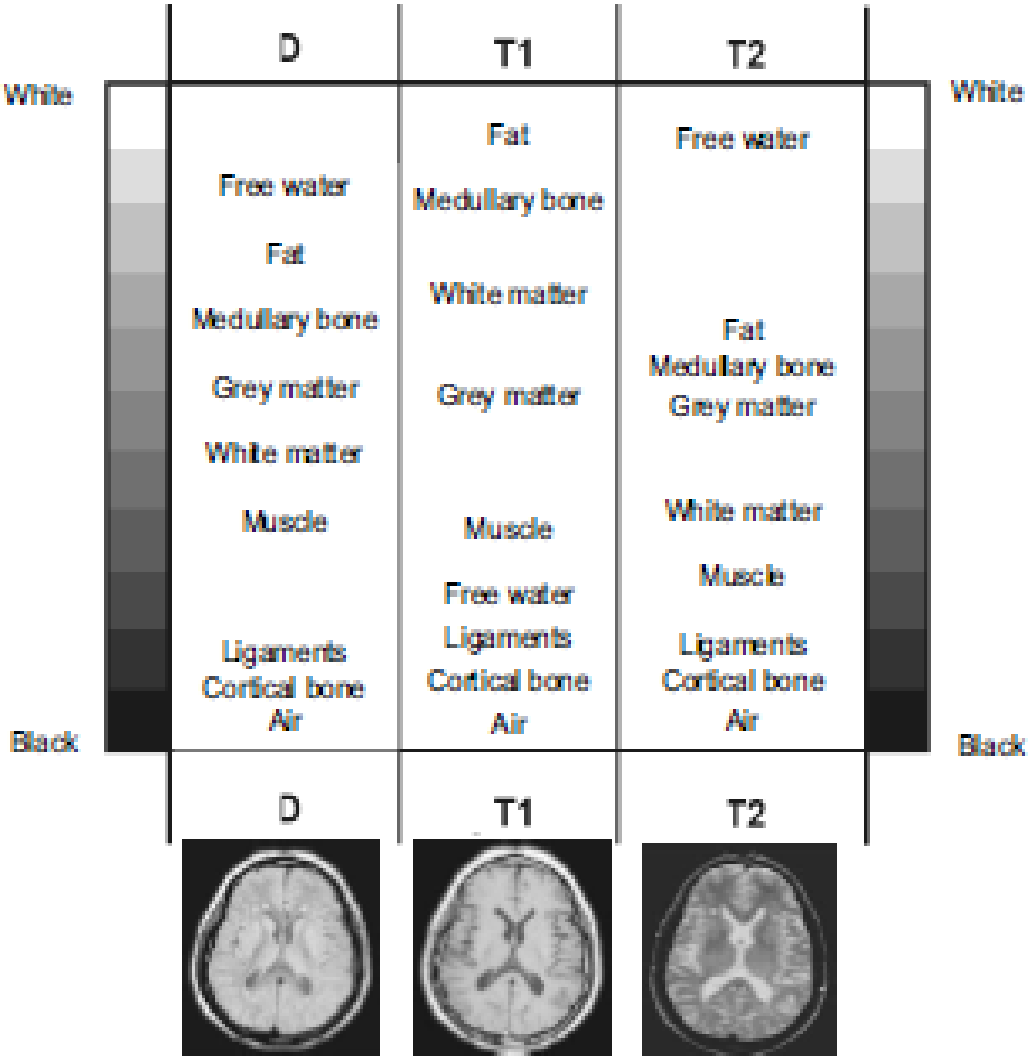

Figure 1.6 Comparison between the gray level of different tissues in spin density weighted, T1-weighted and T2-weighted MR images(Gili, 20007)

1.4 Conclusion

In this chapter, we have presented the anatomy of the human brain and its cerebral structures. Then, we shortly mentioned the different medical imaging modalities used to visualize the brain. Due to the brain nature i.e. its softness, it has been concluded that the best technique to study it is the MR imaging.

Next, we have presented different basic concepts on the MR imaging, its different weighted images: T1, T2 and DP and the artefacts during the MR acquisition. For brain MRI measuring, visualizing anatomical structures, analyzing brain changes, for delineating pathological regions and further image-guided interventions, brain segmentation is needed.

In the next chapter, we will review the different recent segmentation methods in the literature, that are devoted to brain MR images. Highlighting differences between them and discuss in non-invasive way their specificities among each other, their advantages, and their limitations.

Chapter 2

Image Segmentation Techniques

Contents

2.1 Introduction

Medical image segmentation is one of the most important tasks in computer vision applications, its aim is to divide the image into homogeneous regions. These regions should be pertinent, non-overlapping, present zones of interest to make it easy and more meaningful to understand.

Segmentation in MR images is to subdivide the brain into its different tissues: white matter, gray matter, spinal fluid and pathology (if it exists), etc...

In this chapter, after giving formal definition of the segmentation, we describe the recent segmentation methods applied in medical image analysis. Two main categories are mentioned: Region-based segmentation techniques, which considers gray-level of the neighboring pixels to identify the region, is examined in Section 2.4.1. and edge-based segmentation, which detects an abrupt change in intensity of the image, is discussed in Section 2.4.2.

2.2 What is image segmentation?

Segmentation is one of the most important steps in medical image analysis. It is generally defined as the partitioning of an image into nonoverlapping, constituent regions which are: homogeneous with respect to some characteristic such as intensity, color or texture(Pham, Xu, & Prince, 2000) and heterogenous: texture or color that in one region should be distinct from those in another region.

A formal definition is given(Horowitz & Pavlidis, 1976) as follows:

Let ***I*** be the domain of the image and ***P*** a homogeneity predicate is defined on subsets of ***I*** with U(i, j) the uniformity criterion (to be defined)as follows *:*

predicate ***P***(R) = True, if $\exists\ a\ \ni |U(i, j) - a| < \varepsilon, \forall\ (i, j) \in R$

Segmentation of image ***I*** into subsets R_i, i = 1... m, such that:

- Complete: $\boldsymbol{I} = \cup R_i$, i = 1,.., m
- Disjoint subsets: $R_i \cap R_j = \varnothing, \forall\ i, j:\ i \neq j$
- Uniform regions: $P(R_i) = True, \forall\ i$
- Maximal regions: $P(R_i \cup R_j) = False, \forall\ i, j:\ i \neq j$

The four above conditions were more explained by Zucker in (Zucker, 1976) :

- The first condition is about to ensure that every pixel belongs to only one region
- The second condition ensures the convexity of each region obtained.

- The third condition examines the homogeneity of each region.
- The fourth and last condition is a maximality condition, it ensures that two regions must not produce homogenous region.

2.3 Brain MRI segmentation

The objectives of image segmentation are to partition the image into areas of interest that satisfy predefined conditions. The segmentation of medical images(Priyanka, 2013) provides the study of the anatomical structures, identify the regions of interest, localization of (tumors, lesions and other anomalies), measure the tissue volumes to have the tumor growth state and assists in pre-radiology treatment planning, in calculating the radiation dose.

In the case of MRI brain images, as well as other medical images, they contain complex structures so their accurate segmentation is crucial for clinical diagnostics. We cite in non-comprehensive way: tissues classification (Beare et al., 2016) ,structures segmentation(Visser et al., 2016) , segmentation of objects volumes(tumor)(Meier, Knecht, & Loosli, 2016) and segmentation of the brain tumors(Cark, Hall, & Goldgof, 1998),(Işın, Direkoğlu, & Şah, 2016) as well as brain MR tumor classification(Anitha & Murugavalli, 2016),(Gurusamy & Subramaniam, 2017). Segmentation of the brain in white matter, gray matter and spinal fluid(Jokinen et al., 2015),(Chazen et al., 2017)

2.4 Brain MRI segmentation methods

Over the past century there has been a dramatic increase in medical image segmentation methods. Until recently, there has been no ideal method and the choice of a good method stills delicate for researchers in this field.

We present int this thesis in non-exhaustive way the recent approaches proposed in the literature. They can be categorized based on various features found in the image, on three groups of approaches(Scherrer, 2008) :Boundary based approaches, region-based approaches and hybrid approaches see Figure 2.1.

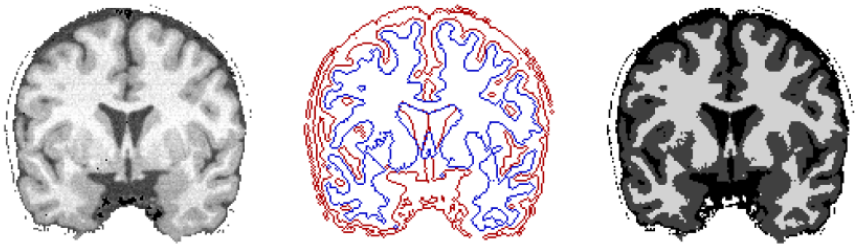

(a) (b) (c)

Figure 2.1 Segmentation approaches: (b)Boundary-based (c) Region based (Scherrer, 2008)

2.4.1 Region-based approaches

The aim of region-based methods is to divide the image into sub regions or clusters that have similar features: color, grey level, texture ...etc. In the following sections, we present the principles approaches in the recent literature.

2.4.1.1 Region growing

Region growing is one of the famous methods. It starts with an initial seed points and will grow by searching for neighborhood pixels and adding the pixels with similar predefined properties (such as gray level, texture, color, shape) to the region, repeat until all pixels are treated and belong to some region.

In (Javadpour & Mohammadi, 2016) the seed points of the region growing algorithm are automatically selected by the genetic algorithm from brain MRI images of patients suffering Alzheimer to produce better and more accurate segmentation results.

Zabir et al. (2015)proposed a Glioma brain tumor detection method where they have used the outcome region of the region growing method as the initial contour to the distance regularized level set method (DRLSE). Then, with number of iterations, the final decision is made. Their approach has improved the detection and segmentation performance of tumor for different glioma brain tumors. Another brain tumor detection presented in (Nerurkar, 2017)

Region growing based algorithms are simple to implement and fast in execution. However, they are expensive in computational time, the absence of the global view of the problem due to the local application iteration process besides they are sensitive to noise.

2.4.1.2 Split & merge

Split and merge unlike the region growing. ,its principle is to consider the whole image as one region. First split the image successively into square subregions (quarters) based on homogeneity criterion, If the pixels in the region have different intensity value then the region is divided until no more splitting is required and a complete homogenous region is achieved. Afterwards, a merge process is applied, if two adjacent segments verify the criterion of homogeneity.

Split and merge have been widely used in brain MR segmentation(Manousakas, Undrill, Cameron, & Redpath, 1998; Saad, Abu-Bakar, Muda, & Mokji, 2010). An adaptive Geometric Split Merge (*AGSM*) segmentation is proposed by Maras et al. (2014),The method has been applied to brain MRI medical dataset and it provided better results with comparison to 3D segmentation methods.

Mary et al.(2016) have proposed a new modified segmentation method. The process includes three steps, the split and merge is the last process where similar regions are merged by using a distance comparison between regions. These results are obtained from the texture feature generation phase and combined with the results of Thresholding step.

2.4.1.3 Thresholding

The concept of thresholding methods is very simple. The pixels are grouped depending on their gray scale levels and the output is a binary image. Generally, the thresholds values are obtained from the histogram of the image. Two types of thresholding can be distinguished: global, local. If threshold T is used consistently throughout the image, T is a global threshold into. Otherwise it is a local threshold, and only applies for a particular area of the image.

A considerable amount of literature has been published on Thresholding. Some of these studies have been extensively used for brain MR image segmentation. In their paper, Sujji et al. (2013)proposed a thresholding technique that can distinguish the pathological tissues such as edema and tumor from the brain tissues :White Matter, Grey Matter and Cerebrospinal Fluid .Suganya and Krishnaveni (2016) uses a threshold technique as first level of their algorithm to extract white and grey matter from the MRI brain image .The obtained binary is forward used for active contour model.

Suresh at al.(2018) have recently developed a new method used thresholding and morphological process with histogram-based method to detect brain tumor and provide specific tumor features (size, place, type). Another improved thresholding approach for brain tumor has successfully detected Alzheimer disease (Priya & Kalavathi, 2018)and separated the brain tissues form MR images.

Overall, Threshold-based segmentation Methods are efficient if there is high contrast between the background and the object. However, these segmentation methods have a number of limitations., they are very sensitive to noise due to the absence of the neighborhood information, no relationships between voxels are considered.

Another crucial drawback is the choice of the threshold value whether manual of automatic (based on preselection process). Generally, Most of Thresholding based segmentation algorithms have incorporated forwards approaches to enhance the segmentation process or they can be used as first step for segmentation process

2.4.1.4 Watersheds

Another region-based method is watershed. Watershed algorithm was first proposed by Digabel and antuéjoul(1978). It represents the morphological approach of a gray level image. The gradient values of an image are then considered as the altitude levels in a topology surface. Water flooded into this surface will flow to the lower parts (local minimum) of this surface, the water will rise until the immersing of all points. When two catchments basins (regions) are met, a dam is built between them. These dams are called watersheds that segment the image.

This technique has widely used for brain tumor segmentation. Dhage et al.(2015) provided a successful approach to extract the abnormal tissues from brain MR image using several parameters such that perimeter, eccentricity, entropy and centroid. Another brain tumor watershed-based method is proposed in (Benson, Lajish, & Rajamani, 2015) , a set of features were used as inputs for the marker watershed-based algorithm such as: color, edge, orientation and texture. In(Shanthakumar & Ganesh Kumar, 2015), After five stages to extract and classify brain tumor as normal or abnormal, the watershed algorithm is combined with morphological operation to segment the tumor region.

Kwon et al.(2016) carried out a study evaluating the effectiveness of a combination between watershed algorithm and the expectation maximization (EM)algorithm. They showed improvement in their results in comparison with other methods.

Although There is a valuable progress in Watershed segmentation algorithms, there still no perfect solutions yet. Watershed method stills suffer from the problem of over segmentation.

2.4.1.5 Markov random fields (MRF)

A Markov random field model (MRF) is a stochastic process that incorporate neighborhood relations as a priori model. The MRF itself is a *conditional* probability model, where the probability of a voxel depends on its neighborhood

Several papers were interested in developing brain MRI segmentation based on this method. Pereira et al. (2016)have designed a new framework based on conditional Markov random field to segment the different brain tissues. They provide a random forest to encode the likelihood function. A robust obtained result insured refinement of the skull stripping at segmentation time.

In (T Krishnan, Balasubramanian, & Krishnan, 2016), the authors presented a new metaheuristic Markov random field where they have used the priors of particle swarm optimization algorithms (PSO). In an inverse concept, Guerrout et al. (2018) have investigated the Markov random field for the PSO algorithms to segment brain MR Images.

2.4.1.6 Neural Networks (NNs)

The Concept of Neural networks (NNs) is inspired by the human brain nervous system. They are statistical learning methods connected together to form a network. NNs are classifiers for MRI images segmentation. The learning process of the neural network consists of adjusting the weight values. In MRI image segmentation, this process is based on set of MR images where the segmentation results are known in advance.

Several approaches based NNs segmentation were presented in the literature. Clarke (1991) was one of several researchers who attempt to present a brain MR image segmentation based on the NNs. His work was done on Different brain MRI sequences.

Later NNs have been developed where the popularity of classical NNs aspect start to increase and deep learning approaches were added as in Convolutional Neural Networks (CNNs). Zhang et al. (2015) employed CNNs for segmenting infant tissue images in the isointense stage. They used combination of T1, T2 and fractional Anisotropy (FA) brain MRI modalities, their approach performed better than other well-known segmentation methods. However, their method is crowded with a huge number of parameters, which lead to difficulties in network converge besides to the sensitivity to patch size. To skip these difficulties, Nie et al. (2016) proposed an improvement fully convolutional networks (FCNs). They trained separately for each modality one network then the resulted high layer features for the final segmentation are combined.

Havaei et al. (2017) proposed an automatic brain tumor segmentation method based on deep convolutional neural networks. They used a variety of architectures to investigate their impact on the performance. They provided fast and accurate approach in comparison with several recent brain MRI segmentation methods.

Another brain tumor MRI segmentation based deep convolutional neural networks algorithm is presented by Hussain et al. (2018). To train the network, they used a patch-based approach after a pre-processing step where the bias field was corrected and the images were normalized. After the application of the convolutional neural network, a post-processing is made to remove the small positives around the edges.

2.4.1.7 Support vector machine (SVM)

Support vector machine (SVM) is a supervised learning machine method introduced by Cortes and Vapnik (1995). SVM algorithms are based on the construction of hyperplanes of N dimensions which separate the high dimensional feature space into subspaces according to the training data. SVM provides a good generalization of classification problem. In recent years, it has achieved a remarkable progress in the brain tumor segmentation hence many approaches based-SVM segmentation have been published in the literature.

Zhang et al. (2015) introduced a brain image classification algorithm. Two types of SVM were investigated: generalized eigenvalue proximal SVM and twin SVM. The SVMs have used about 26 spectral features that have been reduced from different samples after extraction

of the spectrums from the MRI images. Their method has showed good results in comparison with studied state of the art algorithms.

SVM technique was used for brain tumor segmentation by Alfonse and Salem (2016). They proposed a hybrid approach for brain tumor detection and classification in DICOM MR Images. First stage of the proposed approach concerns with image preprocessing which includes image enhancement and cropping. The second stage deals with segmentation using the Expectation Maximization (EM) algorithm and adaptive thresholding, next stage is devoted for feature extraction from MRI data set using Fast Fourier Transform (FFT), feature selection using Minimal-Redundancy-Maximal-Relevance criterion (MRMR) to select most valuable features. Final stage deals with classification of the obtained features using SVM, into normal or abnormal brain MRI. The results of classification shoed a good performance against reviewed methods.

Halder and Dobe (2016) proposed an algorithm which at first, generates a set of features from brain MRI images that allow in precise manner the separation between normal and abnormal MR images. The features have been reduced to be used for SVM algorithm for training with radial basis function to classify the brain MRI images into tumor present and tumor free.

Another brain tumor classification is proposed in (Rasel, Sen Swakshar, Foisal, & Md. Abdur, 2017). They combined SVM and ANN to classify the brain MR images. As preprocessing step, a TKFCM algorithm is used to extract two types of statistical features. The hybrid algorithm is considered as robust method for brain tumor classification. Polepaka et al. (2019) used a method based on three steps. The proposed approach at first, reduces the noise presence in the brain MR images then the tumor is localized using Bounding Box (BB). At last, SVM is used to mope the classification of the tumor.

Despite its success, SVM has a number of problems in developing. We cite: the expensive computationally time, requirement of a large memory and the input training data might be slow. In addition, SVM is designed at first place to deal with binary problems such as the normality or abnormality of brain tumor images, so many extensions must be added. Another drawback is the define of the parameters how can they be chosen.

2.4.1.8 Clustering

Clustering is an unsupervised learning method unlike the previous mentioned methods (SVM, NN, MRF). It consists of regrouping pixels automatically into several groups, therefor, no need for training phase or a training data set. Among clustering-based methods, we cite: K-means (MacQueen, 1967), Fuzzy c-means (FCM) (Bezdek, 1981), Possibilistic c-means (PCM) (Krishnapuram & Keller, 1993) and Expectation maximization (EM) (Dempster, Laird, & Rubin, 1977), Mean shift (Comaniciu & Meer, 2002).

The general idea behind K-means is to define K classes with an iterative process, it minimizes the sum of distances from each data sample to the centroid it is assigned to.

Ganesh et al (2017) used K-means algorithms to separate different brain tissues in MRI images. An enhanced method named adaptive fuzzy K-means (EAFKM) K-means was presented. They showed in their paper, a good and adaptive clustering process.

A brain tumor diagnosis is presented in (Zeinalkhani, Jamaat, & Rostami, 2018).The authors proposed a combination of genetic algorithms (GA) and K-means algorithm to detect malignant tumor in brain MR images. the approach provided a good result using BRATS standard collections of brain MRI. Another combination with K-means algorithm is proposed by Sharma et al. (2018). A Grey Level co-occurrence matrix used for feature extraction. Fuzzy Inference System is created using extracted feature which followed by thresholding, morphological operator and Watershed segmentation for brain tumor detection. The approach is designed to identify affected part of brain and size of tumor.

Dobe et al. (2019) recently published a brain tumor segmentation method using a rough set-based K-means algorithm as first phase then thresholding and morphological operations are investigated to finally extract the tumor form from T1-type magnetic resonance imaging (MRI) scan images. The proposed algorithms have been showed as robust approach against other recent methods.

Fuzzy c-means (FCM) also known as soft K-means. The concept of FCM is the possibility of each pixel to belong to more than one class. FCM method fails to carry out segmentation well enough due to intensity inhomogeneity in MRI. Li et al. (2016) introduced an improved FCM by including the spatial information influence and the correction of bias field. The

proposed approach has showed good results in brain tissues segmentation: white matter (WM), gray matter (GM), and cerebrospinal fluid (CSF) from MRI.

Another neighborhood information managing is included in the work of (Mangla & Singh, 2019). They proposed an FCM-based method in the presence of noise. the preprocessing phase is to eliminate the noise presence using different filters such as: Bilateral Filter, Anisotropic and Filter Total Variation Filter.

2.4.2 Edge-based methods

Unlike region-based segmentation methods which group pixels with similar properties into regions, edge-based or boundary-based methods involves identifying the boundaries of adjacent regions in an image by detecting edges and isolated points. Overall, they use abrupt changes and discontinuities of intensity. In the following, we are particularly interest derivative methods and deformable models.

2.4.2.1 Derivative methods

Boundary-based segmentation involves identifying the boundaries of adjacent regions in an image by detecting edges and isolated points. The classical boundary-based algorithms use abrupt changes and discontinuities of intensity, e.g., Roberts (1963), Prewitt and Sobel (1970)calculate the first-order derivative of a pixel value as a measure of the edge's magnitude and orientation. The Canny operator (Canny, 1986)is a more optimal edge detector that is capable of good detection and localization with a low error rate (Figure 2.2).

In the literature, the contributions of derivatives methods to the segmentation of brain MRI images, are rare. Although these methods are simple and fast, they are very sensitive to noise and do not generate firm contours. Their efficacity is based on the existence of contrast between the structures being researched.

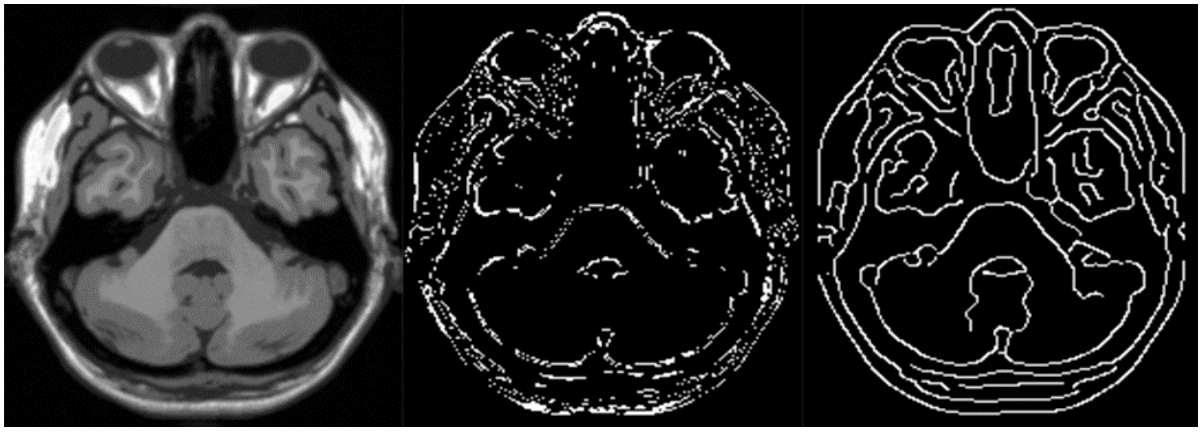

Figure 2.2 An Example of Sobel and Canny filter

2.4.2.2 Deformable models

Deformable models are largely used in volumetric (3D) image segmentation. They require initial estimation of the contour which is done by incorporating a priori knowledge of the object such as shape, location, and orientation. This contour is able to be expanded or contracted over time, within an image and confirm to specific image features. Deformable models can be divided into two groups: parametric and geometric and geometric deformable models

***Parametric deformable models*:** Parametric deformable models are also known as *snakes* or *active contours*. These methods move a deformable contour through the image spatial domain minimizing an energy function. Active contours are widely used for the brain MRI segmentation. As a contribution for active snake methods, Gao, Yang and Yan (2014) suggest a multiphases active contour model devoted to magnetic resonance (MR) and natural images segmentation. this method for simultaneous regions classification of MR images and natural images without bias field correction. As first step, a speed up process is made to the curve evolution. After this initialization, a multiphase level set is introduced for the segmentation of different regions. Their method had proven its efficiency to extract multiple object with smooth boundaries on real and synthetic images.

Active contour model is used by (Soomro, Akram, Kim, & Choi, 2016) and (Akram, Garcia, & Puig, 2017) to inhomogeneity brain MR images. Both methods started by using an energy functional based on local and global fitted images. Moreover, both methods reclaimed that they obtained better results in use a quantitative and qualitative comparison on real and

synthetic MR images. Despite its effective performance, the active contour models can be sensitive to the initialization phase.

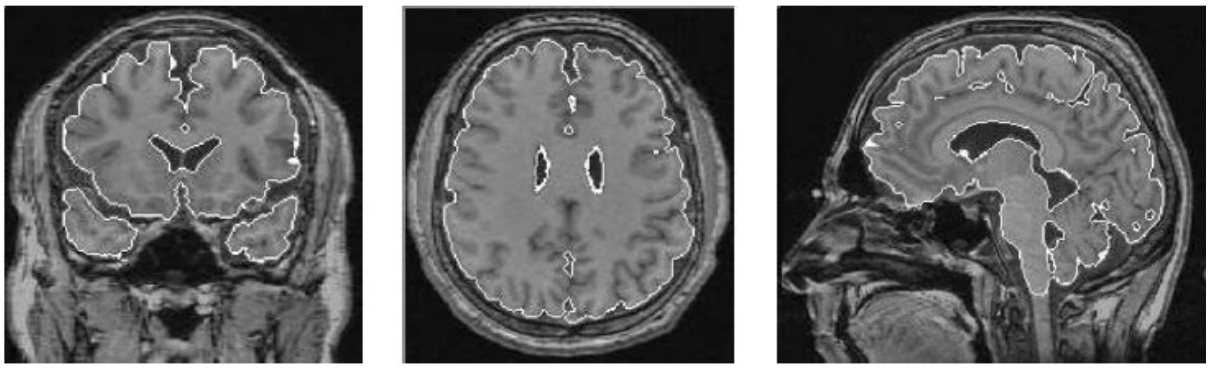

Figure 2.3 Level set segmentation (Ciofolo, 2005)

Geometric deformable models: Geometric deformable models known also as level set methods (EX: Figure 2.3). They are widely used to overcome the limitations of the parametric ones. Recently, in (Meng, Gu, Chen, & Zhang, 2017), the authors introduced a novel level set method for simultaneous brain MR image segmentation and intensity inhomogeneity correction. Their method consists of several stages, they investigated the neighbor pixel to develop anisotropic spatial information for noise reduction. Then a multivariate Student's t-distribution to fit the distribution of the intensities of each tissue is used for the energy function. Moreover, the obtained means are adapted to minimize the effect of intensity inhomogeneity. As last step, the energy function is reconstructed to be convex. The results showed that the proposed method succeeded in application on real and synthetic brain MR images.

In another attempt to use the level set for image segmentation, Pishghadam, et al. (2019) developed a novel method based level set to extract fetus brain in coronal T2-weighted images. They presented a high score based on radiologist examination and statistically experiments.

2.5 Conclusion

In this chapter, we have described the fundamental presentation of an image segmentation, in particular a brain MR image. Moreover, we have reviewed the different recent brain MRI segmentation methods. The presented review is not exhaustive but we have tried to point out the variety of the recent approaches discussed by the various authors. The purpose of the

approaches varied between different criterions such as: normal brain tissues and pathological brain tissues (tumors detection), different noise levels and MRI inhomogeneities. We have briefly attempted to highlight their strengths and their weakness.

In our thesis, we are interested in boundary-based segmentation methods. To detect edges in the hole MR image, the classical edge detectors seem to be appropriate. However, they still have challenging limitations and drawbacks depending on different variables in the MR images, such as several objects with similar intensities, noise, and MRI inhomogeneity. Overall, they are designed for the gray-level images. Our aim is to investigate the texture characteristic in brain MR images to designed an efficient edge detector for brain MRI. At first, we have designed a novel texture descriptor based local binary pattern, then, three contribution for this model are introduced in the next chapters. The following chapter presents our model QuLBP based LBP for brain MR images. In addition, our model is introduced for the first application as combination with Canny-deriche for the noise reduction in brain MR images.

Chapter 3

LBP and the proposed QuLBP model

Contents

3.1 Introduction

Texture analysis plays an important role in machine vision and image analysis. Texture can be broadly defined as an important aspect to describe the content of the image. There is no precise definition of image texture; it can consist of small elements forming an object or huge elements like the stars in the Milky Way. However, different researchers, in general, defines the texture depending upon their particular area of application. (Tuceryan & Jain, 1998). In our work, the texture is considered as the spatial variation of image pixel intensities; this definition is widely used in many machine visions tasks.

In this chapter, the objective is to define the texture taking into consideration the techniques used in medical imaging, and finally presenting the Local binary pattern (LBP). LBP is known in the literature as simple yet powerful grey scale invariant texture descriptor, which encodes the neighborhood into binary patterns. we present the LBP basics besides the different variants of LBP methods then we introduce our proposed model "QuLBP" as local descriptor and classifier for brain MR images. A second application, is to present a salt and pepper noise reduction for the canny-Deriche filter. Our QuLBP model is adjusted as enhancement procedure to reduce the noise effects for Canny-deriche edge detector.

3.2 How can we define an image texture?

The definition of word "texture" in general is difficult to precise due to its wide variability. The academic definitions of texture are often limited to particular cases; they are usually associated with specific domains of activity.

Several definitions of texture have been proposed in the computer vision literature. Some definitions are given below:

- "The notion of texture appears to depend upon three ingredients: (i) some local 'order' is repeated over a region which is large in comparison to the order's size, (ii) the order consists in the nonrandom arrangement of elementary parts, and (iii) the parts are roughly uniform entities having approximately the same dimensions everywhere within the textured region" (Hawkins J.K, 1970).

- "Texture is defined for the purposes as an attribute of a field having no components that appear enumerable. The phase relations between the

components are thus not apparent. Nor should the field contain an obvious gradient. The intent of this definition is to direct the attention of the observer to the global properties of the display i.e., its overall "coarseness," "bumpiness," or "fineness." Physically, non-enumerable (aperiodic) patterns are generated by stochastic as opposed to deterministic processes. Perceptually, however, the set of all patterns without obvious enumerable components will include many deterministic (and even periodic) textures" (Richards & Polit, 1974).

- "A region in an image has a constant texture if a set of local statistics or other local properties of the picture function are constant, slowly varying, or approximately periodic" (Sklansky, 1978).

- "We may regard texture as what constitutes a macroscopic region. Its structure is simply attributed to the repetitive patterns in which elements or primitives are arranged according to a placement rule" (Tamura, Mori, & Yamawaki, 1978).

- "An image texture is described by the number and types of its (tonal) primitives and the spatial organization or layout of its (tonal) primitives. A fundamental characteristic of texture: it cannot be analyzed without a frame of reference of tonal primitive being stated or implied. For any smooth gray-tone surface, there exists a scale such that when the surface is examined, it has no texture. Then as resolution increases, it takes on a fine texture and then a coarse texture" (Haralick, 1979).

A large part of the algorithms of artificial or industrial vision is a continuation of attempts to overcome the inability of the human visual system to discriminate certain patterns textured. A number of studies have been carried out to highlight the perception of texture by the human eye. Examples include psychovisual experiences from Julesz, he has established reliable data on the performance of the human vision to discriminate certain categories of texture. These studies on perception in the context of texture discrimination, have been based on the statistic's spatial gray levels of the image. Julesz defined the concepts of spatial statistics as follows:

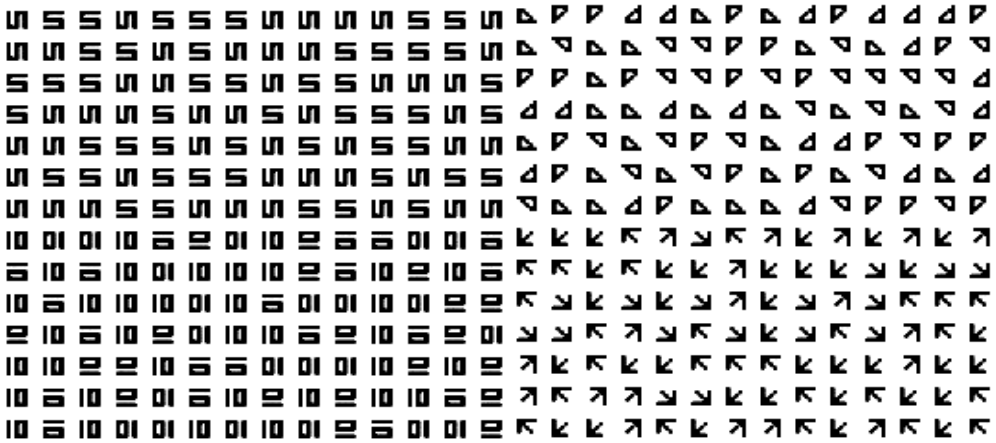

Figure 3.1 Two types of textures

3.2.1 Texture analysis applications in the medical imaging

Several texture analysis operators for extracting texture features are described in the litterature. In (Massich, et al., 2014) the self-invariant feature transform (SIFT) with low-level and high-level descriptors is used to differentiate the tissues present in breast images, a Gaussian Markov random field has also been used for texture recognition (Krishnamachari & Chellapa, 1997) and the Gabor filtering method (Manjunath & Ma, 1996)has shown good results in comparative studies of texture analysis. In addition, Ojala et al. (1996) have developed a robust, fast, and simple texture analysis operator to meet the requirements of real-world applications extracting texture features are described.

In (Massich, et al., 2014) the self-invariant feature transform (SIFT) with low-level and high-level descriptors is used to differentiate the tissues present in breast images, a Gaussian Markov random field has also been used for texture recognition (Krishnamachari & Chellapa, 1997) and the Gabor filtering method (Manjunath & Ma, 1996)has shown good results in comparative studies of texture analysis. In addition, Ojala et al. (1996) have developed a robust, fast, and simple texture analysis operator to meet the requirements of real-world applications.

Liu et al. (2017) presented an application of texture analysis based on apparent diffusion coefficient maps to discriminate different stages of rectal cancer and nodal status.

3.3 LBP and the proposed QuLBP model

3.3.1 Local Binary Pattern (LBP)

The LBP is a local texture descriptor for an image divided into overlapping windows of 3x3 blocks of pixels, as shown in Figure 3.2. Computation of the original LBP is simple and fast. It is obtained by thresholding the pixel values in the neighborhood with the center pixel. If a neighborhood pixel value is not less than the value of the central pixel, the result will be set to one. Otherwise, it is set to zero. Then the results are multiplied by weights given by powers of two, and these are summed up together, resulting in the LBP code for each pixel (see Figure 3.3) as follows:

$$\boldsymbol{LBP_{N,R}\left(i_c, j_c\right) = \sum_{n=0}^{N-1} s(gv_n - gv_c)^{2^n}} \tag{3.1}$$

Where

$$\boldsymbol{s(gv_n - gv_c) = \begin{cases} 1, if\ gv_n - gv_c \geq 0 \\ 0, if\ gv_n - gv_c < 0 \end{cases}} \tag{3.2}$$

gv_n and gv_c are the gray values of the nth neighbor and the central pixel, respectively. The LBP is characterized by two parameters; N and R, where N is the number of neighborhood pixels and R is the radius of the LBP operator (see Figure 3.4).

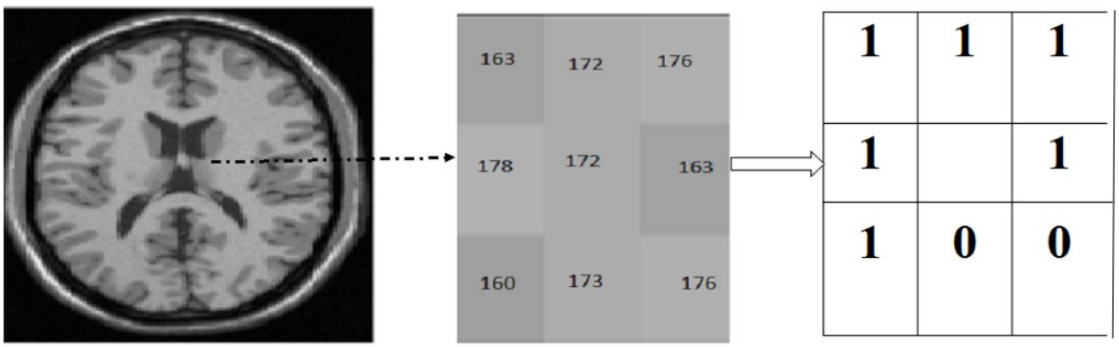

Figure 3.2 LBP model for a 3x3 window taken from the T1 MRI white matter region

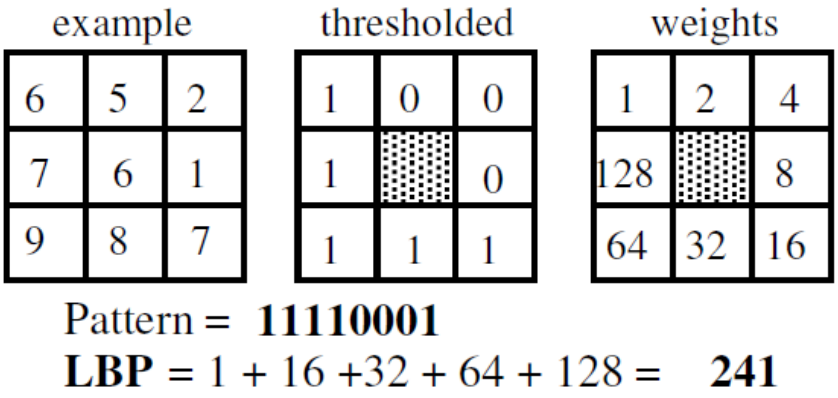

Figure 3.3 Calculating the original LBP

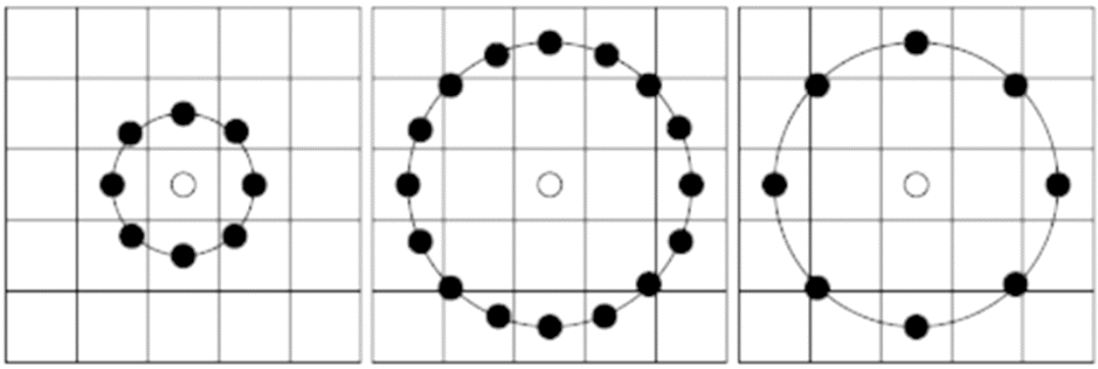

Figure 3.4 The circular (8, 1), (16, 2) and (8, 2) neighborhoods

3.3.2 LBP variants in medical imaging

Many variants of the local binary pattern (LBP) procedure are proposed in the literature. These methods have covered several tasks for medical image analysis and the list is continuously updating.

In (Oliver, Lladó, Freixenet, & Martí, 2007) the authors used another efficient and effective LBP-based model to describe the salient mass micro-patterns in mammographic images in order to reduce false positives; in this model, a support vector machine (SVM) was used to classify the detected masses.

Lakovidis et al. (2008) combined fuzzy logic and the LBP, which proved to be a good, effi0cient combination for ultrasound texture extraction. They used the Fuzzy LBP (FLBP)

approach for supervised classification of nodular and normal samples from thyroid ultrasound images.

Sørensen et al. (2008) use local binary patterns (LBPs) as texture descriptors in a classification framework to classify the different patterns of texture in pulmonary computed tomography. The proposed method was evaluated on a set of 168 regions of interest (ROI) including a normal fabric and different patterns of emphysema. The classification was carried out using the classifier of the k-nearest neighbor (k-NN) with the similarity of histograms as a distance measure.

Ghose et al. (2011) proposed a segmentation method for prostate images that used the LBP to propagate their Active Appearance Model (AAM) and provided an enhancement of texture features for its training. Their approach was validated on a transrectal ultrasound (TRUS), and it showed good results in the presence of intensity heterogeneities and imaging artifacts as well as computationally efficient performance.

Mishra et al (2011). have described a new 3D descriptor of local binary patterns (3DLBP) which seems to be particularly suitable for comparing the evolution of local patterns of 3D bone in longitudinal studies. This new variant of LBP was used to the assessment of bone strength in a condition such as osteoporosis. The results showed that 3DLBP descriptors are useful for comparing changes in structure Local 3D that may occur during the bone loss.

Recently, Subramoniam et al (2013). used the LBP technique for classification of knee arthritis on radiographic images using two classifiers, k-NN and Bayesian. The results showed that the k-NN classifier is more efficient compared to Bayesian.

In (Nosaka & Fukui, 2014) the authors proposed a novel method for classifying six categories of patterns of fluorescence staining of a HEp-2 cell. The proposed method is constructed as a combination of the powerful rotation invariant co-occurrence among adjacent local binary pattern (RIC-LBP) image feature and a linear support vector machine (SVM). RIC-LBP provides high descriptive ability and robustness against local rotations of an input cell image. To further deal with global rotation, we synthesize many training images by rotating the original training images and constructing the SVM using both the original and synthesized images. The proposed method has the following advantages: (1) robustness against uniform changes in intensity of an input cell image, (2) invariance under local and

global rotation of the image, (3) low computational cost, and (4) easy implementation. The proposed method was demonstrated to be effective through evaluation experiments using the MIVIA HEp-2 images dataset and comparison with typical state-of-the-art methods.

Rampun et al. (2018) proposed a variant of LBP called Local Quinary Patterns (LQP) for breast density classification in mammograms. The proposed operator is used to detect the characteristics of the fibro-glandular disk region (FGDroi) texture. A good performance was presented by the LQP in the comparison with different methods. Another LBP variant was presented by Galshetwar et al. (2018). A multi-dimensional multi-directional approach is designed as descriptor for the relationship of neighbor pixels in adjacent planes of a multi-dimensional in bio-medical images. The three stages algorithms showed good results against conventional LBP and recent variants of LBP.

3.4 Contribution 1

3.4.1 QuLBP based framework

Brain MR Images differ from other types of images in the number of textures that are presented. There are four basic textures: white matter, gray matter, spinal fluid in the background, and, in some pathological images, the texture of the pathologies. The textures of the same tissue may vary, producing an intensity inhomogeneity. Spatial intensity inhomogeneity induced by the radio-frequency (RF) in MR images is known to systematically appear by modifying local characteristics of tissues. The advantage of the LBP feature is that it is very fast to calculate, and is invariant to monotonic illumination changes Intensity. However, it failed to overcome the inhomogeneity in its calculation.

For further explanation, in (Figure 3.5), the LBP outputs are 1 or 0. However, since the window is taken from the same region of different tissues in 0% RF MR image, all outputs of same region should be 1. These different intensities level variations caused by the inhomogeneity of MR images and the . As noticed, the conventional LBP failed to overcome this problem.

Based on this concept, the QuLBP is a local classifier for a 3x3 window that preserves the simplicity of the original LBP with number of neighbors N=8 and radius R=1.

To reach this goal, a quantum mechanical system model is incorporated, that of the quantum bit, to generate a probabilistic numerical output as the unit state instead of the strict binary presentation in the LBP.

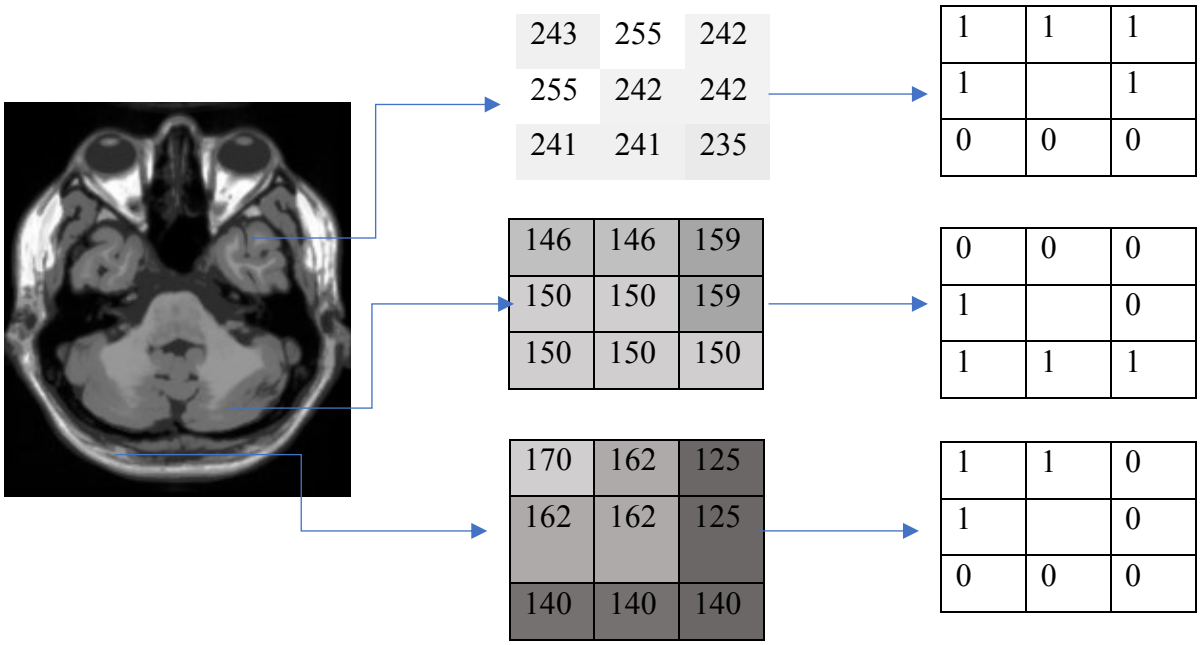

Figure 3.5 LBP for different 3x3 windows taken from different regions in 0% RF MR image

3.4.1.1 Incorporation of Quantum Information

Quantum information uses the specificities of quantum mechanics for manipulating information. According to Narayanan (1999), Narayanan and Menneer (2000) computational methods can use quantum-computing resources to obtain good performance. In quantum computing, the qubit is used instead of the classical bit to quantify information. The Bloch sphere qubit, represented in (Figure 3.6), can be found in quantum system states 0 and 1, denoted as |0> and |1> to differentiate these states from those of the classical bit. Unlike the classical bit, the qubit also can be found in a superposition state:

$$|\Psi \geq \alpha|0\rangle + \beta|1\rangle \tag{3.3}$$

Such that

$$\alpha^2 + \beta^2 = 1 \tag{3.4}$$

Where α and β are equivalent to cos θ and sin θ, respectively, for a quantum angle θ that satisfies the fundamental probability:

$$|\cos(\theta)|^2 + |\sin(\theta)|^2 = 1 \tag{3.5}$$

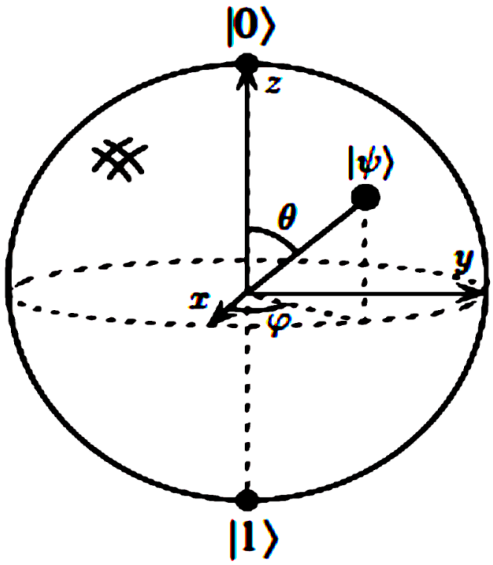

Figure 3.6 Representation of the Bloch sphere for a qubit

Quantum information has been integrated as a mathematical concept with the LBP. The qubit can take an infinite number of states according to the superposition of the quantum system (Eq. 3.6); the probability function has been used to force these and obtain a qubit value (|0> or| 1>).

Incorporating this concept in the LBP, the QuLBP is modeled as follows:

$$Q(p,h) = \begin{cases} |1>, if\ \sin(\varphi) \geq \cos(\varphi)\ \text{and}\ \varphi > 0 \\ |0> \quad otherwise \end{cases} \tag{3.6}$$

φ is the similarity angle between the central pixel gv_c and its neighbor gv_n and represents a local relationship between the two pixels. φ is measured as follows:

$$\varphi = (1-|\ p-h|/\ T) * \frac{\pi}{2} \tag{3.7}$$

Cos and *sin* are two probability functions used to obtain |0> and |1>, respectively, where |0> means that the pixels gv_c and the pixel gv_n belong to different regions and |1> means that they belong to the same region. T is based on the difference between the highest peak and its next valley in the image histogram. The expression is multiplied by $\frac{\pi}{2}$ to return the result value an angle in the range of $[0..\frac{\pi}{2}]$.

From (Figure 3.7) it can be seen that the QuLBP classifies the 3x3 neighborhood pixels for two classes, one class with the value 1 as its central pixel and with its neighbor belonging to the same region, and one class with value 0 where the two pixels belong to different regions.

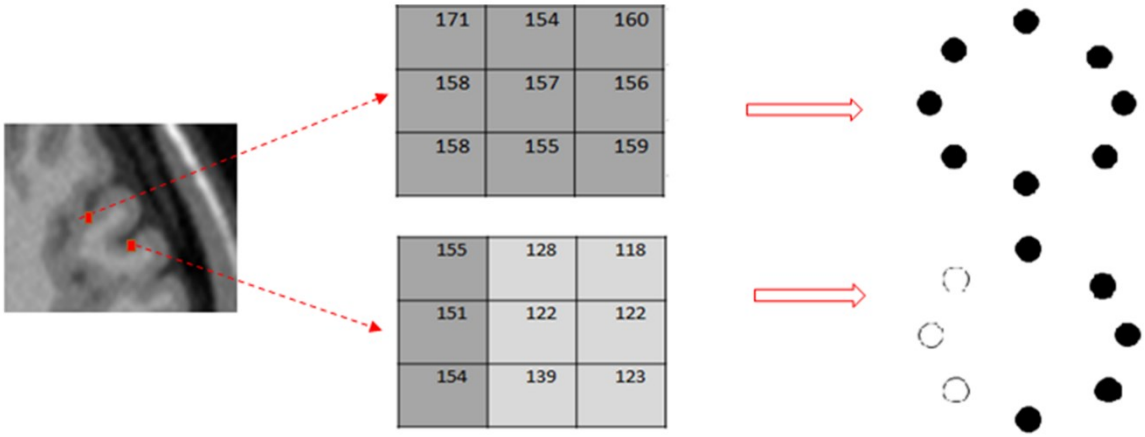

Figure 3.7 QuLBP binary patterns obtained for two image patches, the first row coming from a homogenous region and the second from an edged region

3.5 Contribution 2

3.5.1 Combination of Qulbp with Canny-deriche Edge Detection for Salt and Pepper Noise Resistance

Canny-deriche (Deriche, 1987) is an edge detection algorithm based on the Canny algorithm. Canny is known as one of the edge operators most resistant to noise in the classical methods. We have chosen this filter because it is the most effective and widely used in the literature among other classical filters.

Canny-deriche consists of four basic steps: Gaussian smoothing, gradient calculation, directional non-maximum suppression for gradient magnitudes, and hysteresis thresholding to determine edge pixels. The difference is that the Deriche smoothing filter whose derivative is the exact solution to the Canny equation is extended to infinite support filters.

$$D_\alpha = -m' \, x e^{-\alpha|x|} \tag{3.8}$$

Where m' is given as:

$$m' = -\frac{(1-e^{-\alpha})^2}{e^{-\alpha}} \tag{3.9}$$

The Canny-deriche output can be adjusted through the α scale parameter to filter out high frequency noise. Usually, the value of α is recommended to be around 1, as a small value of α (0.25 to 0.5) or a large value (around 2 to 3) will, given two choices, fail to exhibit good detection for the first or proper localization for the second. An edge detector must be precise and robust against noise and able to handle edge detection drawbacks, and although Canny-deriche is a good candidate for such tasks it still has limitations with respect to noisy images, i.e., salt and pepper.

The basic idea behind the application is to combine the QuLBP model with the Derriche algorithm as the process immediately before the Canny-deriche algorithm; this enhances the edges and presents a better localization in the presence of salt and pepper noise. The proposed algorithm is presented in figure 3.9

In Figure 3.8, it is obvious that the QuLBP preserves all edges and the obtained codes are not affected by the noisy pixels. The model also localizes the image boundaries with good performance.

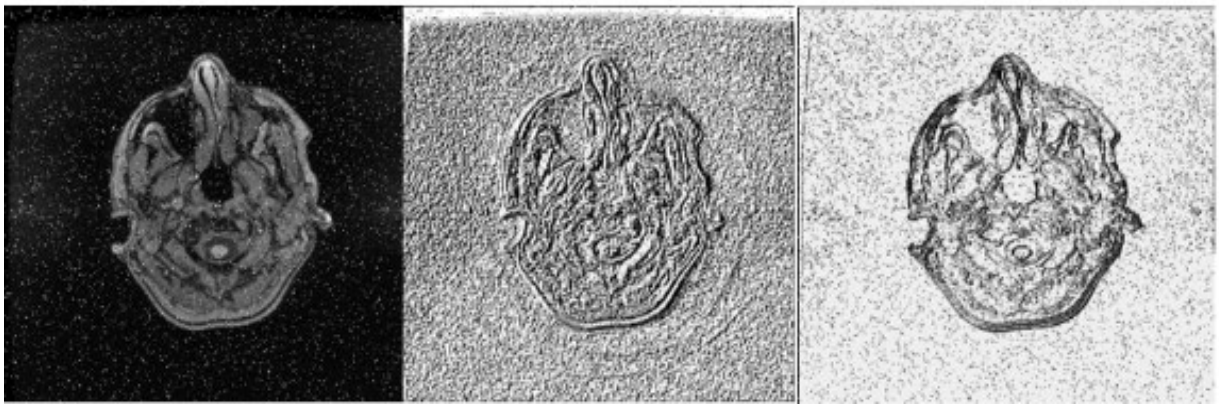

Figure 3.8 Application of LBP and QuLBP, in the 2nd and 3rd columns, to a noisy (salt and pepper) T2 weighted MR image

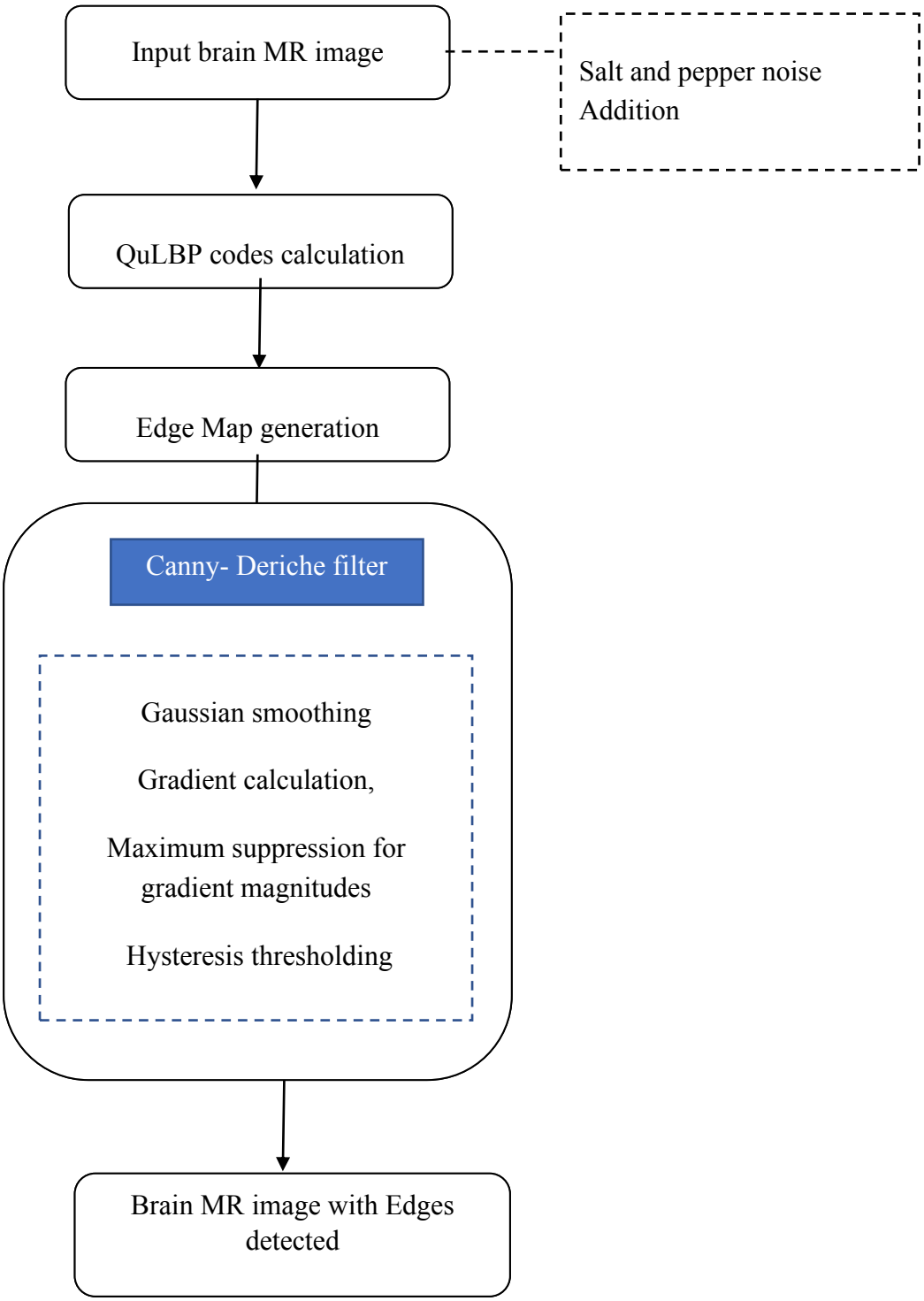

Figure 3.9 Combination of QuLBP with Canny-deriche Edge Detection for Salt and Pepper Noise Resistance

3.6 Experimental results

In order to evaluate the proposed QuLBP model, we have used 24 generated MRI volumes using the Brain web simulator (1996) MR images. We first, discuss the T Parameter as the crucial parameter that guide the performance of the QuLBP, then, an evaluation for the proposed model and the Deriche- canny filter are presented.

Note that, for the different evaluations presented in this chapter for the first application: QuLBP model, they are applied on selected patches in different predefined sizes. The specification of this model is based on the local classification concept. Thus, a local application is needed to show the performance of the proposed model.

3.6.1 T Parameter Analysis

According to the QuLBP description, T is considered as major parameter of QuLBP. It controls the performance of QuLBP as a local classifier. To adjust the threshold value T for each image in the experimental section, several patches of a (9*9) window were taken from the same region (note that there are four main regions in an MR image: white matter (WM), grey matter (GM), spinal fluid (SF), and the background (BG)) in a variety of 24 of the training MR images, including normal and noisy ones . First, the range of the T value is obtained in approximately way from the histograms; specifically, the highest peak value and the next valley. as shown in Figure 3.10, taking one image as an example, the best values of T are between 10 and 15 for normal MR images and 15 and 30 for noisy MR images.

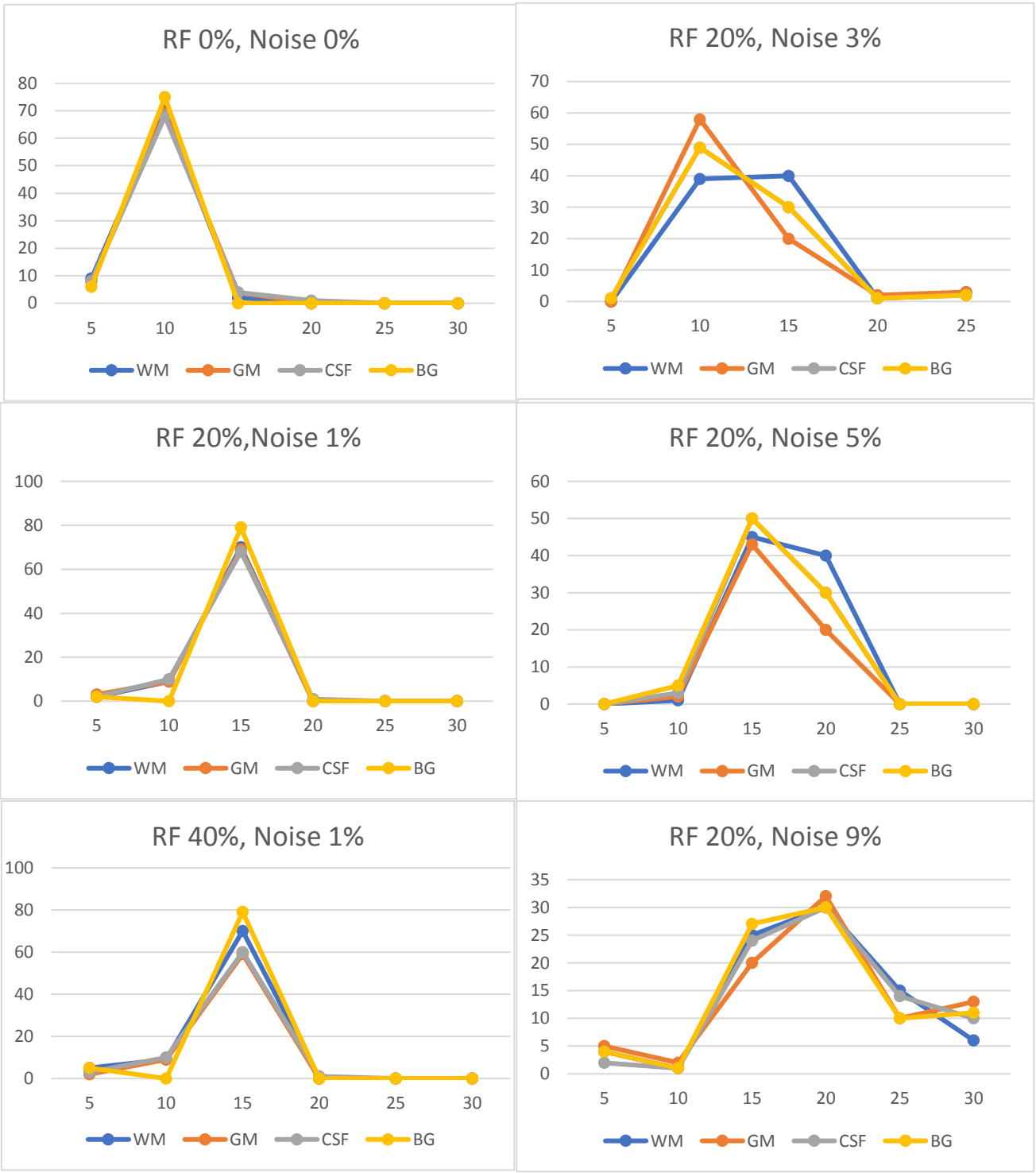

Figure 3.10 T threshold adjustment for eight patches taken from T1 MR images with different types of inhomogeneity and noise levels

3.6.2 Validation and results for QuLBP as local classifier (providing edge map)

After set up the T threshold parameter, a set of different images are tested to validate the proposed model as local classification against the conventional LBP. T1, T2 and DP synthetic MR images are available for the test purpose. Each volume of the synthetic MRI has 181 slices with 217x181 pixels with different inhomogeneity level RF (0% ,20%, 40%) and different Gaussian noise level (1% ,3% ,5%,9%).

An accuracy measurement is presented for the proposed model QuLBP in comparison with classical LBP, which is defined as:

$$Accuracy = \frac{\text{TP}}{all\ true\ pixels} \tag{3.10}$$

TP represents the true classification pixels regarding to the all true pixels. The range of the accuracy values is [**0; 1**], where Accuracy = 1 expresses the exact similarity.

To make the experiments more visible and more efficient, the selected patches for test are in (10x10) pixels for each window from the slice 88/181 in simulated MR images, keeping same patches positions for all images.

Figure 3.11 and Figure 3.12, present the results of LBP and QuLBP with three different types of real and synthetic MR images. The different four textures, GM, CSF and BG are well smoothed and clear unlike the LBP regions where we observe crowding textures especially in the background and in different pixels where the intensities variation is present. Some textures on LBP boundaries are missing and more useless ones are appeared. Not the case with the QuLBP where the boundaries are well presented and better located. It can be seen that the QuLBP algorithm plays a discriminative role between regions and boundary areas in the brain MRI image.

For further experiments validation, the results of QuLBP on different brain MR tissues (BG, WM, GM and CSF) are shown in Figure 3.13. Each texture is well presented with a unique pattern. Even the small details are presented and this example is added to more validate the QuLBP as local classifier for Brain MR textures.

For more clarification, Table 3.1 , Table 3.2 and Table 3.3 present the effect of local classification of each descriptor, where we try to cover the different variety of synthetic brain MR images. The values in bold presents the best obtained values.

The graphical interpretation for each table (Table (3.1) Table (3.2) and Table 3.3)) are given in Figures 3.14,3.15 and 3.16, respectively. The accuracy is presented for synthetic brain MR images where the range of inhomogeneity is variated between (0% ,20% and 40%) and noise level in (0%,3%, 5% and 9%).

According to results, the QuLBP is better than LBP in different image types. The proposed model has succeeded to classify the region pixels in good way and showed a good accuracy. The best obtained value is 1 in the 0% inhomogeneity and 0% of noise. However, the proposed model may lose its accuracy when the noise level and RF increase where the 40% inhomogeneity value and the noise levels (5%-9%) RF, disrupts too much the grayscale distributions.

The QuLBP model plays a significant role in discrimination between different regions in brain MR images. The textures here are considered as pixels with same characteristics (gray level value). An edge map is appeared after execution the QuLBP model with clear and precise region division. That can be clearly showed in Figure (3.11) where the different brain tissues are well presented with smooth perfect smooth regions and accurate boundaries. This model forms a good base to find the edges in previous studies in cooperation with cellular automata in section 4.

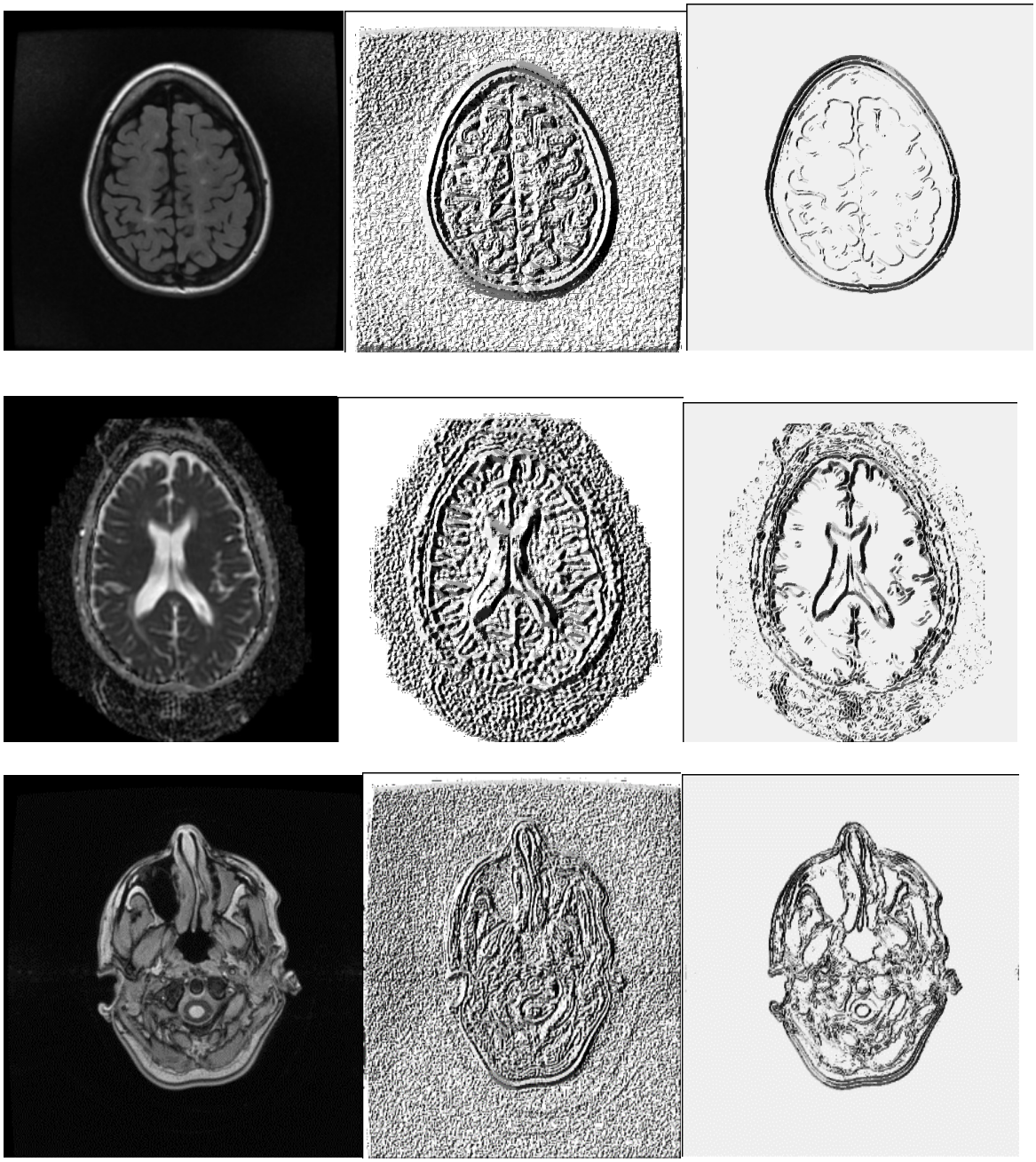

Figure 3.11 Application of LBP and QuLBP models, in 2nd and 3rd columns, respectively, to a real T1 and T2 weighted MR image

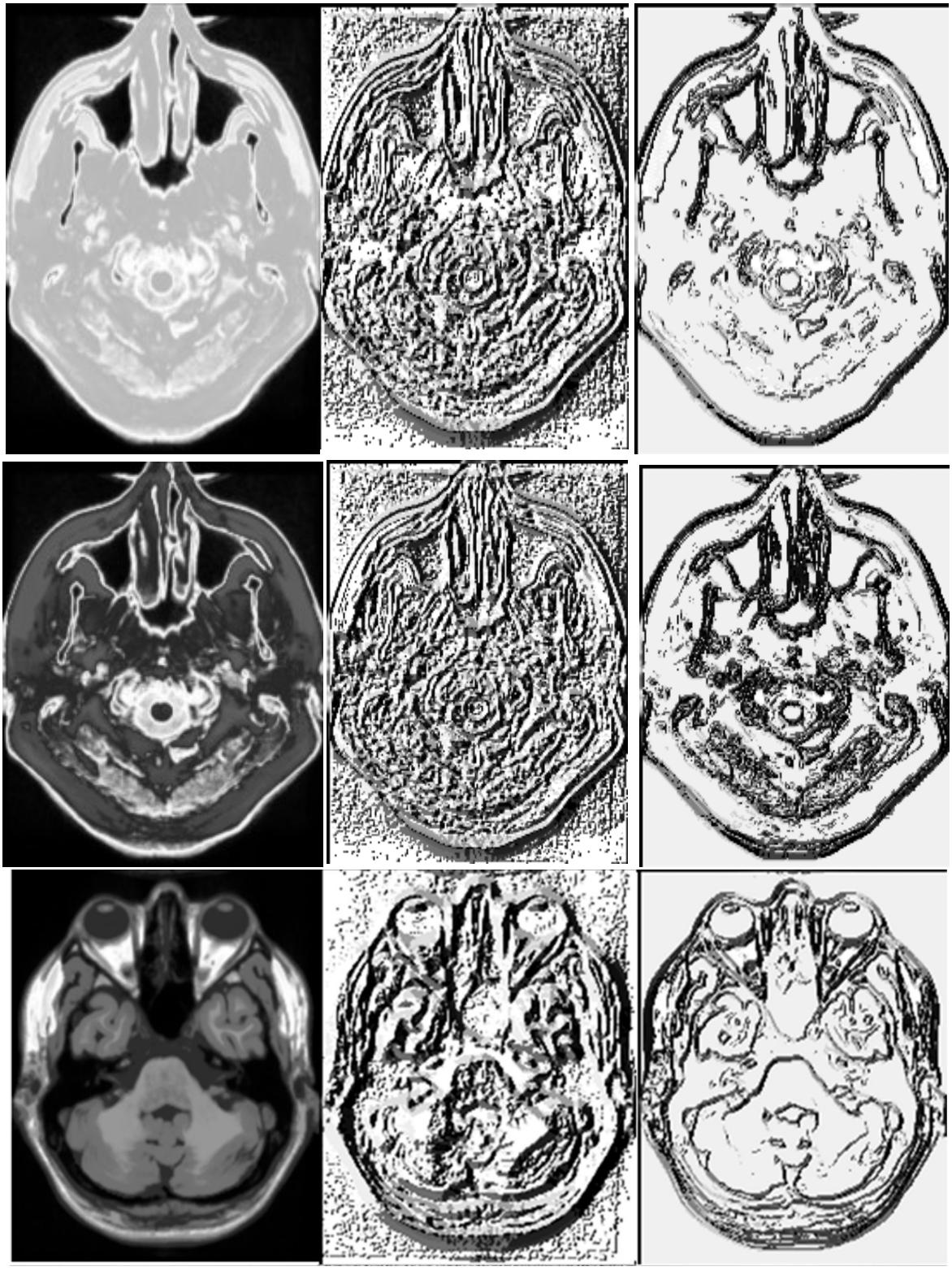

Figure 3.12 Application of LBP and QuLBP models, in 2nd and 3rd columns, respectively, to a DP weighted MR image, real T2 weighted MR image and a synthetic brain T1 weighted MR Image

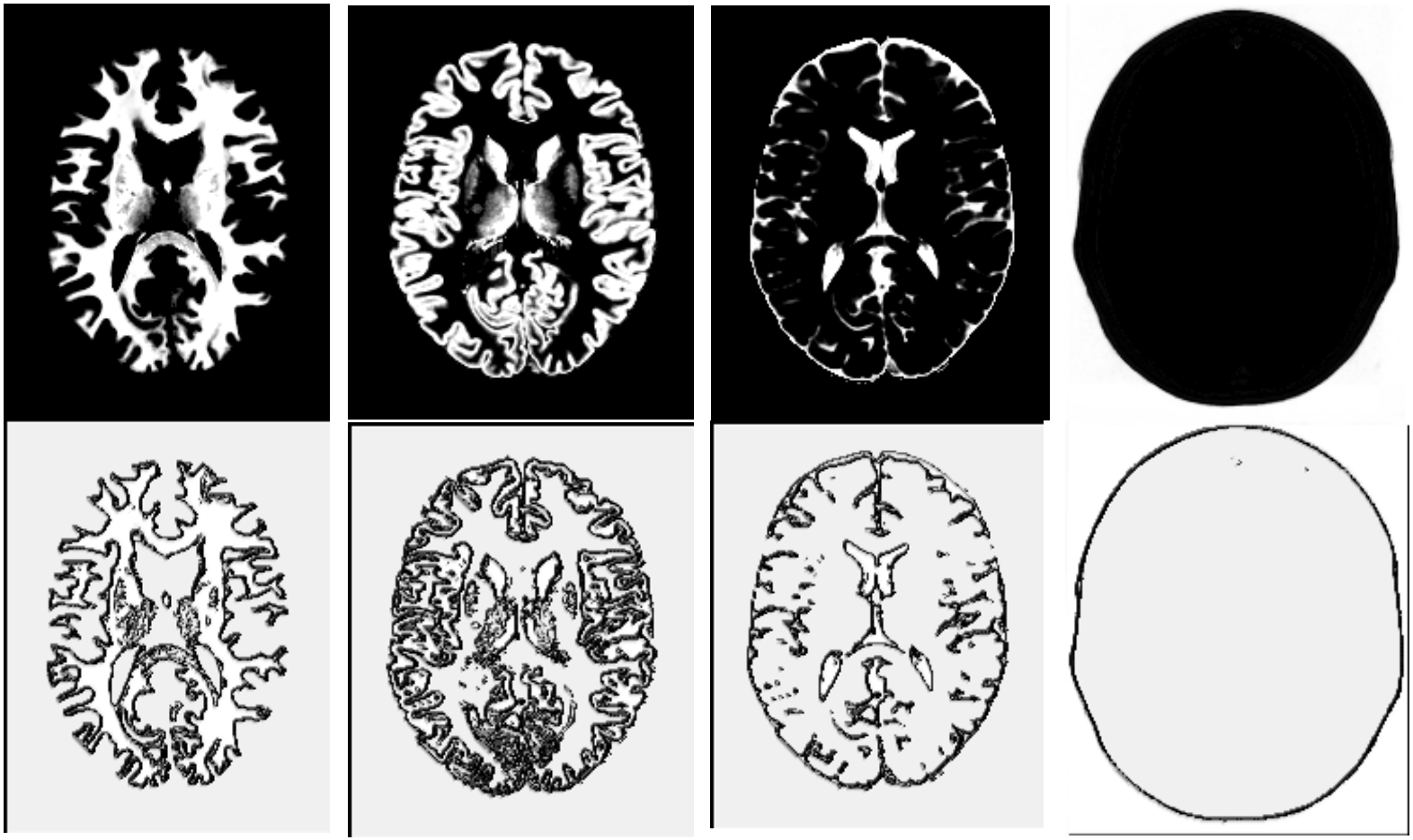

Figure 3.13 Application of QuLBP model on different brain MR different tissues: respectively, background, Cerebro spinal fluid, grey matter and white matter

Table 3.1 Accuracy Comparison between LBP and QuLBP for T1 simulated MR images

Noise		**0%**		**3%**		**5%**		**9%**	
RF		**LBP**	**QuLBP**	**LBP**	**QuLBP**	**LBP**	**QuLBP**	**LBP**	**QuLBP**
0%	**WM**	0,72	**0,97**	0,26	**0,70**	0,11	**0,54**	0,06	**0,34**
	GM	0,48	**1,00**	0,23	**0,64**	0,14	**0,52**	0,10	**0,40**
	CSF	0,49	**0,99**	0,24	**0,62**	0,15	**0,55**	0,05	**0,32**
	BG	0,53	**1,03**	0,34	**0,68**	0,18	**0,59**	0,08	**0,36**
20%	**WM**	0,55	**0,79**	0,22	**0,58**	0,06	**0,28**	0,04	**0,08**
	GM	0,58	**0,82**	0,23	**0,55**	0,05	**0,33**	0,05	**0,12**
	CSF	0,44	**0,84**	0,15	**0,52**	0,08	**0,32**	0,03	**0,13**
	BG	0,63	**0,91**	0,13	**0,58**	0,13	**0,34**	0,05	**0,14**
40%	**WM**	0,36	**0,81**	0,09	**0,50**	0,04	**0,15**	0,03	**0,05**
	GM	0,42	**0,72**	0,05	**0,46**	0,05	**0,18**	0,05	**0,06**
	CSF	0,32	**0,74**	0,12	**0,42**	0,07	**0,22**	0,03	**0,06**
	BG	0,43	**0,81**	0,13	**0,48**	0,07	**0,23**	0,04	**0,12**

Table 3.2 Accuracy Comparison between LBP and QuLBP for DP simulated MR images

Noise		**0%**		**3%**		**5%**		**9%**	
RF		**LBP**	**QuLBP**	**LBP**	**QuLBP**	**LBP**	**QuLBP**	**LBP**	**QuLBP**
0%	**WM**	0.60	**0.94**	0.23	**0.67**	0.08	**0.51**	0.03	**0.31**
	GM	0.45	**0.97**	0.20	**0.61**	0.11	**0.49**	0.07	**0.37**
	CSF	0.46	**0.96**	0.21	**0.59**	0.12	**0.52**	0.02	**0.29**
	BG	0.50	**1**	0.31	**0.65**	0.15	**0.56**	0.05	**0.33**
20%	**WM**	0.52	**0.76**	0.19	**0.55**	0.03	**0.25**	0.01	**0.05**
	GM	0.55	**0.79**	0.20	**0.52**	0.02	**0.30**	0.02	**0.09**
	CSF	0.41	**0.81**	0.12	**0.49**	0.05	**0.29**	0.00	**0.10**
	BG	0.60	**0.88**	0.10	**0.55**	0.10	**0.31**	0.02	**0.11**
40%	**WM**	0.33	**0.78**	0.06	**0.47**	0.01	**0.12**	0.00	**0.02**
	GM	0.39	**0.69**	0.02	**0.43**	0.02	**0.15**	0.02	**0.03**
	CSF	0.29	**0.71**	0.09	**0.39**	0.04	**0.19**	0.00	**0.03**
	BG	0.40	**0.78**	0.10	**0.45**	0.04	**0.20**	0.01	**0.09**

Table 3.3 Accuracy Comparison between LBP and QuLBP for T2 simulated MR images

Noise		**0%**		**3%**		**5%**		**9%**	
RF		**LBP**	**QuLBP**	**LBP**	**QuLBP**	**LBP**	**QuLBP**	**LBP**	**QuLBP**
0%	**WM**	0,74	**0,99**	0,28	**0,72**	0,13	**0,56**	0,08	**0,36**
	GM	0,50	**1,02**	0,25	**0,66**	0,16	**0,54**	0,12	**0,42**
	CSF	0,51	**1,01**	0,26	**0,64**	0,17	**0,57**	0,07	**0,34**
	BG	0,55	**1,05**	0,36	**0,70**	0,20	**0,61**	0,10	**0,38**
20%	**WM**	0,57	**0,81**	0,24	**0,60**	0,08	**0,30**	0,06	**0,10**
	GM	0,60	**0,84**	0,25	**0,57**	0,07	**0,35**	0,07	**0,14**
	CSF	0,46	**0,86**	0,17	**0,54**	0,10	**0,34**	0,05	**0,15**
	BG	0,65	**0,93**	0,15	**0,60**	0,15	**0,36**	0,07	**0,16**
40%	**WM**	0,38	**0,83**	0,11	**0,52**	0,06	**0,17**	0,05	**0,07**
	GM	0,44	**0,74**	0,07	**0,48**	0,07	**0,20**	0,07	**0,08**
	CSF	0,34	**0,76**	0,14	**0,44**	0,09	**0,24**	0,05	**0,08**
	BG	0,45	**0,83**	0,15	**0,50**	0,09	**0,25**	0,06	**0,14**

Figure 3.14 Accuracy Comparison between LBP and QuLBP for T1 RF simulated MR images

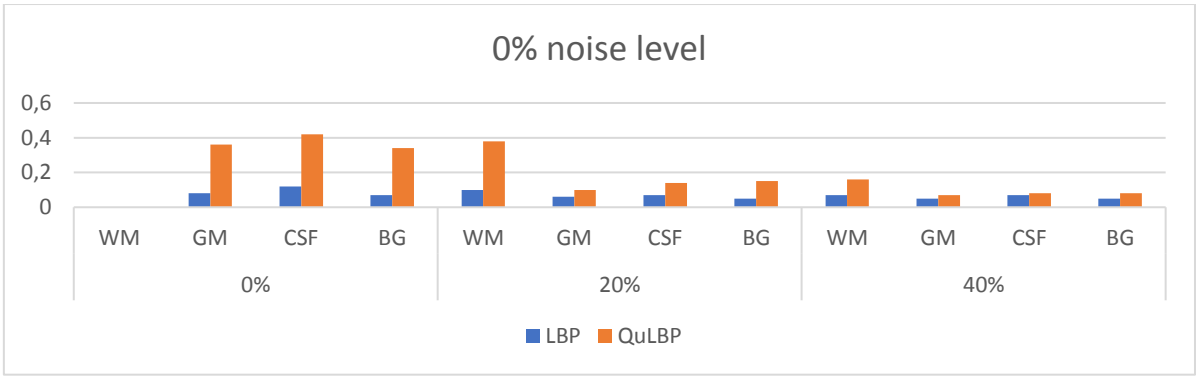

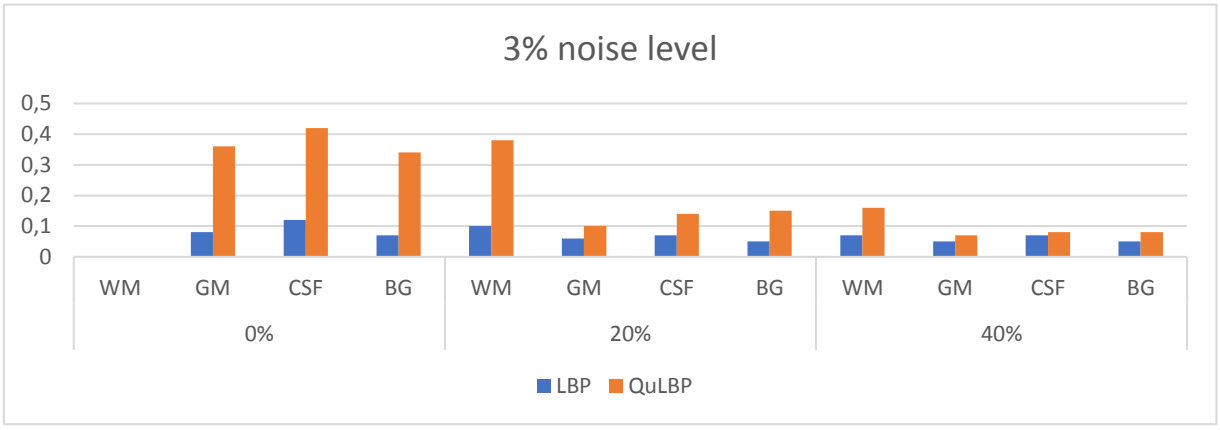

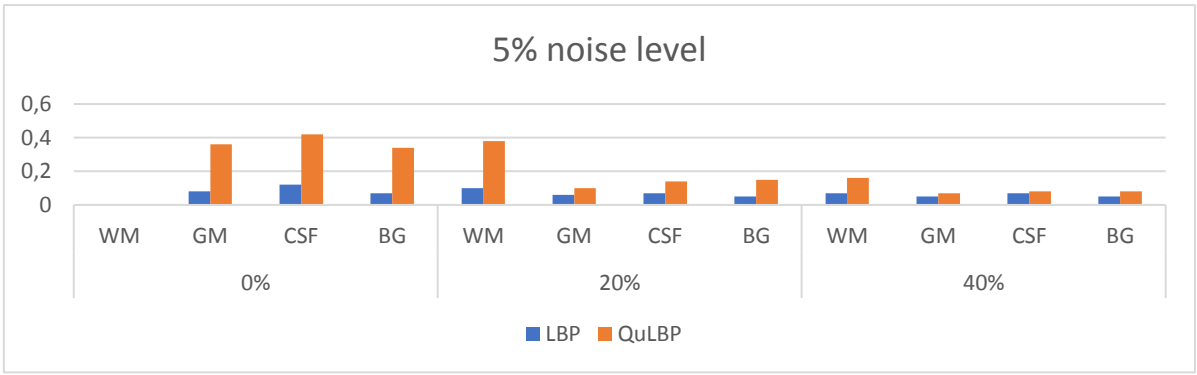

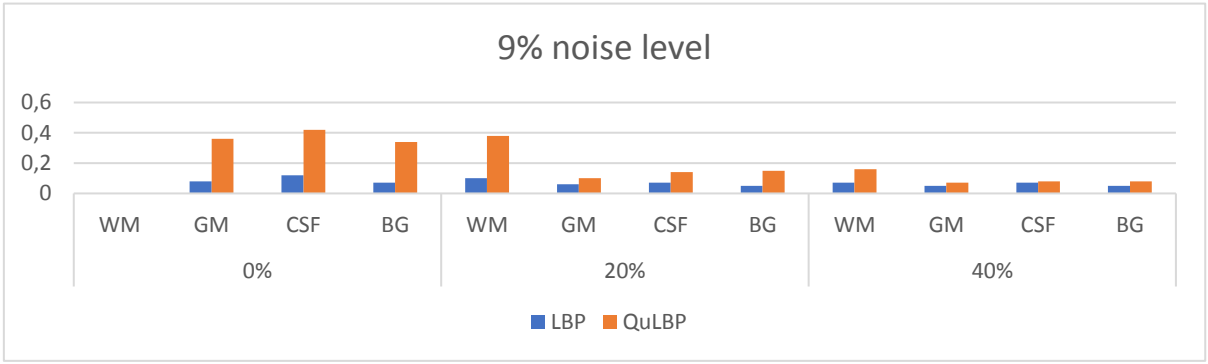

Figure 3.15 Accuracy Comparison between LBP and QuLBP for DP simulated MR images

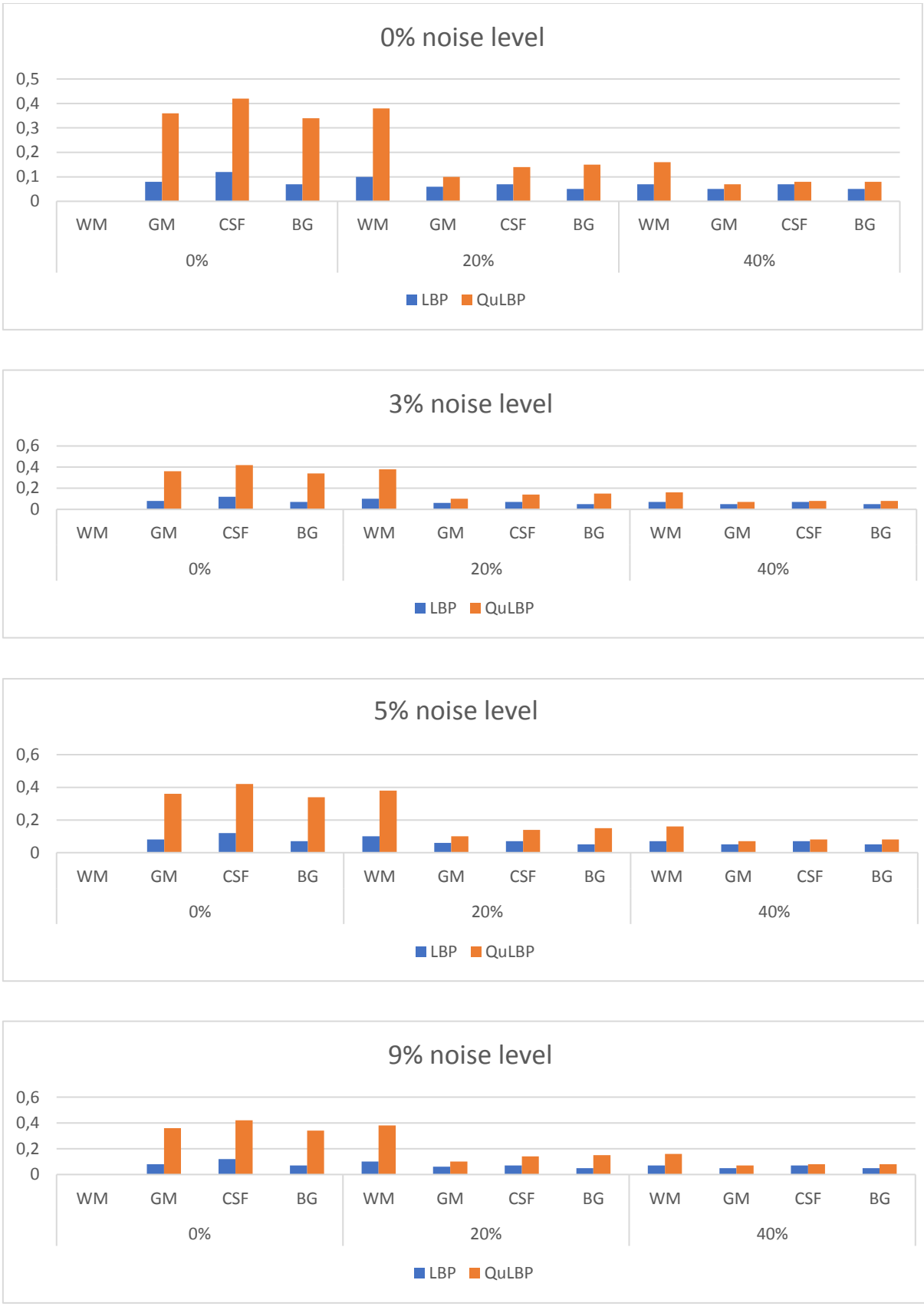

Figure 3.16 Accuracy Comparison between LBP and QuLBP for T2 simulated MR images

3.6.3 Validation and results for QuLBP for Canny-deriche

3.6.3.1 Root mean square error

The root mean square error (RMSE) is an image quality assessment metric. The RMSE calculates the root of the average difference between the original image and the edge detected image such that a lower RMSE means less error between the two images. For the original image *I* and the edge-detected image *J*, the RMSE is calculated as in Eq. (3.11):

$$\text{RMSE} = \sqrt{\frac{1}{m \text{ x } n}\sum_{i=1}^{m}\sum_{j=1}^{n}\left(I_{i,j} - J_{i,j}\right)^2} \tag{3.11}$$

where *m* and *n* are the height and width of the images, respectively.

3.6.3.2 Peak signal to noise ratio

The peak signal to noise ratio (PSNR) is the third image evaluation method the experiments used; it is usually expressed using the logarithmic decibel (dB) scale. A better-quality image is characterized by a higher PSNR ratio between the original image and the distortion signal in an image. The PSNR is calculated as follows:

$$PSNR = 10 \log\left(\frac{R^2}{MSE}\right) \tag{3.12}$$

where $R = 255$ is the maximum variation for an input image with an 8-bit grayscale and *MSE* is calculated by (3.11) regardless of the root.

3.6.3.3 Results and discussion

For the second application of the model, the same data was used as in the preceding test. However, the brain MR images with (0%,20%,40%) only considered, for the noise level we consider two levels (3%, 5%) salt and pepper noise.

The images are affected by salt and pepper noise, and for both applications α is set to 1, the two hysteresis thresholds are set to their best values with the best T parameter, and the radius R is 1.

Figures 3.17(b) ,3.18(b),3,19(b) shows the results for Canny-deriche algorithm on real, T1 synthetic (0%, 20 and 40% inhomogeneity) and T1, T2 and DP of brain MR images, respectively. Figures 3.17(c), 3.18(c), 3,19(c) shows the results for the proposed approach on real, T1 synthetic (0%, 20 and 40% inhomogeneity) and T1, T2 and PD of brain MR images, respectively. The Canny-deriche algorithm produced more noisy pixels for the real MR images and missed most of the MR images' edges, producing a false discrimination of the brain regions. The proposed approach performs better with noisy pixels and eliminates a large range of these while preserving more of the edged structures than the Canny-deriche algorithm. However, some of the edges are lost due to the strong noise.

The results in Table 3.4, Table 3.5 and Table 3.6 confirm the qualitative results for the synthetic MR images on T1, T2 and DP, salt and pepper noise (3%,5%) and intensity inhomogeneity (0%, 20% and 40%).

The application of the model to noisy images affected by salt and pepper noise preserves the boundaries of the MR images as shown previously in Figure 3.17, Figure 3.18 and Figure 3.9 and also strengthens the edge pixels. Moreover, the effect of noise is reduced, and the approach provides a different edge map for the Canny-deriche algorithm instead of the gray values of the original images, on that has less noisy pixels and stronger edge structures. In contrast, using the Canny-deriche algorithm alone, the structure of edges is disfigured due to the strong effect of the noise and a false response to these noisy pixels. It can be seen from results in tables: Tables 3.4, 3.5 and 3.6 that both the proposed approach and canny-deriche gives less accurate results due to the increasing in inhomogeneity levels (40%) and the salt and pepper noise level (5%).

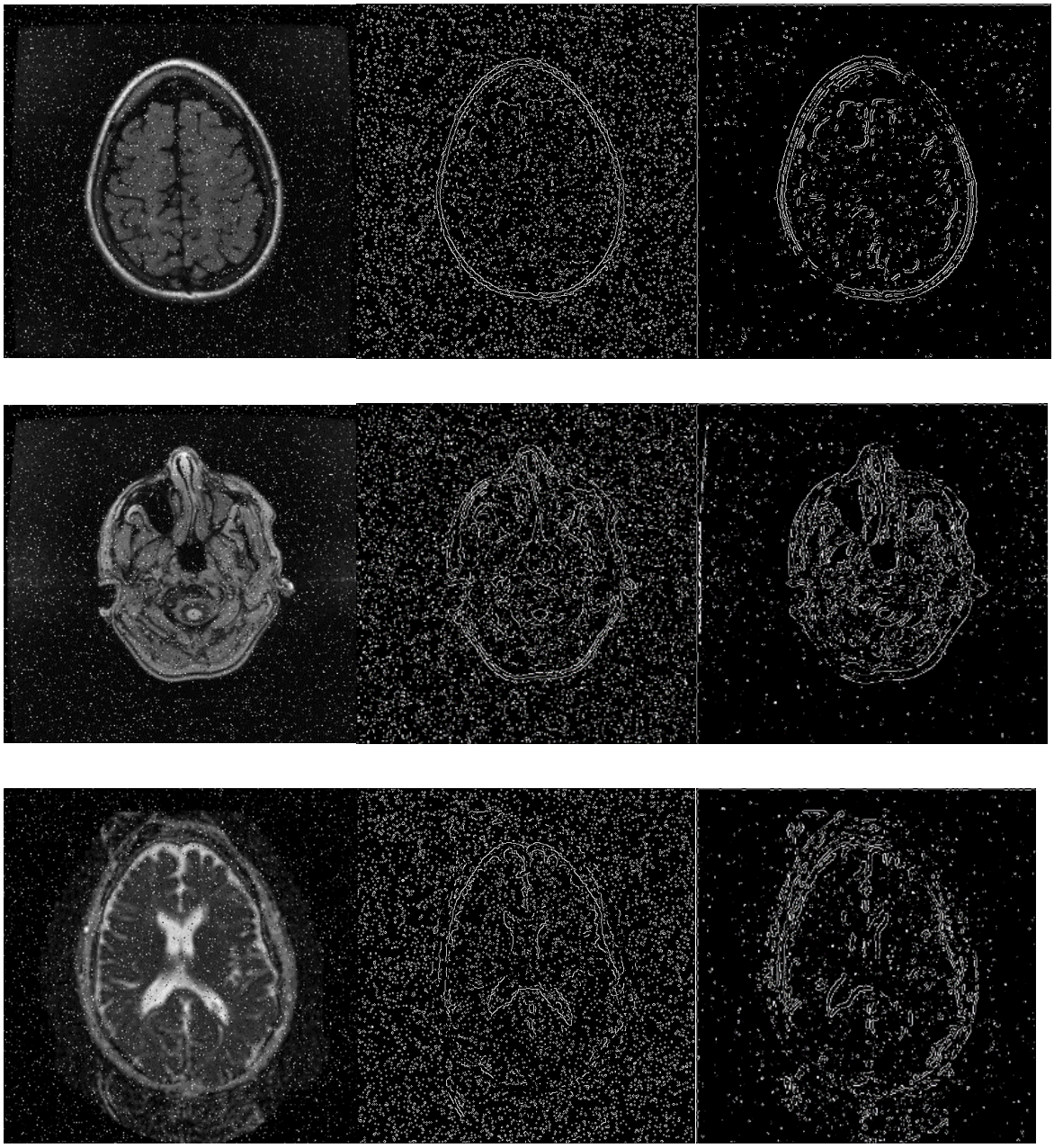

(a) (b) (c)

Figure 3.17 Edge detection of (b) Canny-deriche and (c) the proposed model on (a) real MR images affected by salt and pepper noise.

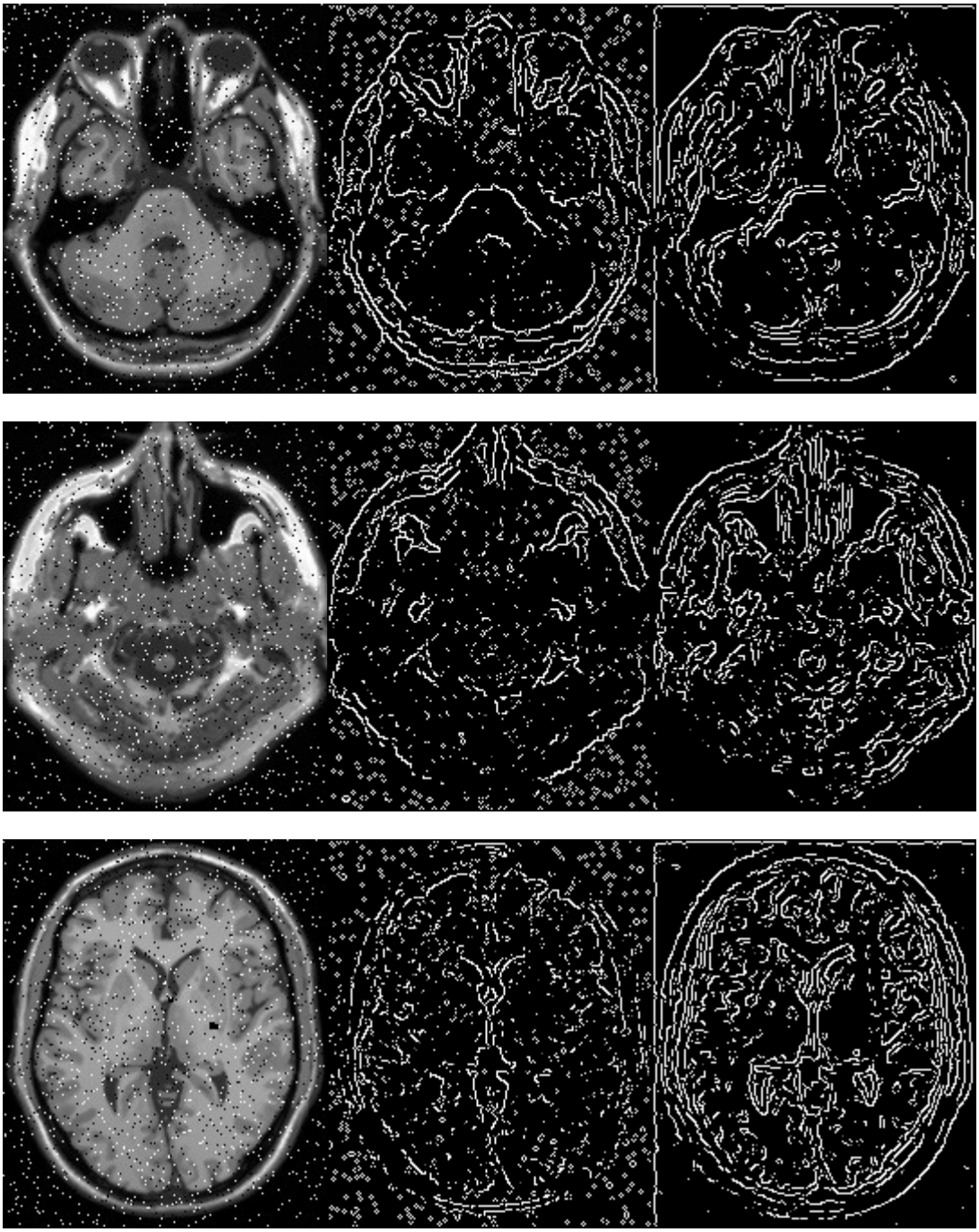

(a) (b) (c)

Figure 3.18 Edge detection of (b) Canny-deriche and (c) the proposed model on (a) synthetic T1 MR images (RF=0%,20%,40%) affected by salt and pepper noise.

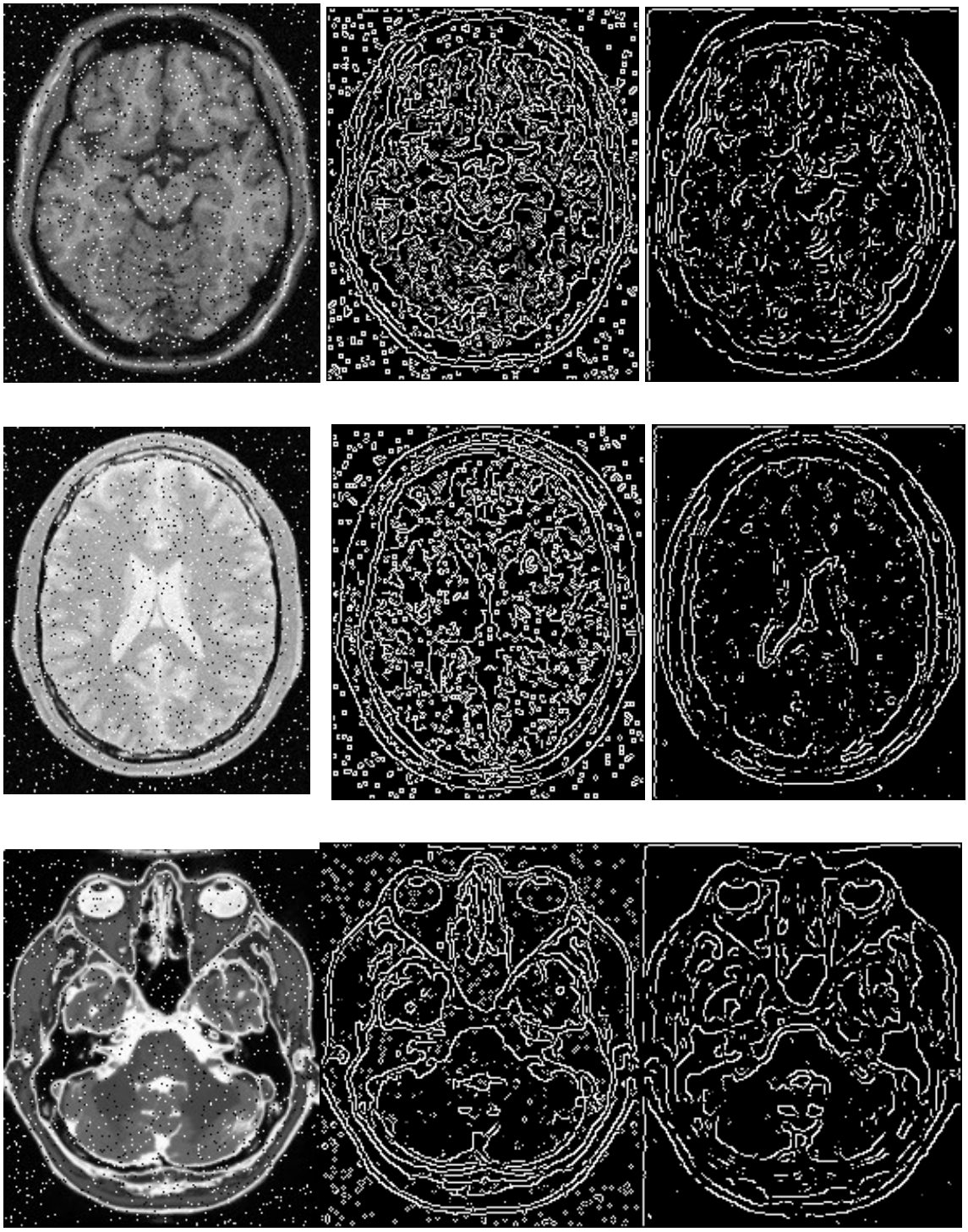

Figure 3.19 Edge detection of (b) Canny-deriche and (c) the proposed model on (a) synthetic T1, T2 and PD MR images, respectively affected by salt and pepper noise.

Table 3.4 Comparison of Canny-deriche and the proposed approach for T1 Edge detection

Noise		**3%**		**5%**	
RF		Canny-deriche	Proposed Approach	Canny-deriche	Proposed Approach
0%	**PSNR**	84,3767	**105,076**	72,9183	**91,9898**
	RMSE	16,4388	**12,2939**	17,7863	**16,4908**
20%	**PSNR**	91,0194	**115,1144**	74,0239	**115,1144**
	RMSE	14,3414	**12,2939**	19,6523	**16,3508**
40%	**PSNR**	83,7108	**91,4487**	79,2457	**79,9183**
	RMSE	18,9512	**15,7173**	19,9856	**19.0326**

Table 3.5 Comparison of Canny-deriche and the proposed approach for T2 Edge detection

Noise		**3%**		**5%**	
RF		Canny-deriche	Proposed Approach	Canny-deriche	Proposed Approach
0%	**PSNR**	80,2563	**104,0080**	69,7532	**89,0147**
	RMSE	16,9512	**12,1174**	16,9897	**15,4230**
20%	**PSNR**	98,0741	**117,6523**	73,3298	**113,**
	RMSE	14,8703	**12,7956**	20,3356	**18,3508**
40%	**PSNR**	84,2108	**89,0021**	80,8520	**81,2007**
	RMSE	18,7781	**16,0258**	18,5623	**18,1199**

Table 3.6 Comparison of Canny-deriche and the proposed approach for DP Edge detection

Noise		**3%**		**5%**	
RF		Canny-deriche	Proposed Approach	Canny-deriche	Proposed Approach
0%	**PSNR**	81,2583	**105,01**	70,7552	**90,0167**
	RMSE	17,9532	**13,1194**	17,9917	**16,425**
20%	**PSNR**	99,0761	**118,6543**	74,3318	**114,002**
	RMSE	15,8723	**13,7976**	21,3376	**19,3528**
40%	**PSNR**	85,2128	**90,0041**	81,854	**82,2027**
	RMSE	19,7801	**17,0278**	19,5643	**19,1219**

3.7 Conclusion

Local binary patterns (LBP) is a simple yet powerful grey scale invariant texture descriptor which encodes the neighborhood into binary pattern. In this chapter, we have presented the LBP method and its main variants in medical imaging tasks. These techniques are very successful for texture analysis. They show that the LBP is flexible to the need of each task and image type. There was need to deal with MR images for the edge detection task so, we introduced a new variant, called QuLBP adapted to projections of brain MRI textures, From the comparative study with the classical LBP presented in this chapter, the model successfully classifies local pixels while preserving the simplicity of the original model. Other application of QuLBP called Canny-deriche QuLBP is presented for salt and pepper noise reduction.

In next chapter, QuLBP will be investigated for the two other application of edge detection task.

Chapter 4

QuLBP based evolutionary algorithms based Cellular Automata for MRI edge detection

Contents

Introduction

The goal of this chapter is to contribute to the edge detection domain, specifically to the field of brain MR images edge detection. The application of the QuLBP model as texture descriptor for edge detection is presented.

At first, the evolutionary Cellular automata is introduced, next, the QuLBP is combined with the CA based on the uniformity concept for edge detection. Finally, the model is combined with Penguin swarm optimization (PeSOA) algorithm to train the CA rules for brain tumor edge detection on real MR images.

3.9 Cellular automata

The simplicity structure of cellular automata (CA) in modeling the complex behavior, make it more attractive to many researchers for various research area. The concept of cellular automata was introduced by (Ulam, 1972) and (Von Neumann & Burks, 1966) in the early 1950s and later by (Wolfram, 2002).

CAs are mathematical, dynamic, and discrete models that are used to investigate the behavior of compound systems. Among its advantages, each cell in a CA contains only a few simple, basic rules. The interactions of cells in a neighborhood area and their communications lead to more sophisticated emergent global behavior.

In recent years, CAs have been investigated for many image-processing applications. In (Rosin l. P., 2010), CAs were trained to deal with convex hulls, feature selection, and noise filtering. Other tasks for which they have been used include object recognition (Dyer & Rosenfeld , 1981), calculating the properties of binary regions (Hernández & Herrmann,

1996), image enhancement, smoothing, and noise filtering (Rosin P. L., 2006), and edge detection (Rosin & Sun, Edge detection using cellular automata, 2014; Slatnia, Batouche, & Melkemi, 2007).

Before introducing the CA-based edge detectors in the literature, first, we would present some definitions given in the literature for CA, then, a brief introduction is presented to the two-dimensional (2D) CA model in the next section.

Definition 1. Automaton is a self-organizing abstract machine (Wolfram, 2002)

Definition 2. Cellular automata are discrete dynamical systems, whose behaviour is completely specified in terms of a local relation. (Ewa & Jaroslaw, 2006)

Definition 3. A cellular automaton is a collection of "colored" cells on a grid of specified shape that evolves through a number of discrete time steps according to a set of rules based on the states of neighbouring cells. The rules are then applied iteratively for as many time steps as desired (Weisstein, 2015).

In a CA, space is defined as a grid of connected cells that evolve through discrete time steps according to a set of rules based on the states of neighbouring cells. More precisely, a CA can be defined as a quadruple consisting of the following:

- **The dimensions of the grid**: 1D, 2D, or 3D. —see Figure 4.1
- **A number of states**: on and off, gray level values, etc.
- **Neighborhoods**: Von Neumann and Moore neighbourhoods—see Figure 4.2 (1) and Figure 4.2(2).
- **Rules** defining the automaton and the progress of the generations at each time t+1, where the initial state is given as t=0.

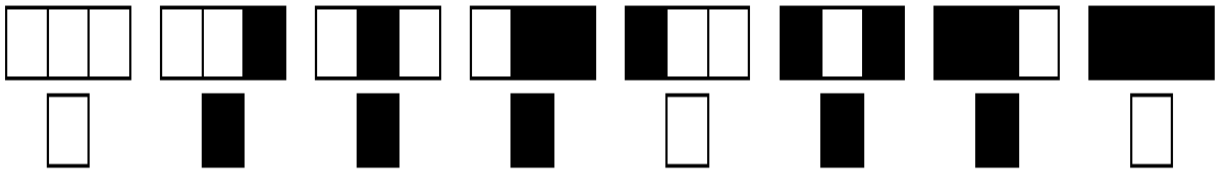

Figure 4.1 A one dimensional (1D) cellular automaton

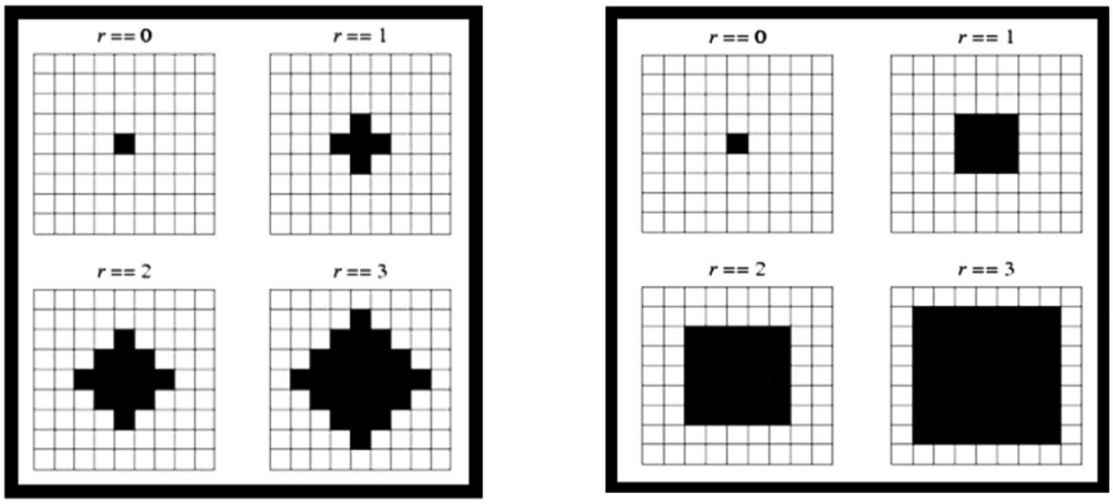

Figure 4.2 (1) Von Neumann neighborhood, (2) Moore neighborhood
Note. r denotes distance in (a) and (b).

3.9.1 Previous works for edge detection using cellular automata

The majority of earlier CA edge detectors are devoted to binary images. The target image is usually considered as cellular automaton, it is presented as a 2D grid of cells, each cell is an image pixel with binary value (0 or 1) connects to its neighboring pixels (CA state values). substantially, the edge detection depends on the transition state process from the initial image (input image pixel values) to the final states (the output image with 1 representing edge pixels and 0 the others). It is critical to find good state transition rules for the CA.

In (Wongthanavasu & Sadananda, 2003), they have designed simple CA rule for edge detection. A VonNeumann neighborhood was used for the cell state. the transition rule changed the pixel value from 1 to 0 if its neighborhood has stated the value 1, otherwise it retains its original state (1 or 0). Though its effectiveness but this model failed with noisy pixels existed in a foreground region.

Some authors have mainly been interested in investigating the genetic algorithm to find the optimal transition rules that define the input image edges in the binary images. Starting with the work of (Selvapeter & Hordijk, 2013) for noisy real image, their method consists of two steps: denoising the image by a simple CA based filter then detect the edges by trained CA rules.

In (Slatnia, Batouche, & Melkemi, 2007), they have trained a single powerful rule to treat the binary image and detect the edges using Moore neighborhood, their resulted transition rule is similar to (Wongthanavasu & Sadananda, 2003).

Another CA based genetic algorithm in the work of (Yang, Ye, & Wang, 2002), they proposed a two steps approach using both Moore and von Neumann neighborhood with one iteration transition rule at the first step and several iterations to find the edged pixels in the second step.

In view of all that has been mentioned so far, one may suppose that all the experiments were done against canny's method. Canny's algorithm is designed to deal with grey images, so this is unfair and inappropriate to present such deferential study.

In recent years, there has been an increasing amount of literature on investigating the CA for intensity images edge detection. In 2015 hasanzadh et al. published a paper in which they described their cellular edge detection (CED) algorithm. In their paper, they combined a cellular automaton and a learning cellular automaton for binary and grayscale images. Both the Moore neighborhood and von Neumann types are used.

Shahverdi et al.(2016) proposed a fuzzy cellular automata-based method for edge detection and image segmentation. Their approach had Three main steps, the first step, they designed a new edge detection method based on fuzzy cellular automata, called the *texture histogram*. In the second step, they proposed an edge detection algorithm, they used the mean values of the edge's matrix with four fuzzy rules. As third and final step, the local edge in the edge detection step is investigated to more accurately accomplish image segmentation.

Recently, Aghaei (2018) proposed an edge detection algorithm for noisy images. His approach used a four-neighborhood under Null boundary cellular automata (FNNBCA) to eliminate the noise effect in a grayscale image. Another concept is proposed in his paper using two-dimensional twenty-five neighborhoods under Null Boundary cellular automata (TFNNBCA). Good results have been showed against literature edge detectors from visual comparison aspect. However, there is no quantitative comparison for real testing.

3.10 MRI edge Detection using uniform QuLBP Cellular Automaton

3.10.1 Contribution 3

In this section, we present the application of the QuLBP model which is combined with the CA procedure for edge detection.

3.10.1.1 Defining the rule set

Edge detection algorithms are usually applied to grayscale or color images, so designing a CA to be used as a practical edge detection application may be subject to one of the disadvantages of CAs, which is that the rule set for edges should be defined by laborious hand-generation, called the inverse problem. To explain this further, consider an MR image coded in 8 bits, which ends up with 8^{256} possible rules in the case of Moore neighborhoods. To train CAs, some previous works (Mofrad, Sadeghi, Rezvanian, & Meybodi, 2015; Uguz, Sahin, & Sahin, 2015) have used evolutionary approaches to select the edges. In this work, a simple model is used to train the CA to find the edge patterns for which the LBP is suitable for a CA; both are presented by a window characterized by a number of pixels (N=8) and a radius (R=1) along with the Moore neighborhood of the CA.

After calculating the QuLBP patterns for an input brain MR image, the question is: How can the edges be defined based on the obtained QuLBP patterns. The answer to this question is given as a second major step, using the CA.

The use of the QuLBP as a local descriptor reduces the rule search space to 2^8 possible rules presented by QuLBP patterns; only 0 and 1 are needed to express the obtained patterns, instead of the gray values. The possible space of edge rules is still a very vast range to search for the appropriate rules.

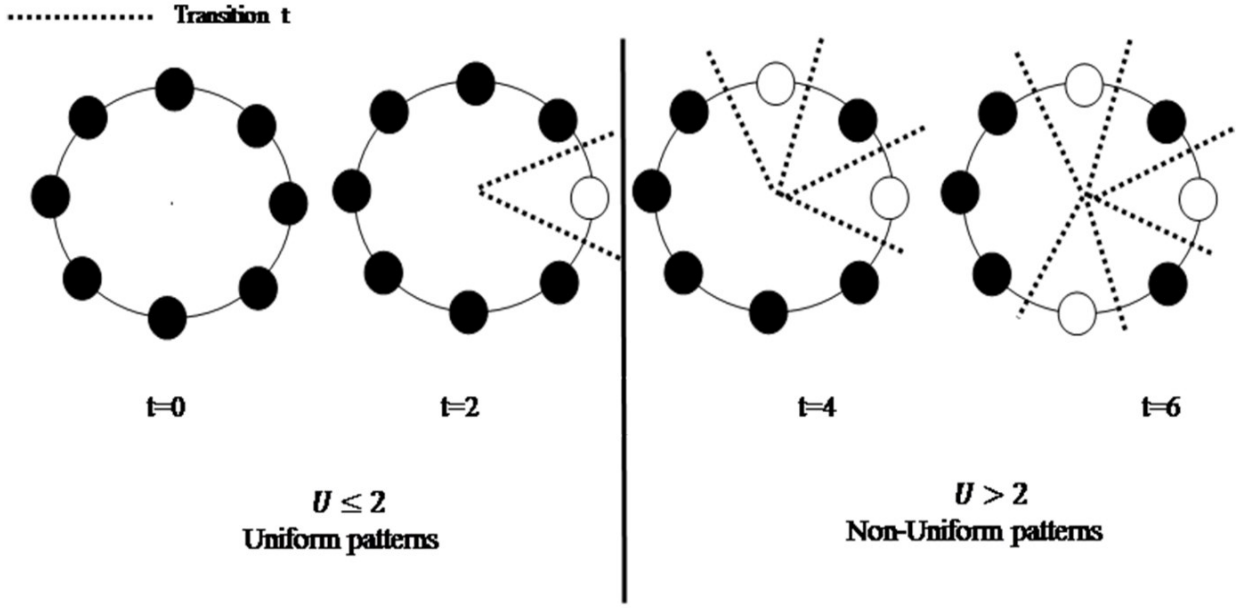

Figure 4.3 Representation of Uniform and Non-Uniform LBP patterns

In (Ojala, Pietikainen, & Maenpaa, 2002) they have worked on what they call uniform patterns. They measured a uniformity called "**U**" by the number of bitwise transitions in the LBP pattern from 0 to 1 or vice versa, see (Figure 4.3). Only ''uniform'' patterns are fundamental patterns of local image texture.

An LBP is called uniform if ***U*** is less than or equal to 2. Its uniformity measure is at most 2. The uniformity od pattern is given as follow given by:

$$\boldsymbol{U}\left(QuLBP_{N,R}\right) = |\boldsymbol{Q}(gv_{n-1}, gv_c) - \boldsymbol{Q}(gv_0, gv_c)| + \sum_{n=1}^{N-1} |Q(gv_n, gv_c) - \boldsymbol{Q}(gv_{n-1}, gv_c)| \quad (4.1)$$

Based on the uniformity concept and the number of pixels with the value 1, as shown in (Figure 4.4), it has been empirically defined, with a limited number of tests, the possible patterns that represent the QuLBP edge patterns. Just the Uniform patterns are considered for this approach since the QuLBP model expressed well the MRI textures and separated the brain structures.

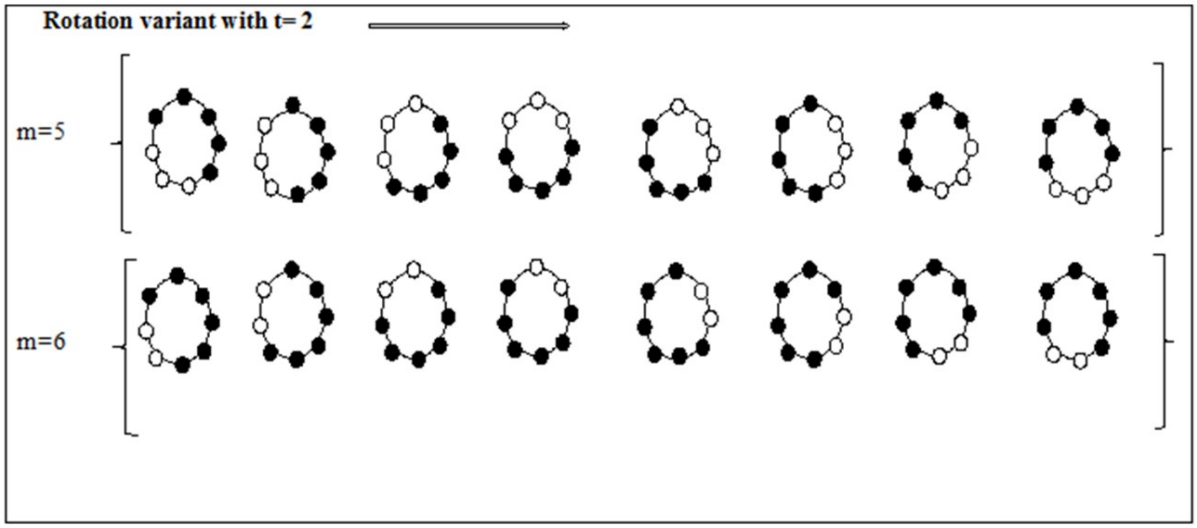

Figure 4.4 Representation of the obtained QuLBP edge patterns

3.10.1.2 The pseudocode for the approach

The CA edge detection algorithm is based on five main steps, as presented in Figure 4.5.

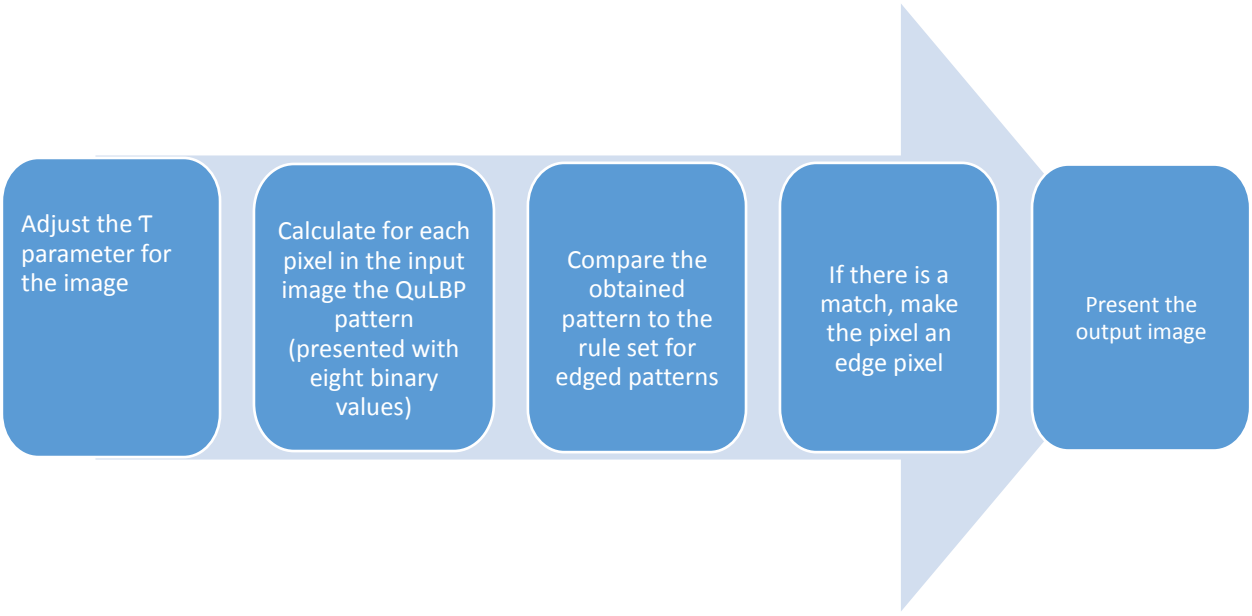

Figure 4.5 The pseudocode for the approach

3.11 Brain tumor edge detection using QuLBP Penguin Search Optimization Algorithm (QULBP-PeSOA) combined with Cellular Automata

In order to investigate other QuLBP-CA rules to detect edges in brain MR images, Penguin Search optimization algorithm (PeSOA) is used. In this section, we present a new method to detect edges in brain MR images based on CA and QuLBP model. All rules set of proposed QuLBP-PeSOA technique are investigated by using PeSOA in order to improve the performance of the brain tumor MRI edge detection. We present for this approach two phases. The first one is training the CA by PeSOA to obtain the edges rules, then, the second one is to applicate these obtained rules to find the edges. At first, we review the recent works that involve the evolutionary algorithms to train the CA for edge detection task. The rest of this section, presents the general definition of PeSOA, and the proposed approach.

3.11.1 Evolutionary algorithms combined with Cellular automata for edge detection

Evolutionary algorithms are bioinspired heuristic-based approach. Generally, their concept is to solve difficult problems, such as classically NP-Hard problems, and the applications that would take long and expensive process.

There were efficient metaheuristic algorithms that proposed in the literature to solve various problems. In this section, we are interested in evolutionary algorithms that presented in combination with CA to detect edges in images, note that CA is also an evolutionary algorithm.

One of the first attempts to combine genetic algorithm with CA for edge detection was described by (Sahota, Daemi, & Elliman, 1994), They involved genetic algorithm with CA to detect edges for binary images. Three simple edge presented for the trainig phase,then , the concluded edges are used for the edge detetcion process. No details are given about the btained rules which make the process a little bit ambiguous.

Also, Batouche et al. (2006) adopted genetic algorithm with CA to detect edges for binary images. The genetic algorithm revealed a simple rule to detect edges. The obtained edge map for each image succeded to locate the different edges. However, the presented edges are thick

.

An Ant colony optimization process is presented in (Etemad & White, 2011). The proposed approach succeeded to extract image features for edge detection task.

Djemame and Batouche (2012) have proposed a combination of particle swarm optimization algorithm (PSO) with CA to detect edge in binary and gray level images. They train 1024 totalistic CA rules. These rules are obtained by evolutionary process based PSO. Three best rules are selected and they showed acceptable results.

In (Sahin, Sahin, & Uguz, 2013) ,the authors presented two dimensional linear cellular automata (CA) rules. The CA rules are defined with the help of fuzzy heuristic membership function optimized with the PSO algorithm. The results showed good performance.

3.11.2 The Penguin Swarm Optimization Algorithm (PeSOA)

Penguin Search optimization algorithm is a new evolutionary algorithm introduced by Gheraibia and Moussaoui (2013). The PeSOA is an optimization nonlinear method inspired by the hunting strategy of penguins.

Although PeSOA is recent algorithm, it succeeded in attracting researchers in various domains. MZILI et al. (2015) have presented a discrete PeSOA to solve the travelling salesman problem. In (Gheraibia, Moussaoui, Djenouri, Kabir, & Yin, 2016), the PeSOA is investigated for association rules mining. Guendouz et al. (2018) have introduced a community detection in complex networks using Penguin swarm optimization algorithm .A modified PeSOA is presented by Mansouri et al. (2018) in order to applicate it in optimal operation of reservoir systems field.

PeSOA is based on the collaboration of penguins for hunting and finding the best position of food. Each penguin presents a possible solution by its position and the amount quantity of eaten fish. These penguins are divided into a set of groups. They are connected to each other by sharing after each dive the position of the eaten fish. The time consuming of each dive is depended on oxygen reserve.

Penguins of one or more groups that have some food follow after a number of dives penguins that hunt the biggest quantity of fish.

In this process the penguins out for the good of all groups and start searching in a specific environment based on the likelihood of food sectors, accordingly, in each cycle the position of the penguin with each new solution is adjusted using the following equation

$$X_{new} = D_{id} + \text{rand}\,() \left| X_{best} - X_{id} \right| \quad (4.2)$$

Where: rand () is a random number for distribution in the range of [0,1], D_{id} is the last best solution accord for this penguin, X_{best} is the best solution in the population, X_{id} is the current solution. The calculations in update solution equation are repeated for every penguin in each group, and after defined number of dives penguins communicate to each other the best solution represented by number of fishes consumed.

The pseudo code of the PeSOA is as follows:

Generate random population of P solutions (penguins) in groups;
Distribute penguins on groups (holes and levels)
For *i* = 1 to number of generations;
For each individual *i* to *P* do
While oxygen reserves are not depleted do

- Take a random step.
- Improve the penguin position using Equation (4.2)
- Update quantities of eaten fish for this penguin.

End While
End For

- Update quantities of eaten fish in the holes, levels, and the best group;
- Redistributes the probabilities of penguins in holes and levels (these probabilities are calculated based on the number of fishes eaten);
- Update best-solution.

End

3.11.3 Contribution 4

In this section, we present the proposed algorithm QuLBP-PeSOA which combines QuLBP model, PeSOA and CA to detect edges in MR images. The main steps to be addressed in applying QuLBP-PeSOA algorithm are selecting an appropriate solution representation (encoding), an adequate evaluation function (fitness function) and amelioration of this solution. We start by presenting the encoding schema, then, the pseudo-code of the proposed algorithm is given.

3.11.3.1 Penguin solution encoding

The choice of a representation for individuals is a very important and a crucial issue in evolutionary algorithms. We choose QuLBP model to encode the penguin solution in this algorithm. From section 4.1.1, QuLBP can provide two presentations: binary and integer encodings. In QuLBP binary encoding, each solution is represented by a vector *v* of *8* elements. However, in integer encoding, the solution is represented by an integer *n* in [0,255]. An illustrative example for both presentations is given in Figure 4.6.

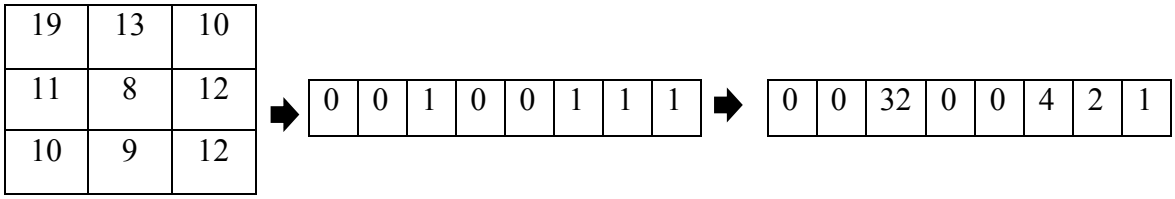

QuLBP binary presentation=00100111

QuLBP integer presentation (QuLBP code) =39

Figure 4.6 Presentation of QuLBP encoding

We investigate in our approach the both of QuLBP presentations: binary and integer. Penguin groups present the rule packets.

3.11.3.2 Fitness function

In order to evaluate the relevance of penguin solution to the problem search space. We propose to use the evaluation function defined by Baddeley, Baddeley's Delta Metric (BDM) in (Baddeley, 1992). Its aim is to measure the dissimilarity of the subsets of featured points, which are generally represented by the value 1.

Let I_1 and I_2 be two binary images and let N×M be their equal dimensions, β ={1,.. ,N}x{1..M} is the set of positions.

Given a value 1 < k < 1 the k-BDM between two images I_1 and I_2 is given as follows:

$$\Delta^k(I_{1,}I_2) = \left[\frac{1}{|\beta|}\sum_{t\epsilon\beta}|w(d(t,I_{1,})) - w(d(t,I_{2,}))|\right]^{\frac{1}{k}} \quad (4.3)$$

Where *w*(.) is a concave increasing function that is used for weighting and $d(t,I_{i,})$ is the distance between position t and the closest edge point of the set *Ii.*

The fitness function is calculated for each penguin in groups. In addition, to obtain the best packet of rules, the fitness function is calculated for the whole group, the penguins of one group are applicated together.

3.11.3.3 Population generation

In bio-inspired metaheuristics algorithms, the generation of the start population of possible solutions, plays an important role where this population is considered as a start point to search for other possible solutions. So, a good initial population will generate better solutions and will speed up the convergence of the algorithm while searching in the search space. The PeSOA uses a random strategy to initialize the first population of individuals without taking into consideration any information about the specified problem.

The purpose is to start the search with a set of diversified initial solutions which have contrasting features benefiting future solution improvement and to control the non-visited region in the coming iterations.

QuLBP starts with a population distributed in K groups

1. Generate a population of QuLBP uniform patterns
2. **For** each penguin i to *P* penguins do
   Eliminate the redundant penguin in each group K and select new one;
   End for.

3.11.3.4 Solution updating

Update Best solution and Best Global solution: After each dive of sharing information, penguins determine the best group, that is to say, the group that ate the highest amount of fish. Best solution that is to say and the best position in the generation. In the original PeSOA updating solution is devoted to the continuous problems unlike the case in our approach. Therefore, the equation (4.2) is not suitable for our algorithm for MRI edge detection. A new concept must be created regarding to the original equation. We rewrite the eqaution as follows:

$$QuLBPB_{new} = QuLBPB_{id} + rand\,() \,(QuLBPI_{best} - QuLBPI_{id}). \quad (4.4)$$

$QuLBPB_{new}$: the binary representation of QuLBP code of the new solution.
$QuLBPB_{i}$: the binary representation QuLBP code of the current solution.
$QuLBPI_{id}$: the integer representation QuLBP code of the current solution.
$QuLBPI_{bes}$: the integer representation QuLBP code of the best solution.

The current solution QuLBPB$_{id}$ is replaced by the difference between best solution and current solution for convergence rand () (QuLBPI$_{best}$ − QuLBPI$_{id}$) return a random QuLBP**I** code named QuLBP$_{\mathbf{random}}$ belongs to {(QuLBPI$_{best}$ − QuLBPI$_{id}$)}.

For the oxygen reserve, it is updated according to the fitness function, and it represents the health of the penguin. After each iteration, the fitness of the solution of the previous iteration updates. If the fitness function increases the oxygen reserve increase and if the fitness function decreases, the oxygen reserve value.

3.11.4 Outlines of QuLBP-PeSOA algorithm

The algorithm 4.1 summarizes how The PeSOA is trained to obtain the CA rules to detect edges in brain MR images.

Algorithm1: ***PeSOA-QuLBP***

```
Read Input image I,
Generate Penguins population
Distribute penguins on groups
 While not End do
     For each penguin_i (solution, oxygen, bestSol, GBest) do
        if Oxygen > 0 do
          calculate solution using equation (4.4)
        applicate the transition rule of CA #which is represented by (penguin_i.solution)
          calculate the fitness
        Endif
     Endfor
       if fitness(penguin_i) < fitness(GBest) (the smallest value for BDM is the best)
            update GBest
            update oxygen
         Endif
  Endwhile
```

3.11.4.1 The pseudocode for the PeSOA-QuLBP for brain MR images edge detection

The PeSOA-Q algorithm consists of four steps. These steps are as follows:

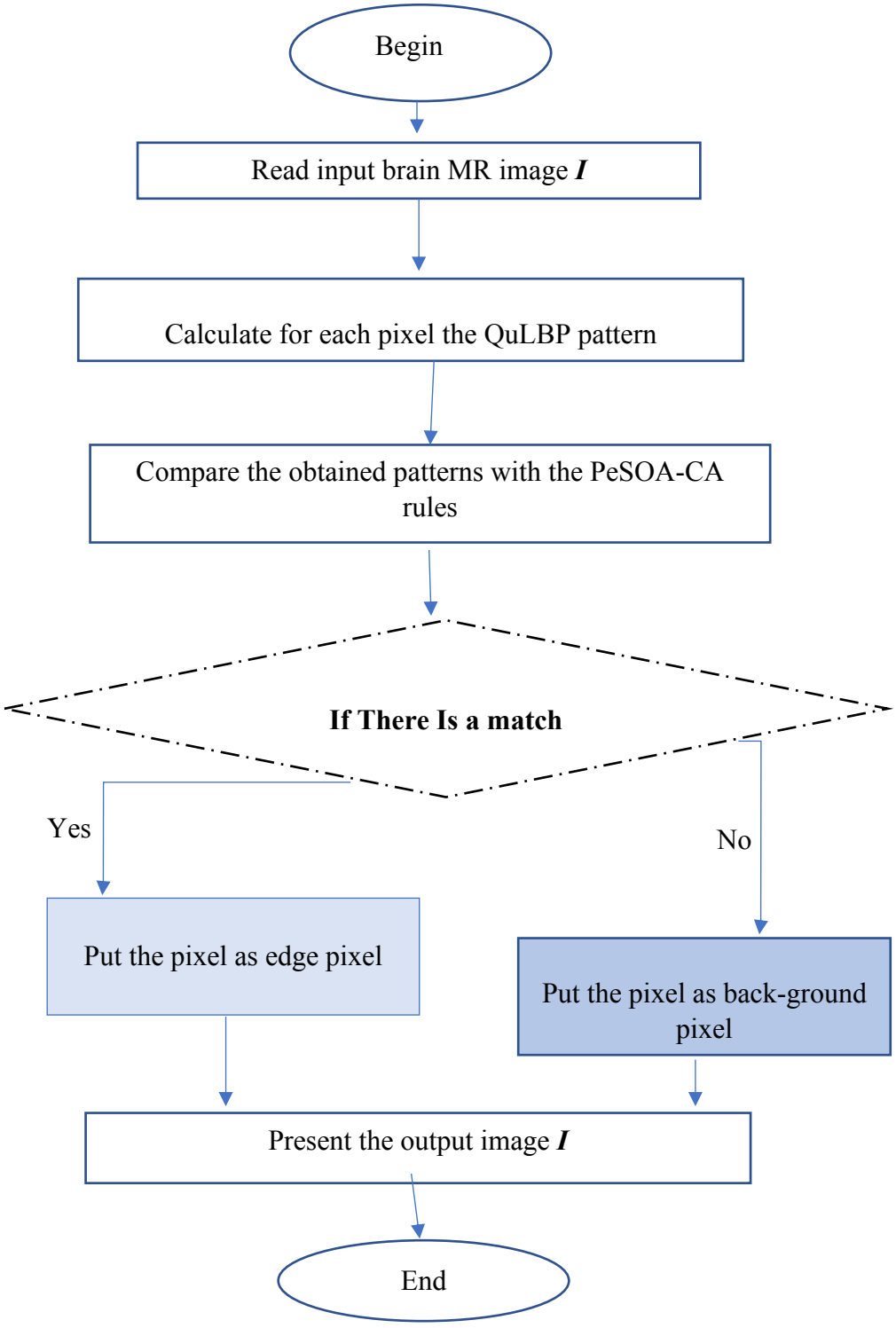

Figure 4.7 The PeSOA-QuLBP edge Detection process

3.12 Experimental Results

To assess the strength of the proposed method to detect edge in brain MR images, the proposed QuLBP had been tested through two different applications: CA-QuLBP edge detection and QuLBP-PeSOA. First the different datasets are described and the evaluation methods. Then the different experiments are describing and ran for each of the models, evaluating and commenting upon these separately.

3.12.1 Cellular Automata Edge Detection

3.12.1.1 Description of Data sets

In this paper, different datasets were used: square synthetic image (Wang, Kong, Yinghua, Qi, & Zhang, 2008)of (256×256) consisting four squares, is generated. The intensity values of the four squares are 0, 57, 166, and 217, respectively (see Figure 4.8).

Real T1 and T2 brain MR images with 256x256 and 512x512 resolutions with 3% typical noise, and a synthetic MR image dataset presented in BrainWeb (Brainweb: Simulated Brain Database, 1996). These are presented through six images to cover this diversity.

BrainWeb is an open access dataset that provides a full three-dimensional data volume of simulated MR images using T1 sequences with a variety of thicknesses, noise levels, and levels of intensity nonuniformity. The algorithm had been applied to the T1 MR sequence with a thickness of 1 mm, 1% noise, and an intensity inhomogeneity ranging from 0% to 40%.

Most of edge detection algorithms avoid one obstacle in the edge detection task by basing their evaluations on visual comparison only. To lay a foundation for the quantitative evaluation and offer a performance evaluation, the ground truth images in the method are provided by the Canny-deriche algorithm, since this last one is known to be an optimal edge detector, then the blurred edges are manually corrected.

3.12.1.2 Evaluation methods

The performance of the proposed approach had been evaluated by using three well-known assessment methods. The structural similarity index (SSIM) was utilized for the quantitative evaluation of the first application.

- ***The structural similarity index***

The SSIM is a method for measuring the similarity between two images, taking three independent channels into account: luminance, contrast, and structure.

The SSIM for two images x and y is calculated as:

$$SSIM(x,y) = \frac{(2\mu_x\mu_y + c_1)(2\sigma_{xy} + c_2)}{(\mu_x^2 + \mu_y^2 + c_1)(\sigma_x^2 + \sigma_y^2 + c_2)} \quad (4.5)$$

where c_1 and c_2 are small positive constants defined as $c_1 = (0.01 \times 2^n)^2$ and $c_2 = (0.03 \times 2^n)^2$, with n being the number of bits used to code the image (n=8 in the case of an image coded in 8 bits); μ_x denotes the mean of x; μ_y denotes the mean of y; σ_{2x} and σ_{2y} are the variance of x and y, respectively; and σ_{xy} is the covariance of x and y.

3.12.1.3 Synthetic square image

The validation process goes throw several tests. As first comparison, the synthetic square image (Figure 4.8(a)) with different gray levels intensity is presented. The image was affected by two types of noise; Salt and pepper noise (Figure 4.8(b)) and Gaussian white noise of mean 0 and variance 0.06 (Figure 4.8 (c)).

In Figure 4.8, we show the edge detection results of the proposed approach present by the second row and Sobel edge detector presented by the third row. In this experiment, we set the T parameter in range of {15 ,20,60}to deal with the two types of noise. Visually, our proposed approach and Sobel performed well on homogenous Synthetic square image, perfect edges are presented with high discrimination between the four regions. In salt and pepper Square image, our approach removes most of the noise and localizes the edges between regions unlike Sobel edge detector which achieve relatively satisfactory for the four regions edge localization but it fails to remove the noise. For the square image that affected by Gaussian noise, the performance of both algorithms is decreased only that our algorithm surpasses Sobel. A less noise is appeared in our approach resulted image.

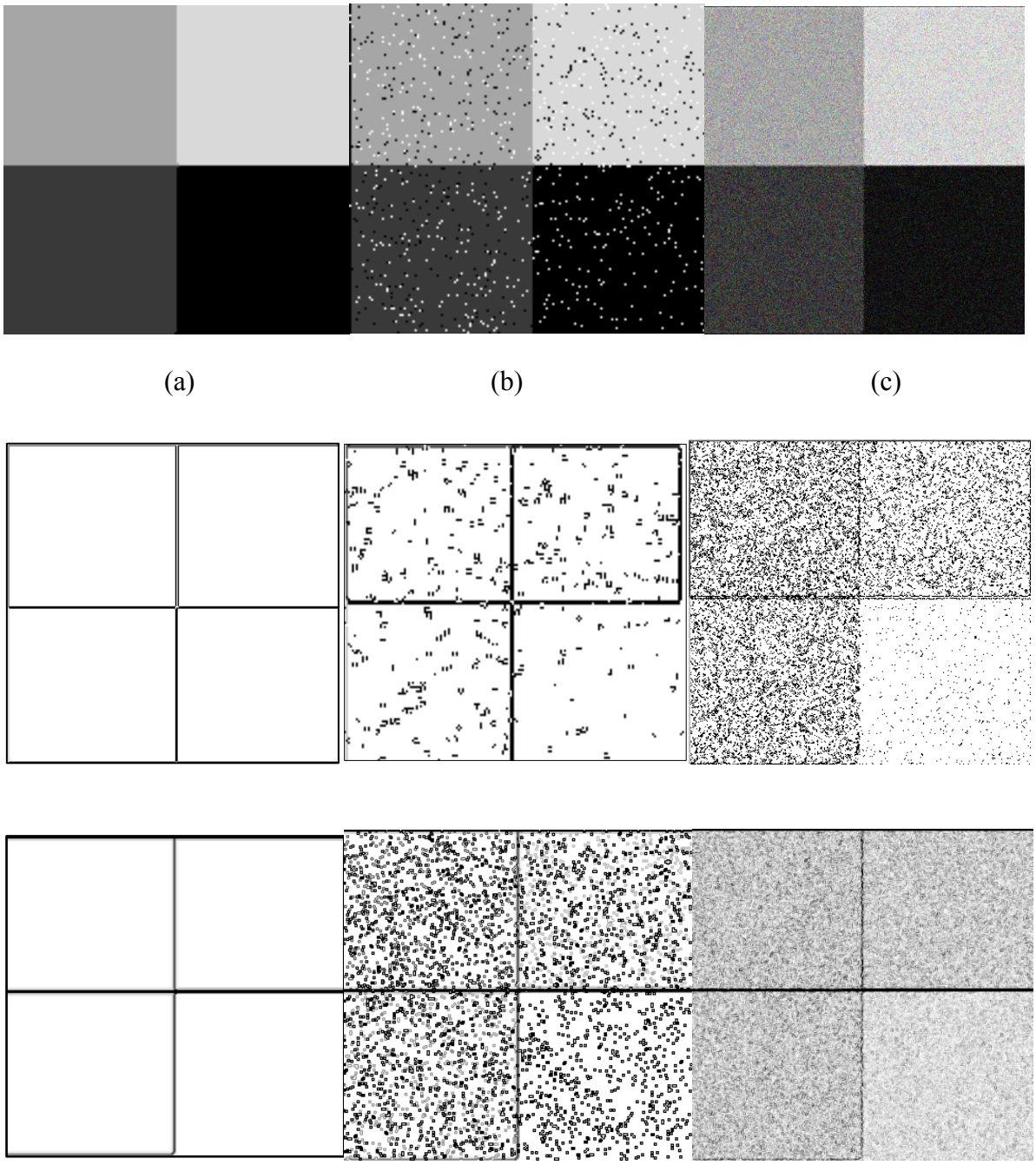

Figure 4.8 Comparison of edge detection results on synthetic square image (a);(b) same image with salt and pepper noise ;(c) with white gaussian noise ,2nd row proposed method results third one is Sobel detector results.

3.12.1.4 Digital Brain Phantom

In order to evaluate our algorithm performance, BrainWeb simulator provides 20 Anatomical models of 20 Normal Brains named subjects. Each subject offers different phantoms with intracranial brain tissues: White Matter (WM), Gray Matter (GM) and Cerebrospinal Fluid (CSF). Among the 20 provided subjects, we test eight.

Figure 4.9 shows, in larger clarification, the edge detection results of the proposed approach on different phantoms for 87^{th} slice in T1 normal brain tissues. It is obvious that our can locate the edges of different given phantoms with accuracy. A high discrimination between the presented tissue of each phantom and the background of the images. The edges are well located with thin presentation and correct edges.

The quantitative accuracy of the average results of the eight phantoms are shown in figure 4.10 Here, different types of noise (salt-and-pepper impulse noise and gaussian) are used.

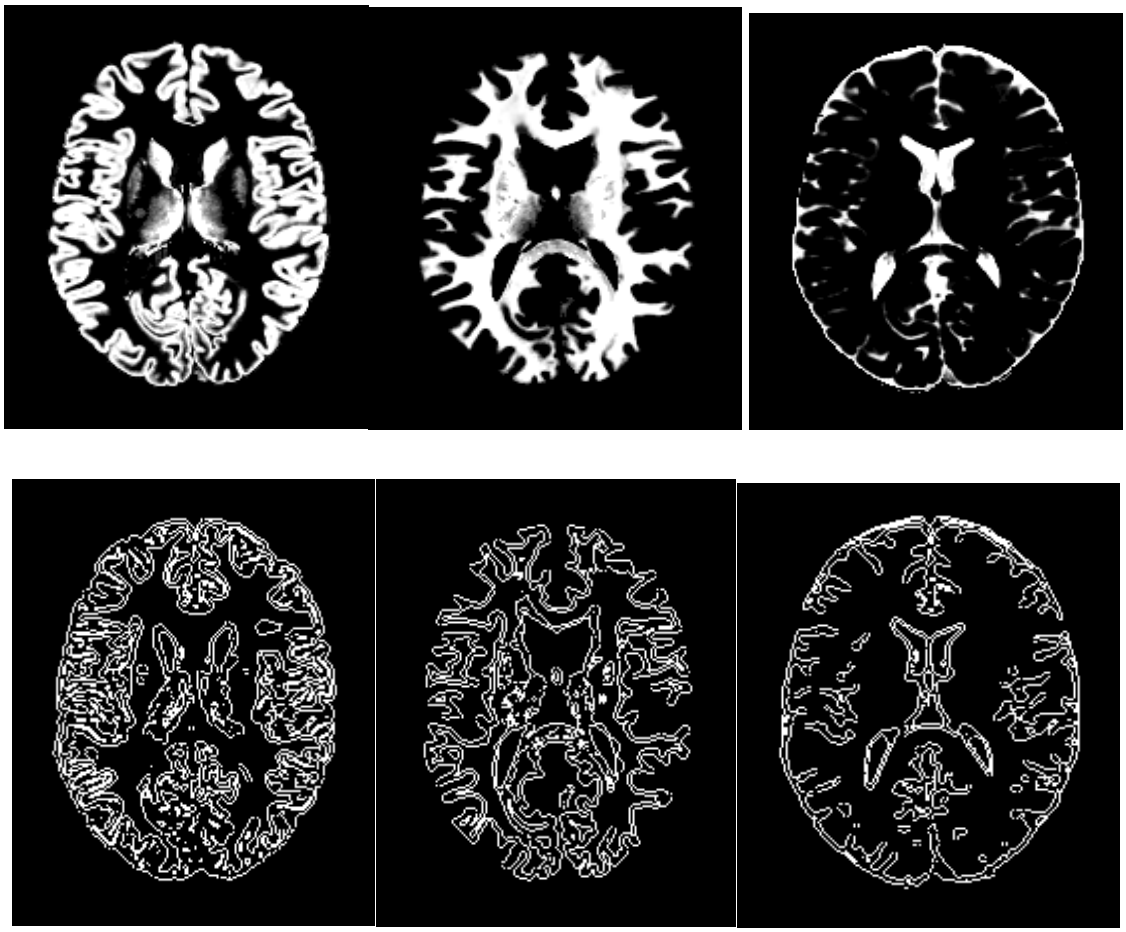

Figure 4.9 Edge detection results of the proposed approach on different phantoms

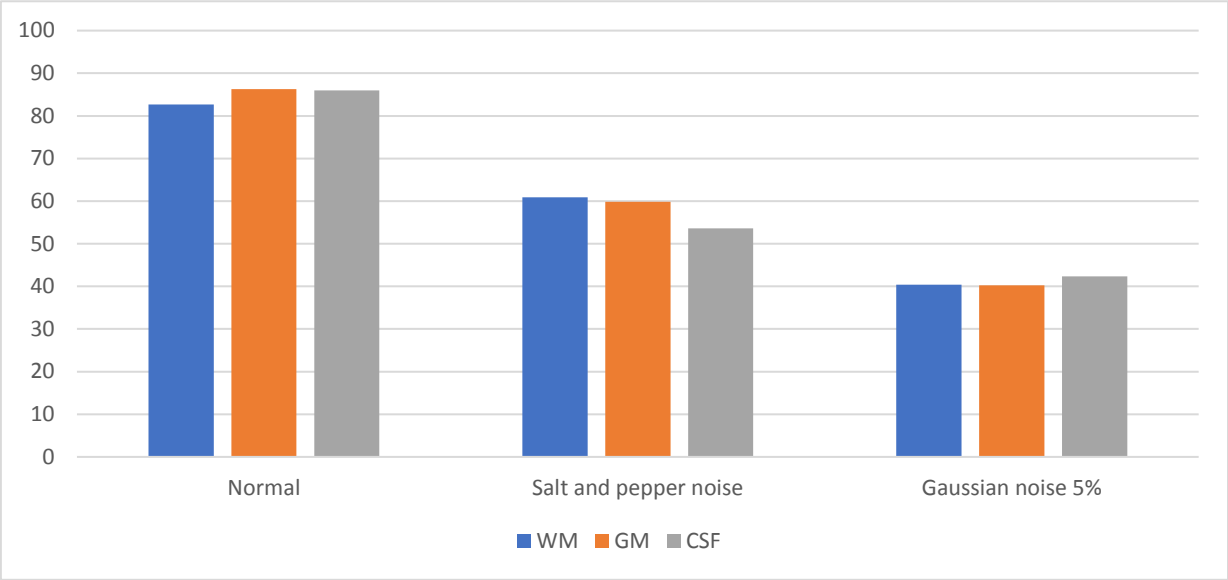

Figure 4.10 Accuracy results of SSIM on normal, noisy (salt and pepper) and gaussian noise of brain phantom

The performance of the CA edge detector touches its high levels in the absence of noise where the value starts to decrease in the presence of noise, especially gaussian noise.

3.12.1.5 Real Brain MR images

For further Tests, the edge detection results for real T1 and T2 MR Images are shown in Figure 4.12. Two classical edge detectors were employed, i.e., Sobel and Canny, to extract edges with a standard threshold technique, and they are compared with the proposed approach. The T parameter was set in the model in the range [14...20] See (Figure 4.11) and the radius R to 1 for all experiments.

As can be seen in Figure 4.12(b), not only does the Sobel operator fail to detect most of the MR images' meaningful edges, but in addition the produced edges are discontinuous and thick. Cranny's edges in Figure 4.12(c) are better than Sobel's in terms of their responsiveness to more of the images' edges. However, Canny misses some critical edge structures, which leads it to produce meaningless images.

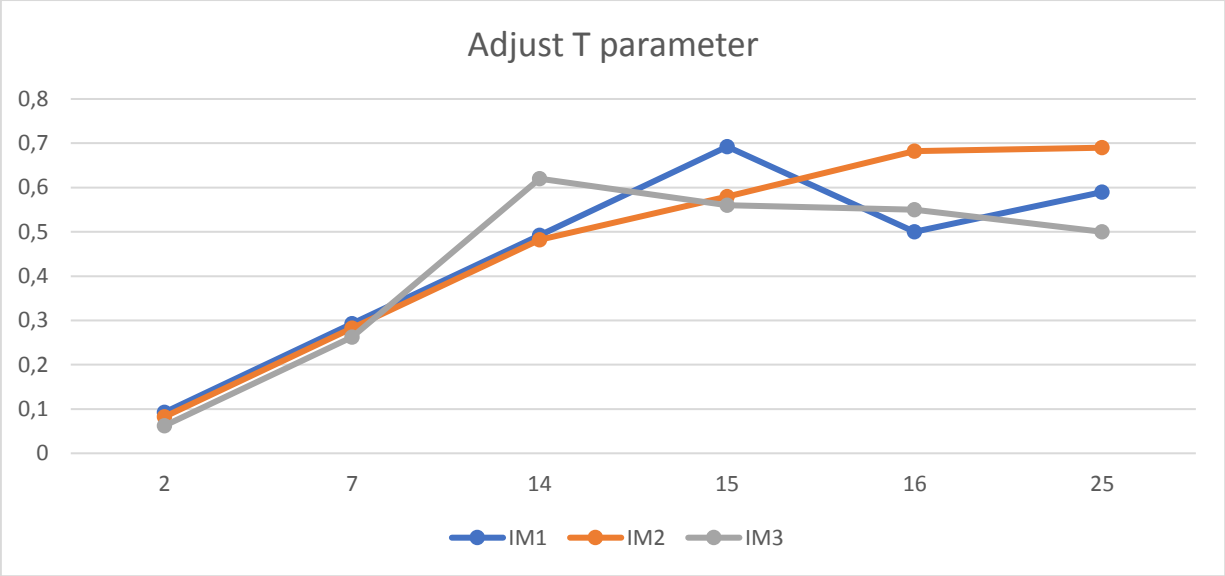

Figure 4.11 Adjusting T parameter for different real brain MR images

The results reveal that the proposed approach successfully detected most of the edges. Figure 4.12(d) shows that the proposed approach detects the outlier edges of the brain textures and provides good localization of the small overlapping regions. The separation between different brain regions is presented with thin and connected edges. However, a double line marks the edges in some areas.

The quantitative accuracy of the results is shown in Table 4.1. The images are given in the same order as in Figure 4.12. For most of the results, the proposed approach has the best values for the evaluation metrics used; as an example, the SSIM value **0.69** is the best value that is achieved. The best values in the table are highlighted in boldface.

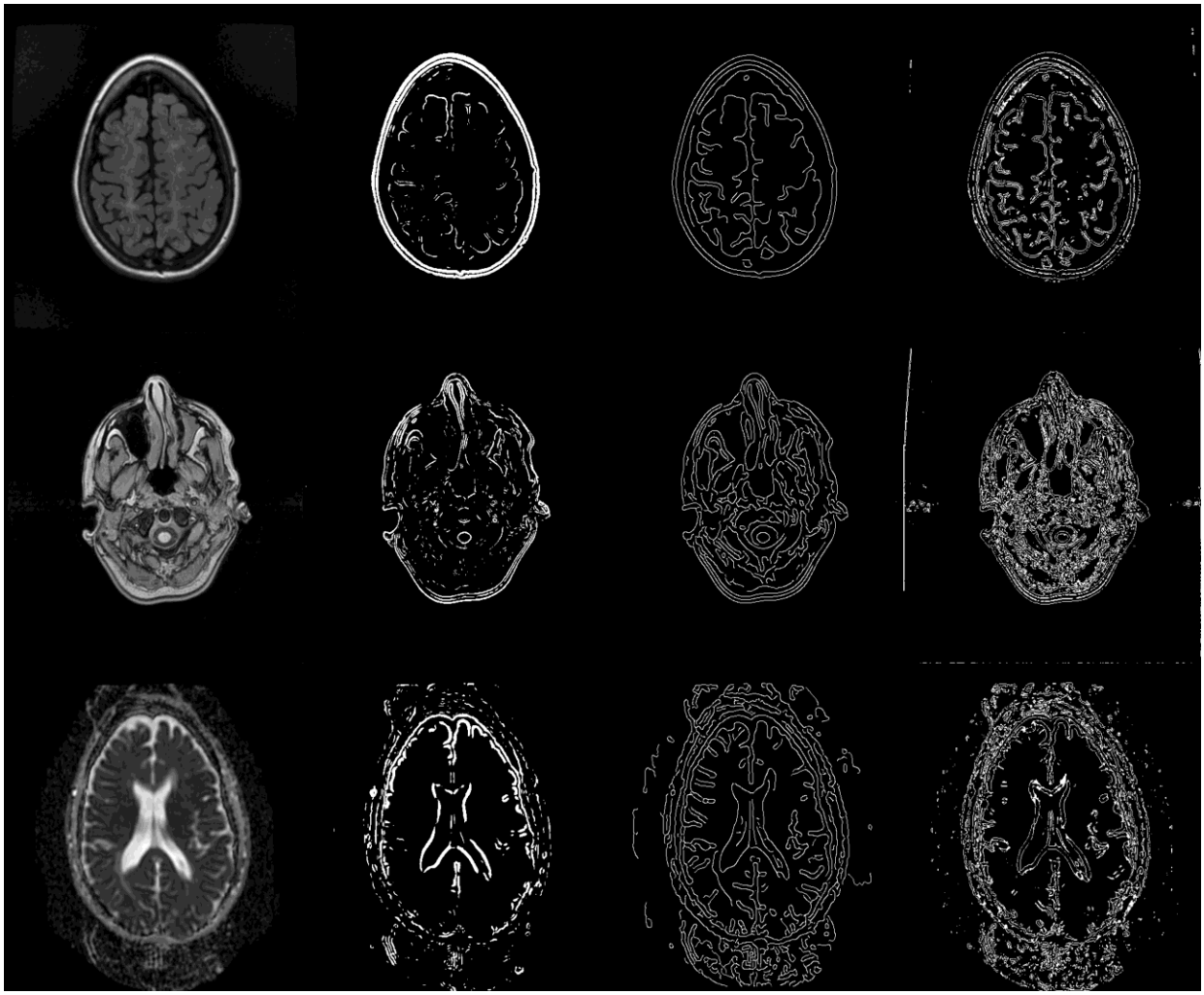

a b c d

Figure 4.12. Edge detection algorithms for real T1 and T2 weighted MR images: (a) MR test images, (b) Sobel algorithm, (c) Canny algorithm, (d) the proposed algorithm

Table 4.1 SSIM values for the real Brain MR images

	Sobel	Prewitt	Laplacian of gaussian	Canny	Proposed Approach
IM1	0.3976	0.4005	0.5485	0.6394	**0.6924**
IM2	0.5192	0.6078	0.5925	0.6064	**0.6640**
IM3	0.4023	0.5325	0.5741	0.5723	**0.5886**

3.12.1.6 BrainWeb Synthetic Brain MR images

This section presents the results of the comparison of several edge detectors algorithms (Canny, Sobel and our proposed method) on T1 and T2 synthetic brain MR images modalities with different noise levels and different inhomogeneous levels.

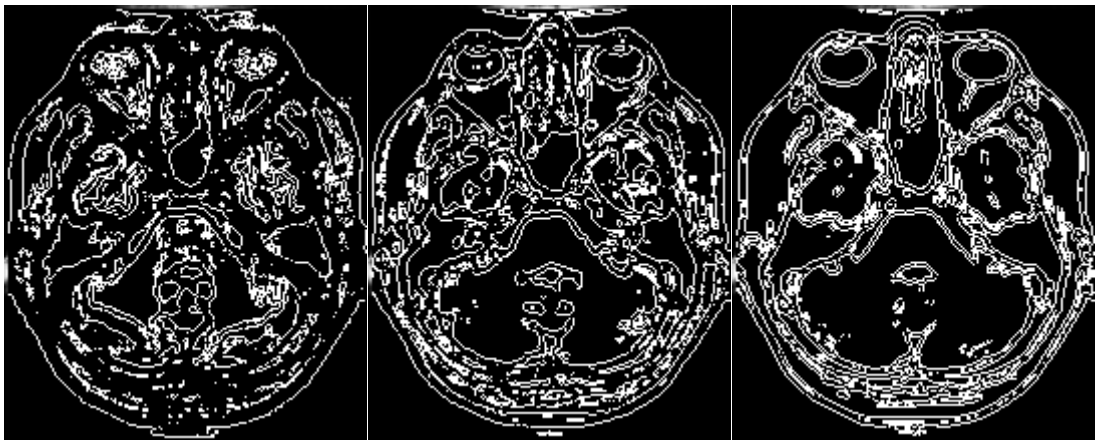

T=05 T=15 T=50

Figure 4.13 Adjusting T parameter for different real brain MR images

The T parameter was set in the model in the range [15...50] See (Figure 4.13) and the radius R to 1 for all experiments.

For a qualitative comparison of QuLBP-CA edge detector with Sobel and Canny, we applied the mentioned algorithms to the T1 and T2 brain MR Images. The resulting images are shown in Figures 4.13and 4.14 after applying the Canny, Sobel and QuLBP-CA on the images.

The resulting images in Figure 4.13 and Figure 4.14 show that QuLBP-CA performed better than the other two algorithms on the three different brain MR images. The Sobel algorithm produces thick and not connected edges, it misses most of brain edges. In Canny detector, even with postprocessing, did not work well for these MR images. It misses most of meaningful edges. In Figure 4.14 (the second and third row), the noise level and the inhomogeneities increase and the performance of the both Sobel and Canny algorithms decrease. They fail to detect the brain edges and misses most of the edges. Our algorithm performed better than the both algorithms, it produces more connected edges in the presence

of the noise and the high level of the non-uniformity. However, some spots are appeared but do not affect the real brain edges.

The quantitative comparison is presented in Table 4.2 and 4.3. More images are used, 24 T1 and T2 synthetic MR images are available for this objective comparison. Each volume of the synthetic MRI has 181 slices with 217x181 pixels with different inhomogeneity level RF (0% ,20%, 40%) and different Gaussian noise level (0% ,3% ,7%,9%). Figures 4.15 and 4.16 the graphical interpretation of the tables.

The best value obtained for our proposed algorithm is presented in T2 brain MR images due to high contrast between the brain tissues: White matter, grey matter and cerebro-spinal fluid.

The results of the classical Canny, Prewitt and Sobel methods are not satisfactory. Sensitivity to each edge and its localization is more important in MR images than in other types of images, from the point of view of medical health.

The proposed method presented the MR images' edges with significantly more detail, which can be very useful for medical analysis, for example, in the presentation of certain anatomical textures such as tumors. Due to the high sensitivity of the proposed model to the images' boundaries. The choice of the T parameter in the QuLBP influences its sensitivity, and this choice can be understood as the crucial point for proper detection—which in some cases can produce double lines, although this may be rare.

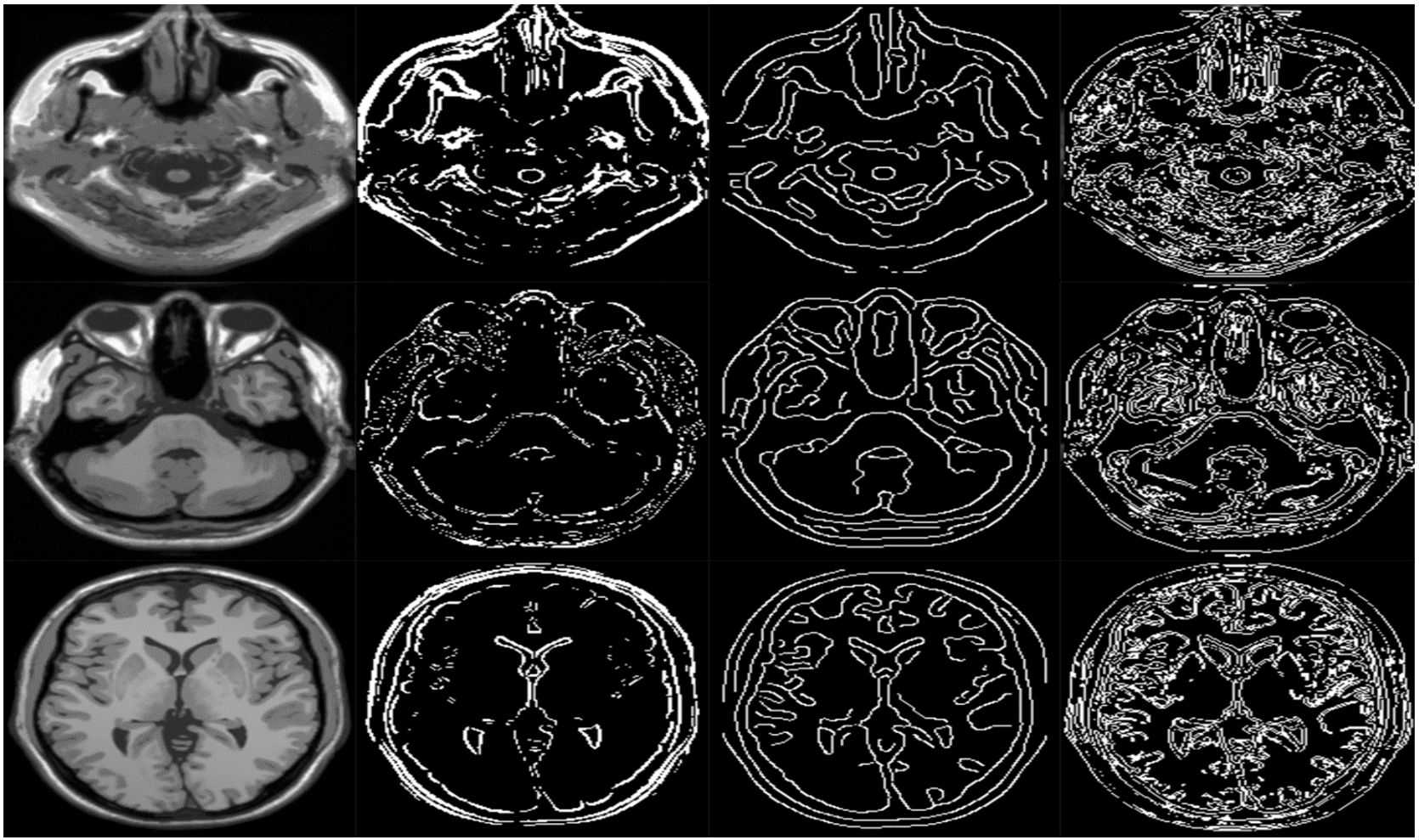

a b c d

Figure 4.14 An example Edge detection algorithms T1 weighted MR images: (a) MR test images, (b) Sobel algorithm, (c) Canny algorithm, (d) the proposed algorithm.

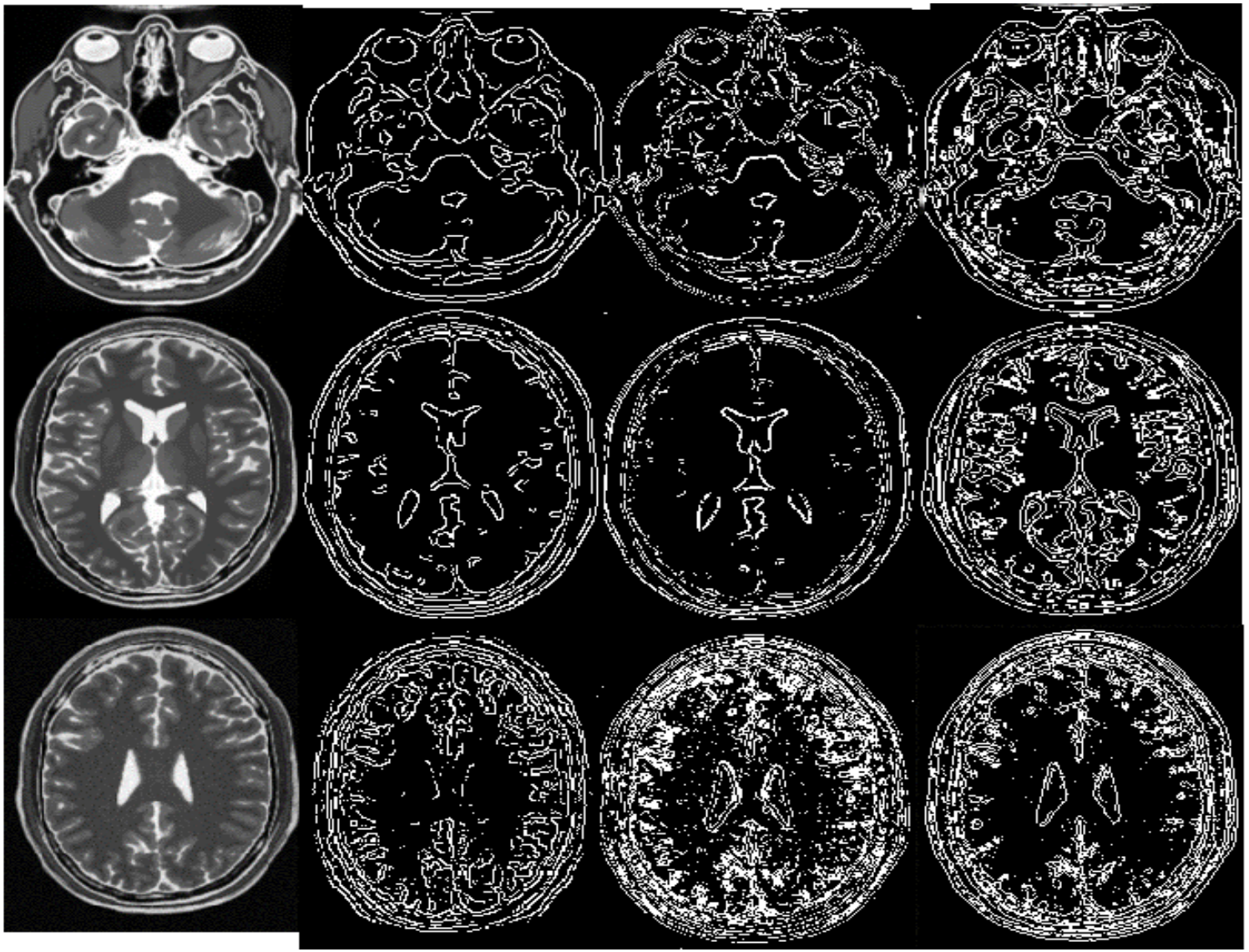

a b c d

Figure 4.15 An example Edge detection algorithms T2 weighted MR images: (a) MR test images (first row 0% RF,0%noise,second row 40%rf,3%noise and third row 40%rf,7%noise), (b) Sobel algorithm, (c) Canny algorithm, (d) the proposed algorithm.

Table 4.2: comparison of the obtained results for T1 MRI image edge detection

RF \ Noise		0%	3%	7%	9%
0%	**Canny**	0,5569	0,3884	0,3856	0,2024
	Prewitt	0,4304	0,3001	0,3753	0,2113
	Sobel	0,4230	0,3985	0,3992	0,1035
	CA-QuLBP	**0,6994**	**0,5784**	**0,4756**	**0,2924**
20%	**Canny**	0,5792	0,2997	0,2004	0,1496
	Prewitt	0,4753	0,2536	0,1967	0,1223
	Sobel	0,4631	0,2312	0,1753	0,1367
	CA-QuLBP	**0,6635**	**0,4684**	**0,3656**	**0,2824**
40%	**Canny**	0,3898	0,2857	0,1720	0,0786
	Prewitt	0,3244	0,1543	0,0720	0,0811
	Sobel	0,3442	0,2723	0,0935	0,0899
	CA-QuLBP	**0,6019**	**0,3584**	**0,2556**	**0,2076**

Table 4.3: comparison of the obtained results for T2 MRI image edge detection

RF \ Noise		0%	3%	7%	9%
0%	**Canny**	0,5668	0,3983	0,3955	0,2123
	Prewitt	0,4403	0,31	0,3852	0,2212
	Sobel	0,4329	0,4084	0,4091	0,1134
	CA-QuLBP	**0,7105**	**0,5883**	**0,4855**	**0,3023**
20%	**Canny**	0,5891	0,3096	0,2103	0,1595
	Prewitt	0,4852	0,2635	0,2066	0,1322
	Sobel	0,4732	0,2411	0,1852	0,1466
	CA-QuLBP	**0,6934**	**0,4783**	**0,3755**	**0,2923**
40%	**Canny**	0,3997	0,2956	0,1819	0,0885
	Prewitt	0,3343	0,1642	0,0819	0,091
	Sobel	0,3541	0,2822	0,1034	0,0998
	CA-QuLBP	**0,6694**	**0,3584**	**0,2556**	**0,2076**

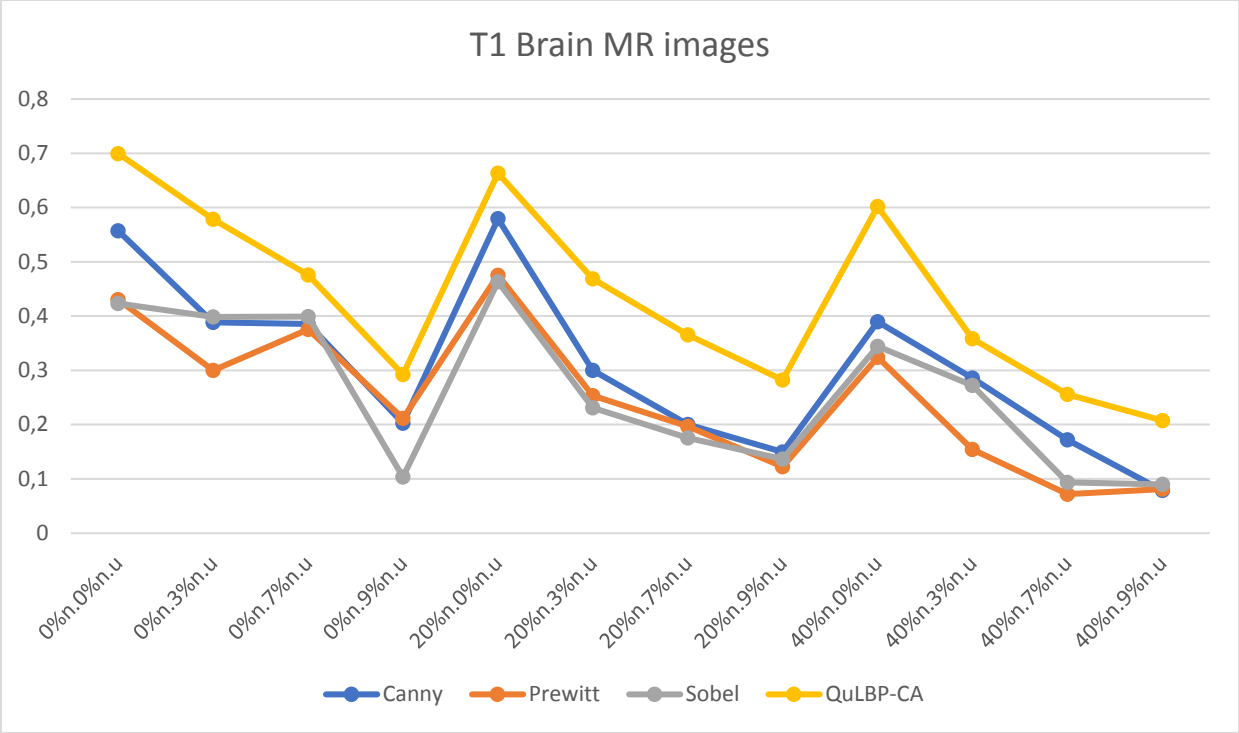

Figure 4.16 Accuracy comparison between Canny, Prewitt ,Sobel and QuLBP-CA on T1 synthetic MR image

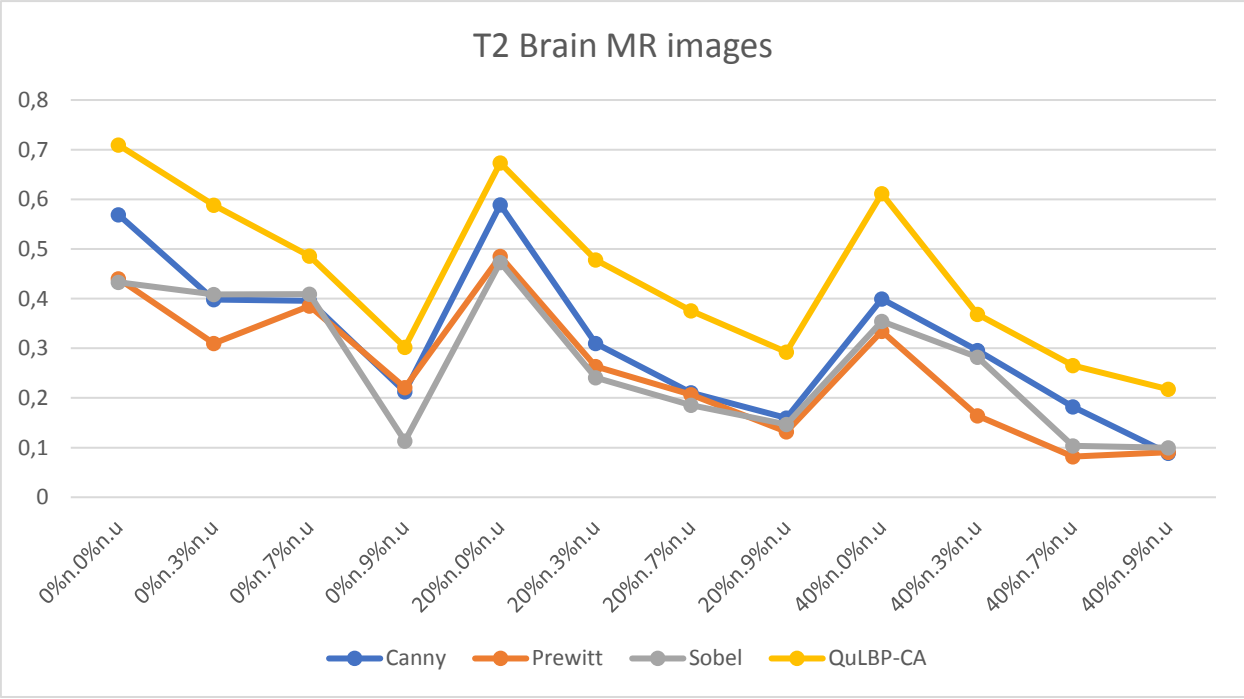

Figure 4.17 Accuracy comparison between Canny, Prewitt, Sobel and QuLBP-CA on T2 synthetic MR image

3.12.2 Brain tumor edge detection using QuLBP Penguin Search Optimization Algorithm (QULBP-PeSOA) combined with Cellular Automata

In order to evaluate effectiveness of the proposed approach, two basic evaluation phases have been used in the experimentation process. Firstly, the training of the CA with the PeSOA to produce the rules that generate the edges of the tumor brain MR image. Secondly, the execution of the obtained rules for the CA to detect the edges.

3.12.2.1 The training phase

3.12.2.1.1 Description of dataset

In this section, 9 clinical real brain MR images are used for the training and the test of proposed method (Table 4.4). The images are obtained by MRI scan of brain with gray levels intensities.

Table 4.4 Description of dataset

Sequences	Resolution	Slices number	Plane
Seq 1	512x512	21	Sagittal, T1
Seq 2	512x512	49	Axial, T2
Seq 3	512x512	24	Flair
Seq 4	512x512	32	Coronal, T2
Seq 5	256x256	24	Axial, T2
Seq 6	512x512	24	Axial, T1
Seq 7	512x512	24	Axial, T1
Seq 8	512x512	24	Coronal, T1
Seq 9	512x512	24	Axial, T1

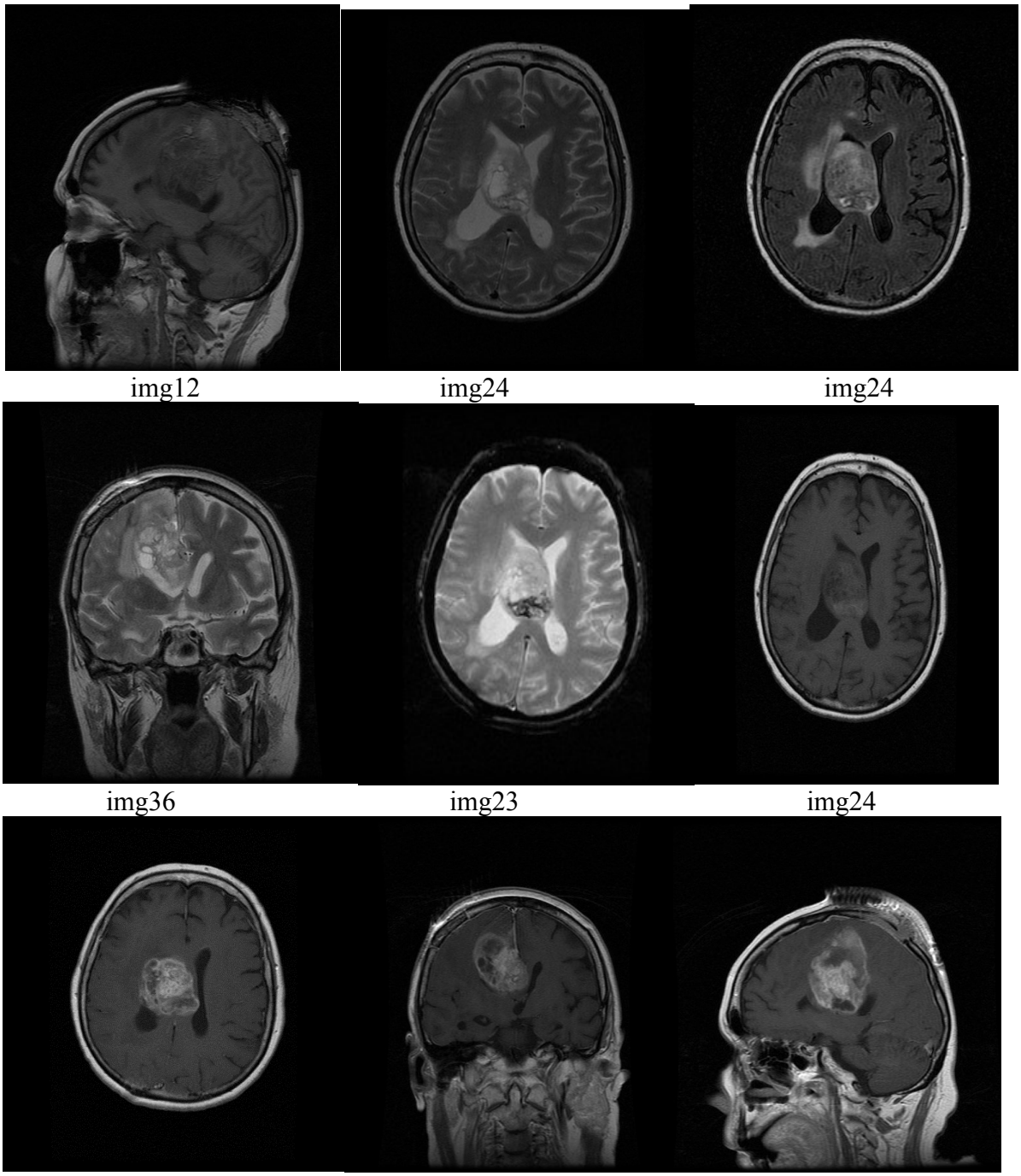

Figure 4.18 Examples of images(slices)for sequences 1 to 9, respectively.

The QuLBP in this approach is predefined to classify the textures according to the tumor texture Instead of four regions (WM, GM, CSF and background). If two pixels belongs to the tumor region are defined similar (value 1), otherwise, the value is 0. This process is done by changing the T parameter value that differs any pixel from the tumor region. The T parameter can reach up to 120 in images where the tumor presence is brighter than other tissues.

During the training process PeSOA requires different parameters to ensure the best obtained results. Our aim here, is to investigate the best parameters values to our optimization process to finally obtain the best rules that represent the edges in the tumor brain MR images.

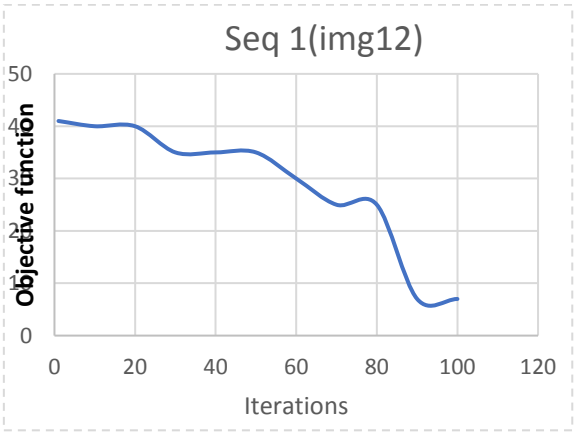

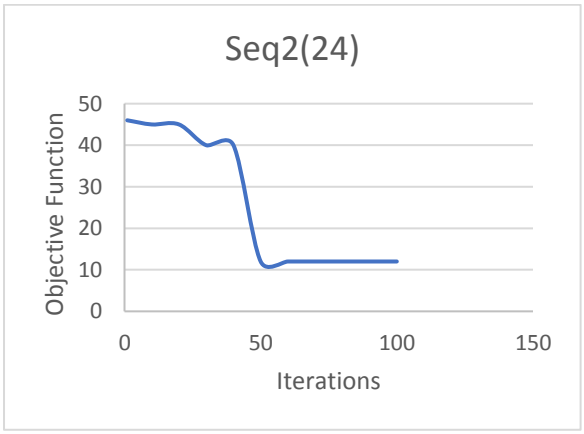

x

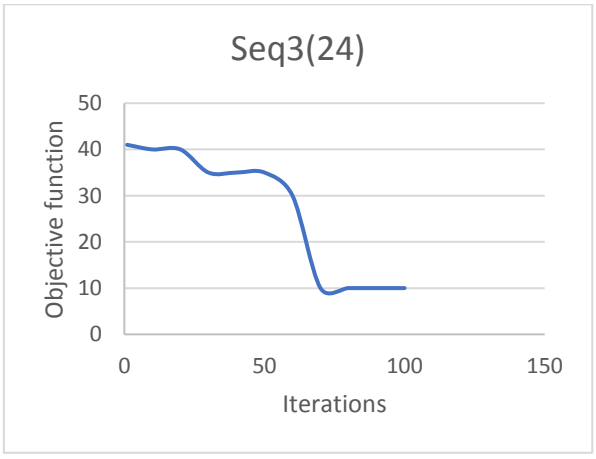

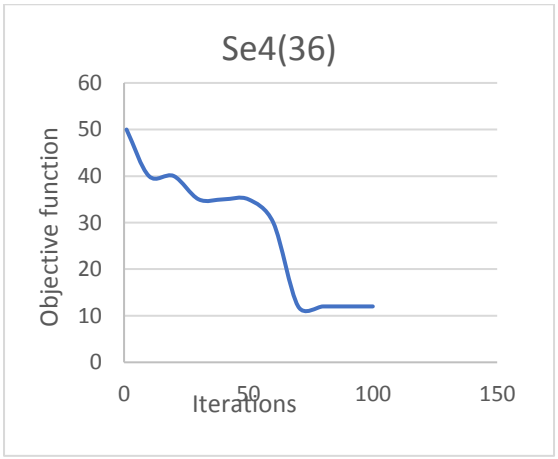

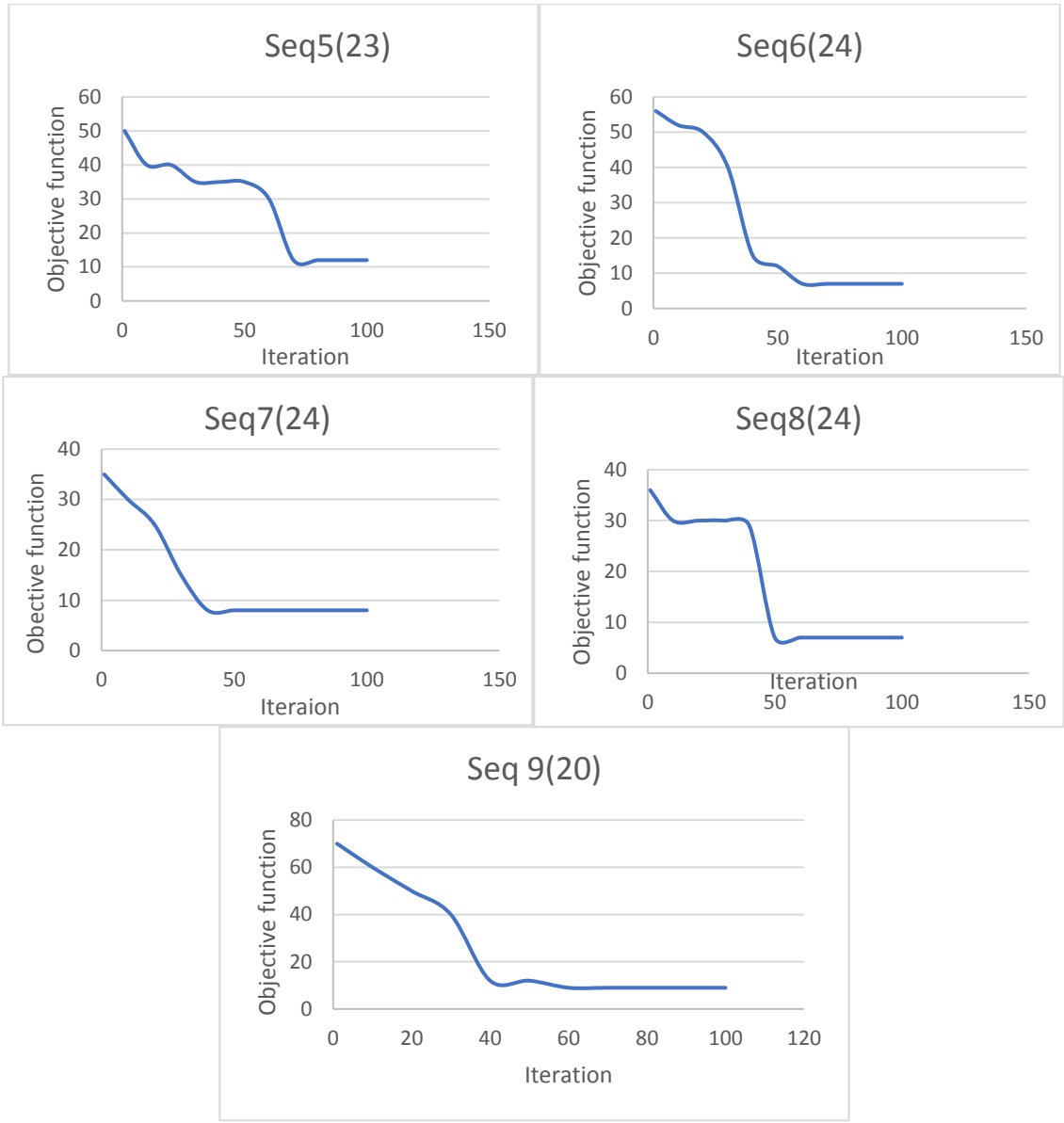

Figure 4.19 Convergence of objective function for each image

Figure 4.18 shows the global convergence of our proposed algorithm accomplished for the dataset images. We notice that the diversification strategy is more effective and the algorithm avoided cyclic behavior with high exploration of the solution space. In the parameter settings, the value of each parameter is changed iteratively in order to find the smallest BDM (objective function) index for this algorithm. we have used 100 generations for all tests.

We set the training algorithm parameters according to the table below (Table 4.5).

Table 4.5 presents the different parameters for running PesOA

Number of penguin population (possible rules)	2^8 possible solution
Number of iterations	100
Oxygen	5
Set of groups	7

The convergence process is different for each seq, that may be affected by the image modality (due to intensity contrast), the population generation and may that due to the image structure where the tumor complex contrast (tumor is presented with more than texture) -see (Figure4.17).

In order to provide the transitions rules, Figure 4.19 shows an example of three obtained rules on same image [Seq6, img24]. The transition rules are applied severally and different results are presented. The results for Rule 31, Rule 15 and Rule 252, can be seen from the figure4.19 for seq6(Img 24). The edges of tumor image are mostly detected without distortion with the proposed method in all rules with missing of some of small parts. Among them the last rule (rule 252) performed better.

Each rule in the obtained rules performed better for different images and that may depend on the image tissues contrast and the adjusting of the primary parameters as the way for the T parameter.

Overall, the best penguins that represent the best rules are: **Penguin 1**: 00011111 (31)

Penguin 2 : 00001111 (15), **Penguin 3** : 01111000 (120), **Penguin 4** : 01111100 (124)

Penguin 5 : 11111100 (252), **Penguin 6** : 10000011 (131).

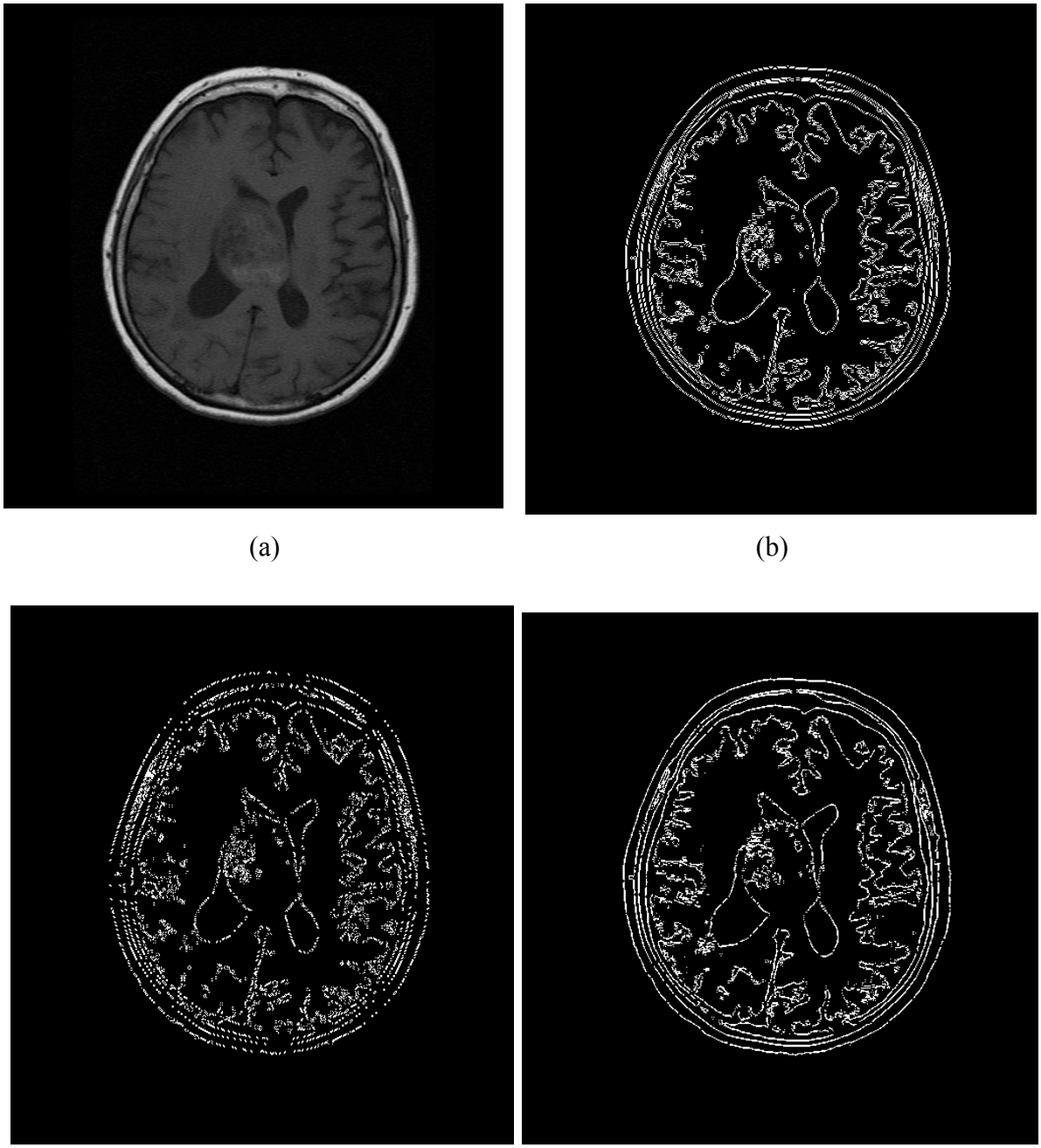

(a) (b)

(c) (d)

Figure 4.20 Performance of the three different obtained rules on (a) brain tumor MRI [seq6, img24] (b) rule31, (c) rule15, (d) rule 252.

3.12.2.2 The test phase

In order to evaluate the performance of the proposed model, we have compared our algorithm against different known edge detectors: Canny, Sobel and Prewitt. In this part, 32 images are

used for the test. The 27 images (Table 4.6) were selected from the dataset described in the test phase besides five tumor brain MR images that are characterized by different locations and different types of pathologies, shape, size, density, as well as the size of the area of the affected tissue near the tumor space.

Table 4.6 The 27 test images

Sequence number	**Seq 1**	**Seq 2**	**Seq 3**	**Seq 4**	**Seq 5**	**Seq 6**	**Seq 7**	**Seq 8**	**Seq 9**
Images slices	11_13	23_25	23_25	35_37	22_24	23_26	23_26	23_26	19_21

As shown in Figures (4.21, 4.22, 4.23 ,4.24 and 4.25) show that our proposed approach performed better where an accurate tumor localization is present. The Sobel and Prewitt algorithm produce not connected edges in Figures (4.21, 4.22, 4.23), they miss most of tumor brain edges. wherein Figures (4.24 and 4.25) the tumor area is fully appeared but with thick edges, In Canny detector, even with postprocessing, its performance varied between full connected edges and missing edges and in general it did not work well for these brain tumor MR images. It misses most of the meaningful edges. Our algorithm performed better than the three other algorithms, it produces more connected edges. The objective results for the presented images are given in Figure 4.26.

To test the effectiveness of the proposed approach against the classical edge detectors for all test dataset, we set the comparative study of all images for the SSIM metric (presented previously) in Figure 4.27. It can be concluded that the proposed approach performed better with the SSIM index in all images and that can be explained by the detection of the hall tumor area in the majority of test images. For Sobel, Prewitt and Canny the specification of the tumor region is missed, it means that all edges are considered including the tumor. The low contrast in majority of images makes their work harder and the tumor border misses most of their edges. Moreover, the thickness of the edges like the way in Sobel and Prewitt cause also the lost of the tumor characteristics (real size).

The T parameter in our approach plays an important and crucial role in discriminating the tumor from other textures. However, some of textures with same tumor intensity may appeared but that doesn't affect the tumor characteristics and show it clear for the expert for further analysis.

For further experiments, we measure the false alarm or the pixels that are erroneously detected as edge pixels by the equation bellows:

$$FA = \frac{FN}{ReC} \quad (4.6)$$

Where FN is the number of pixels that falsely identified as tumor edge and ReC represents the number of edge pixels in reference edged image. The value 0 presents the optimal value.

In Figure 4.28, the percentage of the false alarm metric is given for each image from the test images. High values were presented specially in the case of Sobel and Prewitt, an over edge detection is presented besides the miss detection of the tumor edges. Same way in Canny algorithm but with less false edges due to its superiority over the two algorithms.

Best results are presented by our proposed approach where the tumor edged are well detected and that was approved from previous tests but some of extra edges were presented which increase of the FA values little bit.

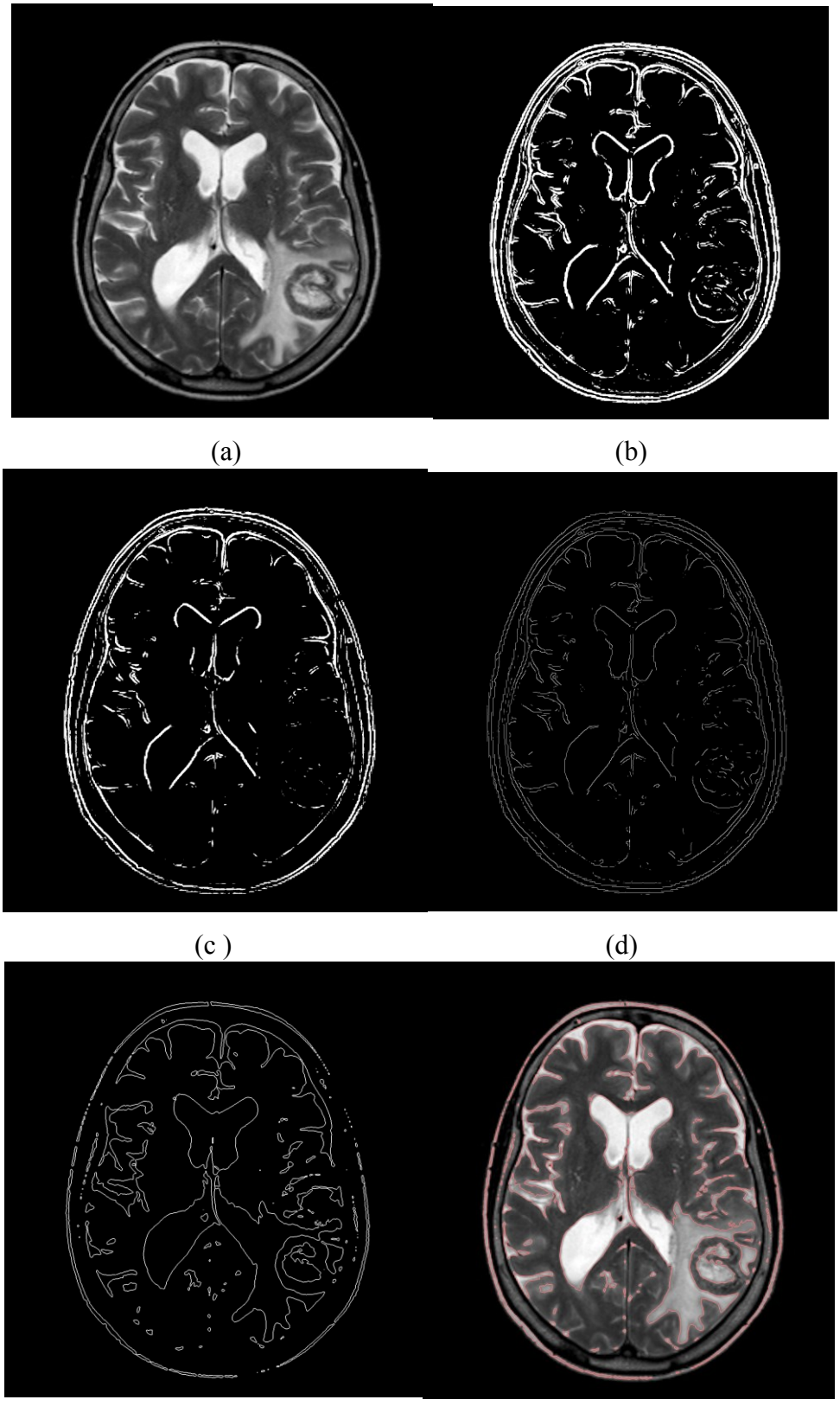

Figure 4.21 Edge detection results(1) (a) original image, (b)Sobel, (c) Prewitt, (d) Canny, (e) and (f) The proposed approach

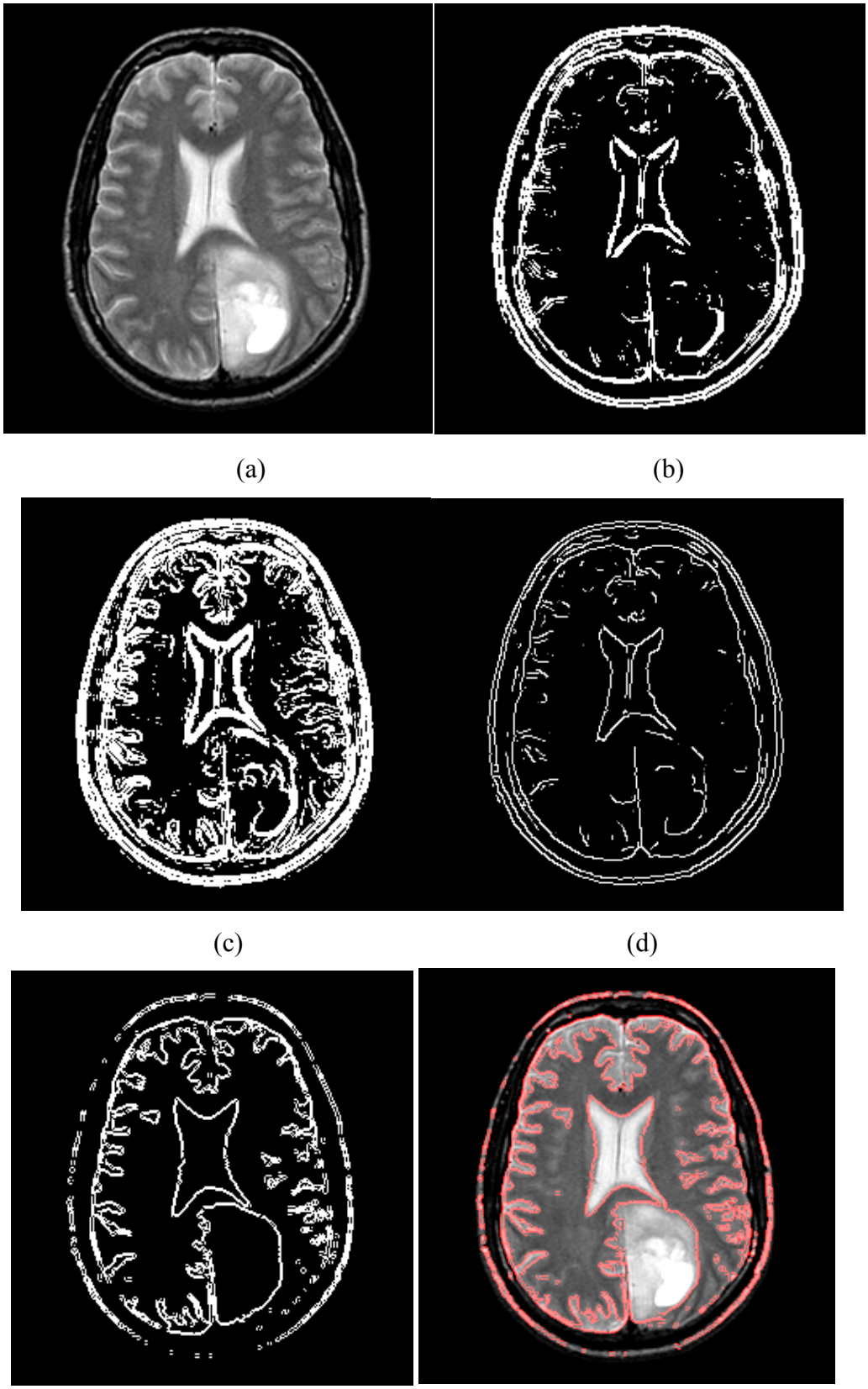

(a) (b)

(c) (d)

(e) (f)

Figure 4.22 Edge detection results(2) (a) original image, (b)Sobel, (c) Prewitt, (d) Canny, (e)and (f) The proposed approach.

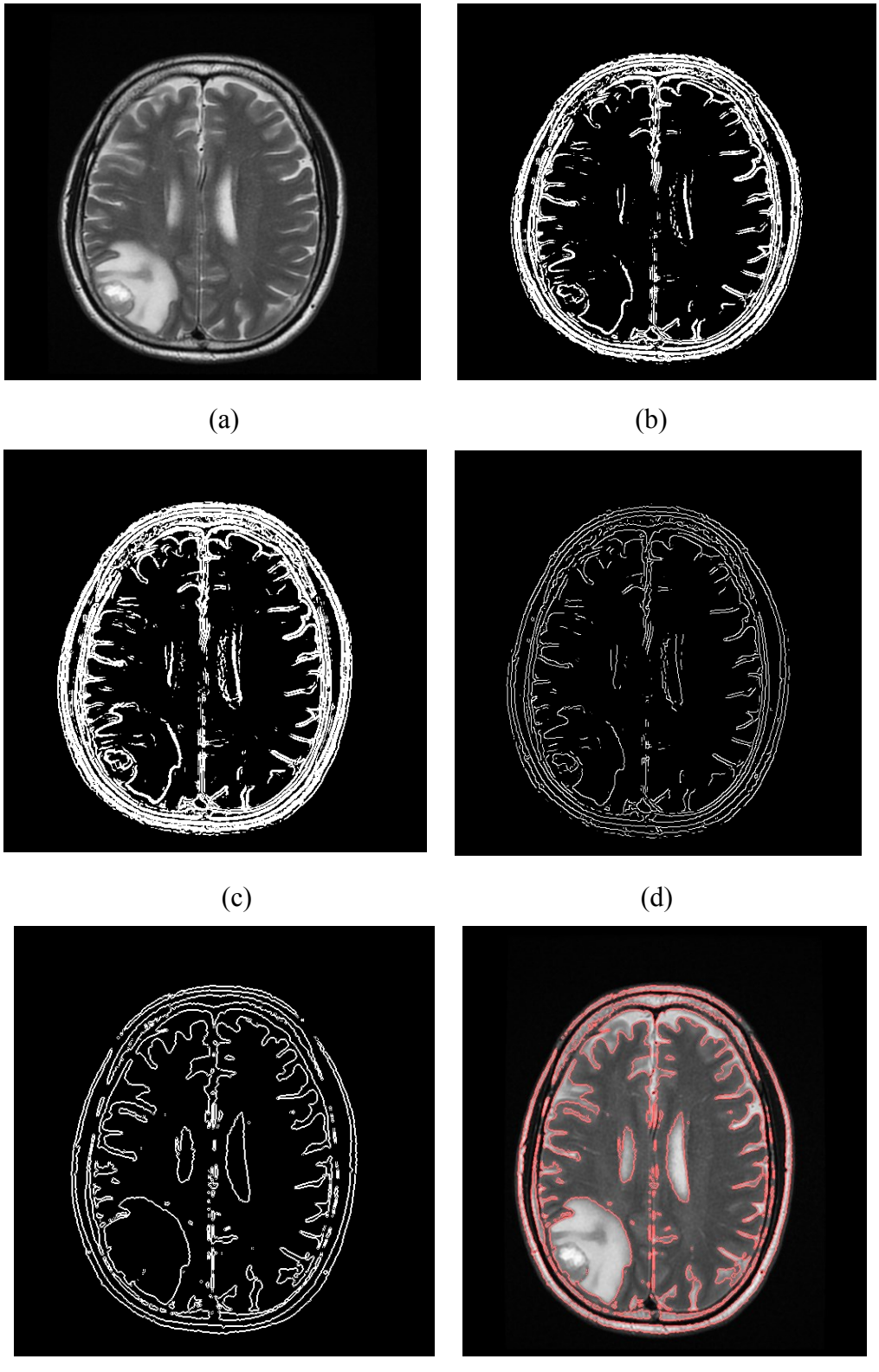

Figure 4.23 Edge detection results(3) (a) original image, (b)Sobel, (c) Prewitt, (d) Canny, (e)and (f) The proposed approach

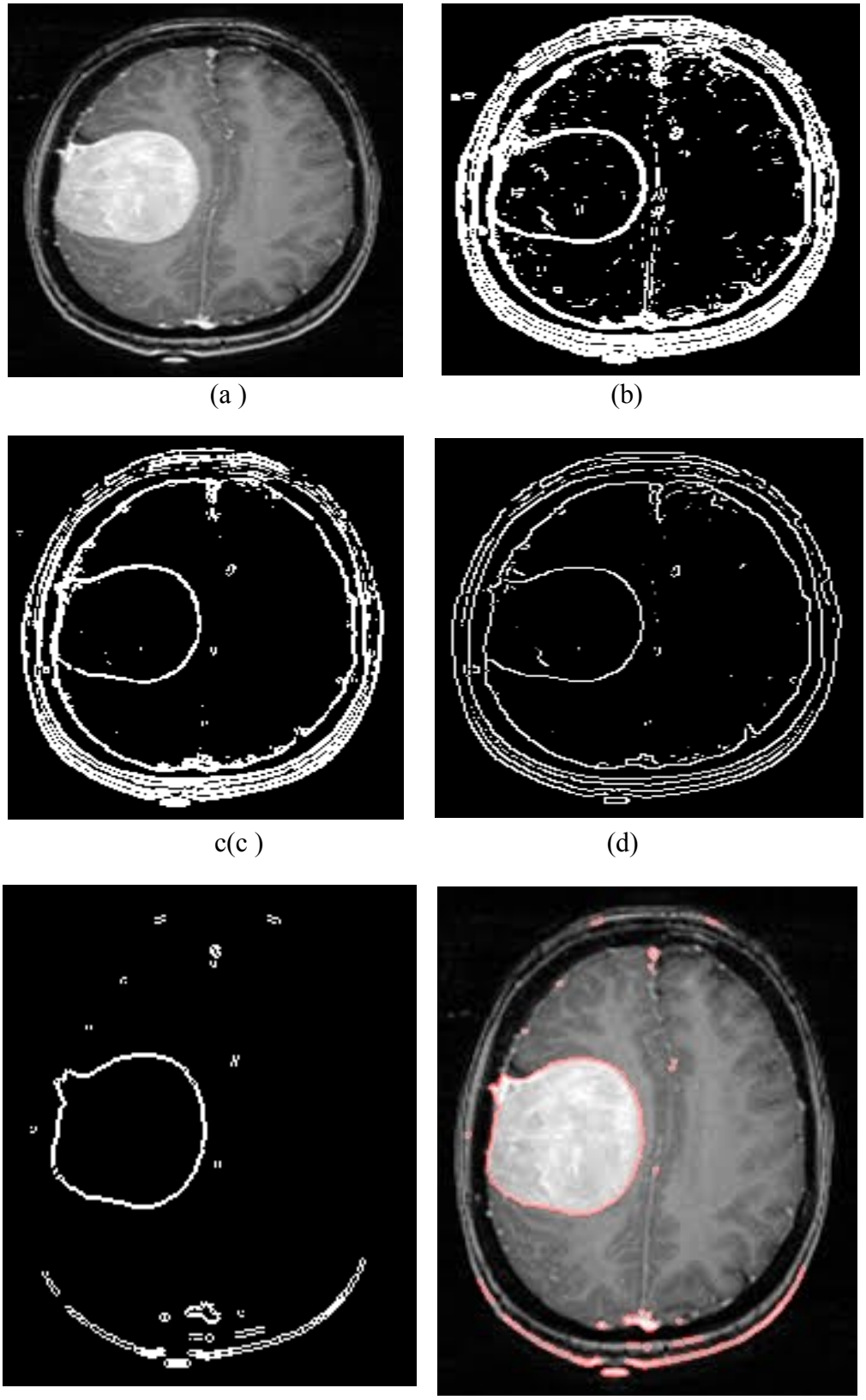

Figure 4.24 Edge detection results(4) (a) original image, (b)Sobel, (c) Prewitt, (d) Canny, (e)and (f) The proposed approach

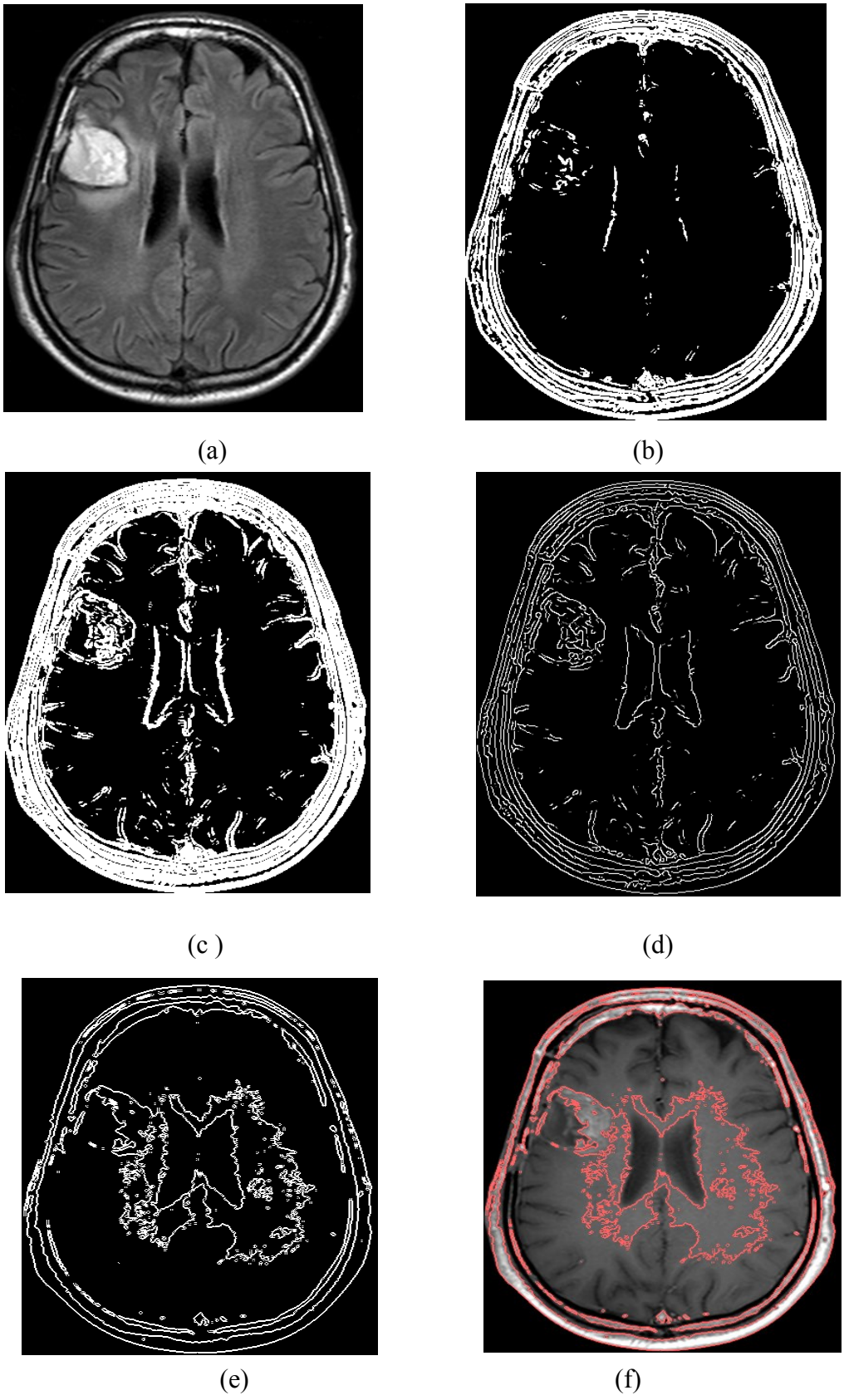

Figure 4.25 Edge detection results (5) (a) original image, (b)Sobel, (c) Prewitt, (d) Canny, (e)and (f) The proposed approach

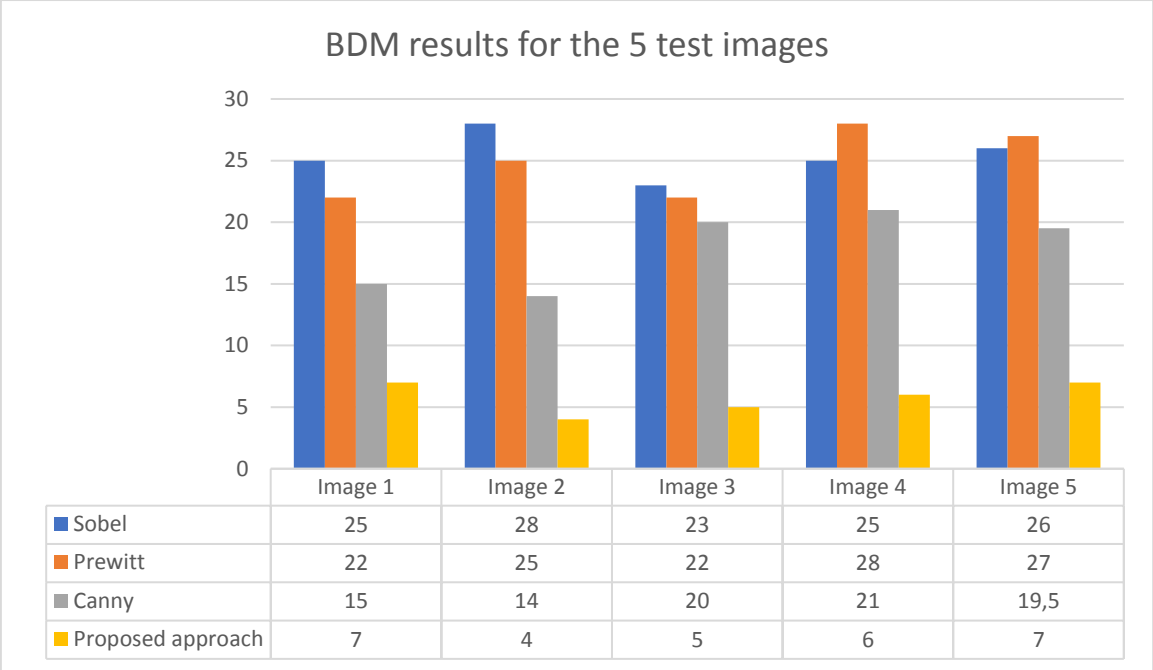

	Image 1	Image 2	Image 3	Image 4	Image 5
Sobel	25	28	23	25	26
Prewitt	22	25	22	28	27
Canny	15	14	20	21	19,5
Proposed approach	7	4	5	6	7

Figure 4.26 BDM results for the 5 test images

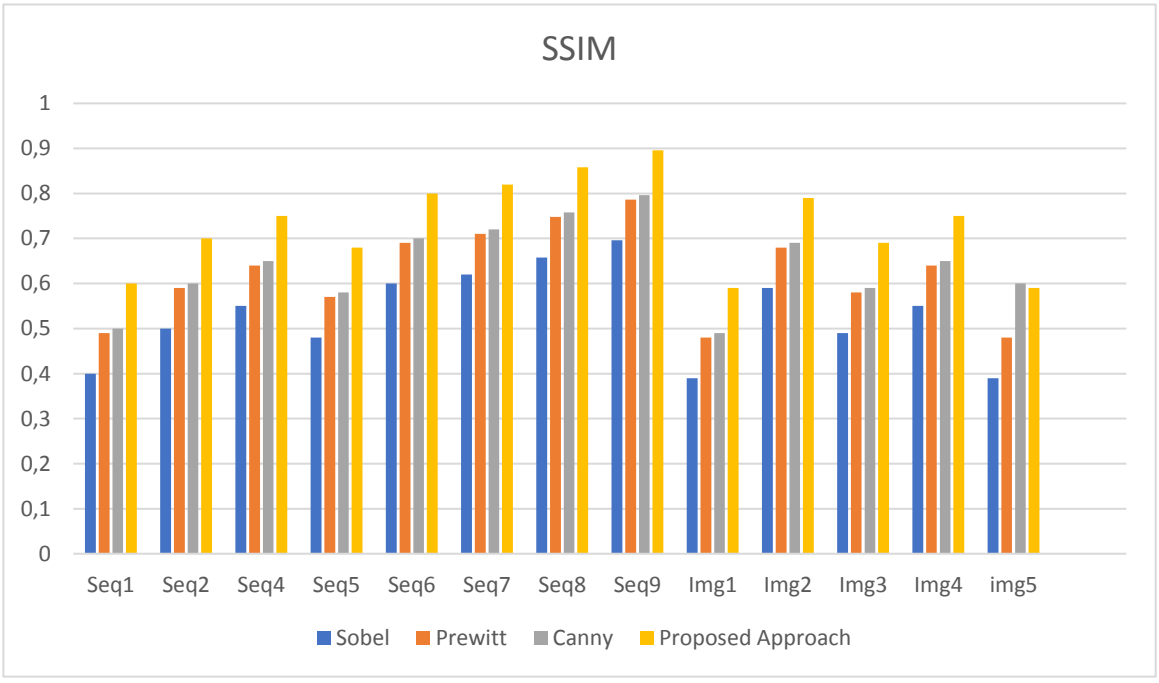

Figure 4.27 SSIM comparison results of dataset for sobel, Prewitt, Canny and the propsoed approach

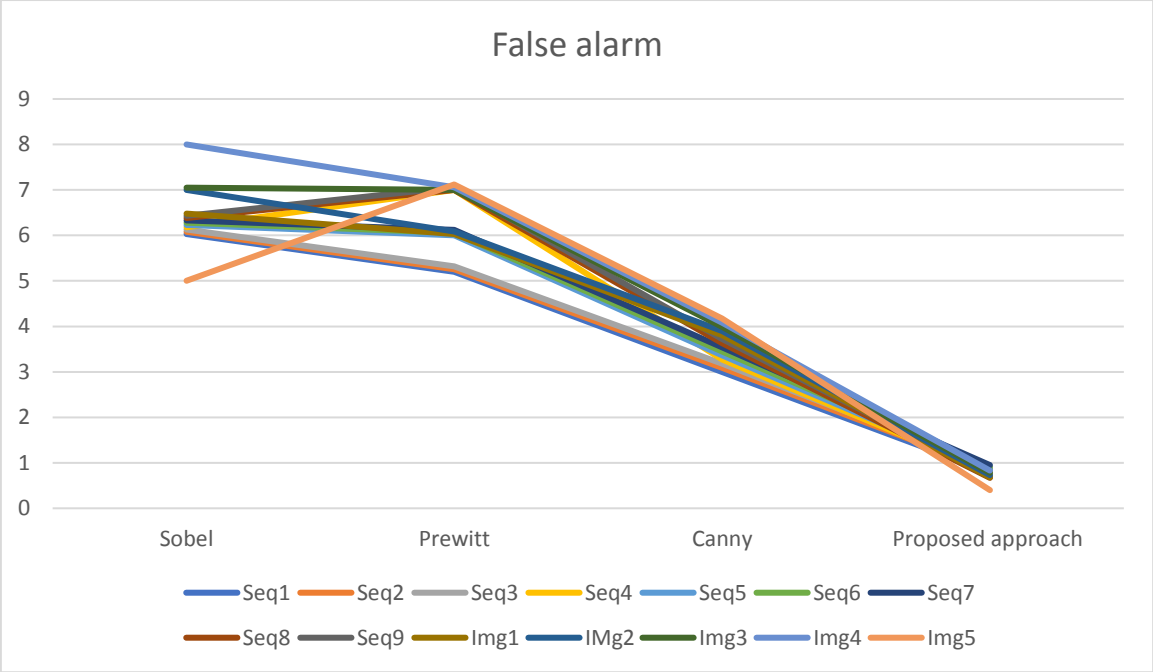

Figure 4.28 The false edged tumor pixels for the dataset images

3.13 Conclusion

In this chapter, we have introduced two main applications for brain MRI edge detection task based on the proposed QuLBP model as third and fourth contributions in this thesis. For the first approach, the Cellular Automata is combined with the QuLBP where the uniformity concept is investigated to detect edges in brain MRI. For the second application, the model is combined with the Penguin search optimization (PeSOA) algorithm to train the CA rules for brain tumor MRI edge detection.

In order to validate the performance of both applications, each application shows a good performance in comparison with classical methods. Different datasets were used: real and synthetic MR images with different homogeneities and different type of noise even a different noise level and brain tumor MR images. The different metrics used for quantitative evaluation were experimented the best performance for our approaches.

Conclusion and perspectives

During this thesis, we were interested in the exploitation of texture analysis in the field of brain MRI image segmentation. The objective was to reformulate the segmentation problem i.e. edge detection to work with a new image characteristic unlike the pixel intensity: the texture. In order to improve the results of edge detection and help the doctor to characterize the different tissues where they are healthy or pathological (tumors).

After having carried out a bibliographical review on the different recent methods of segmentation we found the importance and the difficulty of the problem of the segmentation of brain MR images. There are two reasons for this difficulty: on the one hand, the diversity of approaches that continue to be proposed in the literature, without arriving at a generic method, applicable to a wide variety of images and problems not only caused by artifacts specific to MRI (noise, e and partial volume, etc.), but also, a the complex anatomy of the human brain. As a result, A novel model for MR image edge detection is presented.

The QuLBP is designed as a local texture classifier, and the QuLBP model is investigated through three separate applications. The three applications, CA edge detection and QuLBP combined with Canny-deriche for noise resistance, show good results compared to the classical methods. The main contributions of this thesis can be summarized as follows:

- We have designed a new model that is an extension of the LBP model to deal with MR images with different inhomogeneities; the model successfully classifies local pixels while preserving the simplicity of the original model.

- As a second application, we have successfully reduced the effect of salt and pepper noise for the Canny-deriche algorithm in real and synthetic brain MR images.

- We have relaxed the QuLBP patterns for the Cellular Automata models and improved the performance of the edge detection with two rules based on the uniformity concept

of the local binary pattern that are empirically shown to provide an easy process without the need for evolutionary algorithms.

- Brain tumor MR images edge detection provide a great help to the doctors during diagnosis. Therefore, as fourth application, we have investigated the Penguins search optimization algorithm for detecting tumors in real brain MR images in combination with the CA.

The QuLBP is designed to be investigated for specific applications and specific parameters, such as the type of data and its homogeneity in addition to the type of noise. To determine the generality of the model in medical analysis, future work should investigate a different type of noise for various medical imaging applications, moreover, the proposed model.

Bibliography

Aghaei, A. (2018). A cellular Automata approach for noisy images edge detection under null boundary conditions. *2018 Second International Conference on Computing Methodologies and Communication (ICCMC)* (pp. 771-777). IEEE.

Akram, F., Garcia, M. A., & Puig, D. (2017). Active contours driven by local and global fitted image models for image segmentation robust to intensity inhomogeneity. *PloS one, 12*(4), e0174813.

Alfonse, M., Salem, & M, A. B. (2016). An automatic classification of brain tumors through MRI using support vector machine. *Egyptian Computer Science Journal, 40*(3).

Anitha, V., & Murugavalli, S. (2016). Brain tumour classification using two-tier classifier with adaptive segmentation technique. *IET computer vision, 10*(1), 9-17.

Baddeley, A. (1992). An error metric for binary images. *Rstner WF, Ruwiedel S, editors. Robust computer vision: quality of vision algorithms. Karlsruhe: Wichmann Verlag*, 5978.

Batouche, M., Meshoul, S., & Abbassene, A. (2006). On solving edge detection by emergence. *International Conference on Industrial, Engineering and other Applications of Applied Intelligent Systems* (pp. 800-808). Springer, Berlin, Heidelberg.

Beare, R. J., Chen, J., Kelly, C. E., Alexopoulos, D., Smyser, C. D., Rogers, C. E., & Anderson, P. J. (2016). Neonatal brain tissue classification with morphological adaptation and unified segmentation. *Frontiers in neuroinformatics, 10*, 12.

Benson, C. C., Lajish, V. L., & Rajamani, K. (2015). Brain tumor extraction from MRI brain images using marker based watershed algorithm. *International Conference on Advances in Computing, Communications and Informatics (ICACCI)* (pp. 318-323). IEEE.

Bezdek, J. C. (1981). Pattern Recognition with Fuzzy Objective Function Algorithms. *Kluwer Academic Publishers*.

Brainweb: Simulated Brain Database. (1996). Retrieved from http://brainweb.bic.mni.mcgill.ca/brainweb/

Canny, J. (1986). A Computational Approach to Edge Detection. *IEEE Transactions on pattern analysis and machine intelligence*, 679-698. doi:10.1016/b978-0-08-051581-6.50024-6

Cark, M. C., Hall, L. O., & Goldgof, D. B. (1998). Automatic tumor segmentation using knowledge-based techniques. *IEEE transactions on medical imaging, 17*(2), 187-201.

Chazen, J. L., Dyke, J. P., Holt, R. W., Horky, L., Pauplis, R. A., & Verma, A. (2017). Automated segmentation of MR imaging to determine normative central nervous system cerebrospinal fluid volumes in healthy volunteers. *Clinical imaging, 43*, 132-135.

Ciofolo, C. (2005, December). Segmentation de formes guide par des modles en neuro-imagerie - Intgration de la commande floue dans une mthode de segmentation par ensembles de niveau. *Phd. thesis*. Universit de Rennes I - IFSIC - Ecole doctorale Matisse.

Clarke, L. (1991). MR image segmentation using MLM and artificial neural nets. *Med Phys, 18*(30), 672–682.

Comaniciu, D., & Meer, P. (2002). Mean shift : A robust approach toward feature space analysis. *IEEE Trans. Pattern Anal. Mach. Intell* (pp. 603-619). IEEE.

Cortes, C., & Vapnik, V. (1995). Support-Vector Networks. *Mach. Learn*, 273–297.

Dempster, A. P., Laird, N. M., & Rubin, D. B. (1977). Maximum likelihood from incomplete data via the em algorithm. , 39(1) :. *Journal of The Royal Statistical Society, Series B, 39*(1), 1-38.

Deriche, R. (1987). Using cannys cteria to derive a recursively implemented optimal edge detector. *International Journal of Computer Vision, 1*(2), 167-187.

Dhage, P., Phegade, M. R., & Shah, S. K. (2015). Watershed segmentation brain tumor detection. *International Conference on Pervasive Computing (ICPC)* (pp. 1-5). IEEE.

Digabel, H., & antuéjoul, C. (1978). Iterative algorithm. *Quantitative analysis of micro structures in materials sciences, 1*, 85-99.

Djemame, S., & Batouche, M. (2012). Combining cellular automata and particle swarm optimization for edge detection. *International Journal of Computer Applications, 57*(14).

Dobe, O., Sarkar, A., & Halder, A. (2019). Rough K-Means and Morphological Operation-Based Brain Tumor Extraction. *Integrated Intelligent Computing, Communication and Security* (pp. 661-667). Singapore: Springer.

Etemad, S. A., & White, T. (2011). An ant-inspired algorithm for detection of image edge features. *Applied soft computing, 11*(8), 4883-4893.

Galshetwar, G. M., Waghmare, L. M., Gonde, A. B., & Murala, S. (2018). Multi-dimensional multi-directional mask maximum edge pattern for bio-medical image retrieval. *International Journal of Multimedia Information Retrieval, 7*(4), 231-239.

Ganesh, M., Naresh, M., & Arvind, C. (2017). MRI brain image segmentation using enhanced adaptive fuzzy K-means algorithm. *Intelligent Automation & Soft Computing, 23*(2), 325-330.

Gao, S., Yang, J., & Yan, Y. (2014). A novel multiphase active contour model for inhomogeneous image segmentation. *Multimedia tools and applications, 72*(3), 2321-2337.

Gheraibia, Y., Moussaoui, A., Djenouri, Y., Kabir, S., & Yin, P. Y. (2016). Penguins search optimisation algorithm for association rules mining. *Journal of computing and information technology, 24*(2), 165-179.

Guendouz, M., Amine, A., & Hamou, R. M. (2018). Penguins Search Optimization Algorithm for Community Detection in Complex Networks. *International Journal of Applied Metaheuristic Computing (IJAMC), 9*(1), 1-14.

Guerrout, E., Mahiou, R., & Ait-Aoudia, S. (2018). Hidden markov random fields and particle swarm combination for brain image segmentation. *Int. Arab J. Inf. Technol, 15*(3), 462-468.

Gurusamy, R., & Subramaniam, V. (2017). A machine learning approach for MRI brain tumor classification. Computers. *Materials & Continua, 53*(2), 91-108.

Halder, A., & Dobe, O. (2016). Detection of tumor in brain MRI using fuzzy feature selection and support vector machine. *International Conference on Advances in Computing, Communications and Informatics (ICACCI)* (pp. 1919-1923). IEEE.

Havaei, M., Davy, A., Warde-Farley, D., Biard, A., Courville, A., Bengio, Y., & Larochelle, H. (2017). Brain tumor segmentation with deep neural networks. *Medical image analysis, 35*, 18-31.

Horowitz, S. L., & Pavlidis, T. (1976). Picture segmentation by a tree traversal algorithm. *Journal of the ACM (JACM, 23*(2), 368-388.

Hussain, S., Anwar, S. M., & Majid, M. (2018). Segmentation of glioma tumors in brain using deep convolutional neural network. *Neurocomputing, 282*, 248-261.

Işın, A., Direkoğlu, C., & Şah, M. (2016). Review of MRI-based brain tumor image segmentation using deep learning methods. *Procedia Computer Science, 102*, 317-324.

Javadpour, A., & Mohammadi, A. (2016). Improving brain magnetic resonance image (MRI) segmentation via a novel algorithm based on genetic and regional growth. *Journal of biomedical physics & engineering, 6*(2), 95.

Jokinen, H., Gonçalves, N., Vigário, R., Lipsanen, J., Fazekas, F., Schmidt, R., & Pantoni, L. (2015). Early-stage white matter lesions detected by multispectral MRI segmentation predict progressive cognitive decline. *Frontiers in neuroscience, 9*, 455.

Krishnapuram, R., & Keller, J. (1993). A possibilistic approach to clustering. *IEEE Transactions on Fuzzy Systems. 1*, pp. 98-110. IEEE.

Kwon, G. R., Basukala, D., Lee, S. W., Lee, K. H., & Kang, M. (2016). Brain image segmentation using a combination of expectation-maximization algorithm and watershed transform. *International Journal of Imaging Systems and Technology, 26*(3), 225-232.

L. ,., & MOUSSAOUI, A. (2019). Quantum local binary pattern for medical edge detetcion. *Journal of inforamtion technology Research (JITR), 12*(2), 36-52.

Li, M., Zhang, L., Xiang, Z., Castillo, E., & Guerrero, T. (2016). An improved fuzzy c-means algorithm for brain MRI image segmentation. *2016 International Conference on Progress in Informatics and Computing (PIC)* (pp. 336-339). IEEE.

Liu, L., Liu, Y., Xu, L., Li, Z., Lv, H., Dong, N., & Jin, E. (2017). Application of texture analysis based on apparent diffusion coefficient maps in discriminating different stages of rectal cancer. *Journal of Magnetic Resonance Imaging, 45*(6), 1798-1808.

MacQueen, j. (1967). Some methods for classification and analysis of multivariate observations. *Proceedings of the fifth Berkeley symposium on mathematical statistics and probability*, *4*, pp. 281-297. Berkeley, Calif.

Mangla, A., & Singh, C. (2019). A Local Information-Based Fuzzy C-Means for Brain MRI Segmentation. *Computational Intelligence: Theories, Applications and Future Directions, 799*, 607-619.

Manousakas, I. N., Undrill, P. E., Cameron, G. G., & Redpath, T. W. (1998). Split-and-merge segmentation of magnetic resonance medical images: performance evaluation and extension to three dimensions. *Computers and Biomedical Research, 31*(6), 393-412.

Mansouri, A., Aminnejad, B., & Ahmadi, H. (2018). Introducing modified version of penguins search optimization algorithm (PeSOA) and its application in optimal operation of reservoir systems. *Water Science and Technology: Water Supply, 18*(4), 1484-1496.

Marras, I., Nikolaidis, N., & Pitas, I. (2014). 3D geometric split–merge segmentation of brain MRI datasets. *Computers in biology and medicine, 48*, 119-132.

Mary, M., Padma, L., & John, M. (2016). Modified image segmentation method based on region growing and region merging. *Int. Arab J. Inf. Technol*, 899-907. Consulté le 6A

Meier, R., Knecht, U., & Loosli, T. (2016). Clinical evaluation of a fully-automatic segmentation method for longitudinal brain tumor volumetry. *Scientific reports, 6*, 23376.

Meng, X., Gu, W., Chen, Y., & Zhang, J. (2017). Brain MR image segmentation based on an improved active contour model. *PloS one,, 12*(8), e0183943.

Mohsen, H., El-Dahshan, E. S., El-Horbaty, E. S., & Salem, A. B. (2018). Classification using deep learning neural networks for brain tumors. *Future Computing and Informatics Journal, 3*(1), 68-71.

MZILI, I., & RIFFI, M. E. (2015). Discrete penguins search optimization algorithm to solve the traveling salesman problem. *Journal of Theoretical & Applied Information Technology, 72*(3).

Nerurkar, S. N. (2017). Brain Tumor Detection using Image Segmentation. *Brain, 4*(4).

Nie, D., Wang, L., Gao, Y., & Sken, D. (2016). Fully convolutional networks for multi-modality isointense infant brain image segmentation. *IEEE 13th International Symposium on Biomedical Imaging (ISBI)* (pp. 1342-1345). IEEE.

Pereira, S., Pinto, A., Oliveira, J., Mendrik, A. M., Correia, J. H., & Silva, C. A. (2016). Journal of neuroscience methods. *Automatic brain tissue segmentation in MR images using random forests and conditional random fields*, 111-123.

Pham, D. L., Xu, C., & Prince, J. L. (2000). Current methods in medical image segmentation. *Annual review of biomedical engineering, 2*(1), 315-337.

Pishghadam, M., Nekooei, S., Seilanian-Toosi, F., Hoseini-Ghahfarokhi, M., Kazemi, K., Zabizadeh, M., & Fatemi, A. (2019). A new approach to automatic fetal brain extraction from MRI using a variational level set method. *Medical physics*.

Polepaka, S., Srinivasa Rao, C., & Chandra Mohan, M. (2019). A Brain Tumor: Localization Using Bounding Box and Classification Using SVM. (S. Springer, Éd.) *Innovations in Electronics and Communication Engineering. Lecture Notes in Networks and Systems,, 33*, 61-70.

Priya, T., & Kalavathi, P. (2018). HSV Based Histogram Thresholding Technique for MRI Brain Tissue Segmentation. *International Symposium on Signal Processing and Intelligent Recognition Systems* (pp. 322-333). Singapore: Springer.

Priyanka, B. S. (2013). A review on brain tumor detection using segmentation. *International Journal of Computer Science and Mobile Computing (IJCSMC), 2*, 48–54.

Rampun, A., Scotney, B., Morrow, P., Wang, H., & Winder, J. (2018). Breast density classification using local quinary patterns with various neighbourhood topologies. *Journal of Imaging, 4*(1), 14.

Rasel, A., Sen Swakshar, A. ,., Foisal, H., & Md. Abdur, R. (2017). Classification of Tumours and It Stages in Brain MRI Using Support Vector Machine and Artificial Neural Network. *International Conference on Electrical, Computer and Communication (ECCE)*, (pp. 16-18).

Roberts, L. G. (1963). *Machine perception of three-dimensional solids (Doctoral Dissertation)*. Massachusetts Institute of Technology.

Saad, N. M., Abu-Bakar, S. A., Muda, S., & Mokji, M. (2010). Automated segmentation of brain lesion based on diffusion-weighted MRI using a split and merge approach. *Biomedical engineering and sciences (IECBES.* IEEE EMBS conference.

Sahin, U., Sahin, F., & Uguz, S. (2013). Hybridized fuzzy cellular automata thresholding algorithm for edge detection optimized by PSO. *2013 High Capacity Optical Networks and Emerging/Enabling Technologies* (pp. 228-232). IEEE.

Sahota, P., Daemi, M. F., & Elliman, D. G. (1994). Training genetically evolving cellular automata for image processing. *Proceedings of ICSIPNN'94. International Conference on Speech, Image Processing and Neural Networks (* (pp. 753-756). IEEE.

Scherrer, B. (2008). Segmentation des tissus et structures sur les IRM cérébrales : agents markoviens locaux coopératifs et formulation bayésienne. *PhD thesis*. Institut National Polytechnique de Grenoble, France.

Shahverdi, R., Tavana, M., Ebrahimnejad, A., Zahedi, K., & Omranpour, H. (2016). An improved method for edge detection and image segmentation using fuzzy cellular automata. *Cybernetics and Systems, 47*(3), 161-179.

Shanthakumar, P., & Ganesh Kumar, P. (2015). Computer aided brain tumor detection system using watershed segmentation techniques. *International Journal of Imaging Systems and Technology, 25*(4), 297-301.

Sharma, M., Purohit, G. N., & Mukherjee, S. (2018). Information retrieves from brain MRI images for tumor detection using hybrid technique K-means and artificial neural network (KMANN). *Networking Communication and Data Knowledge Engineering*, 145-1.

Sobel, I. (1970). *camera models and machine perception.* Stanford Univ Calif Dept of Computer Science.

Soomro, S., Akram, F., Kim, J. H., & Choi, K. N. (2016). Active contours using additive local and global intensity fitting models for intensity inhomogeneous image segmentation. *Computational and mathematical methods in medicine*.

Suganya, D., & Krishnaveni, K. (2016). Brain Image Segmentation Methods using Image Processing Techniques to Analysis ADHD. *International Journal of Data Mining Techniques and Applications, 5*(1).

Sujji, G. E., Lakshmi, Y. V., & Jiji, G. W. (2013). MRI Brain Image Segmentation based on Thresholding. *International Journal of Advanced Computer Research, 3*(1), 97-101.

Suresh, A., Suresh, A., Reshmi, R., Rajam, R. A., & Hemalatha, M. (2018). Extraction and Evaluation of Brain Tumor from MRI using Tsallis Entropy and Level set. *International Conference on Recent Trends in Electrical ,Control and Communication RTECC)* (pp. 251-255). IEEE.

T Krishnan, P., Balasubramanian, P., & Krishnan, C. (2016). Segmentation of brain regions by integrating meta heuristic multilevel threshold with Markov random field. *Current Medical Imaging Reviews, 12*(1), 4-12.

Thejaswini, P., Bhavya, B., & Kushal, P. (2019). Detection and Classification of Tumour in Brain MRI. *International Journal of Engineering and Manufacturing(IJEM), 9*(1), 11-20.

Ulam, S. M. (1972). Some ideas and prospects in biomathematics. *Annual review of biophysics and bioengineering, 1*(1), 277-292.

Visser, E., Keuken, M. C., Douaud, G., Gaura, V., Bachoud-Levi, A. C., Remy, P., & Jenkinson, M. (2016). Automatic segmentation of the striatum and globus pallidus using MIST: multimodal image segmentation tool. *NeuroImage, 125*, 476-497.

Von Neumann, J., & Burks, A. W. (1966). Theory of self-reproducing automata. *IEEE Transactions on Neural Networks, 5*(1), 3-14.

Wang, j., Kong, j., Yinghua, L., Qi, M., & Zhang, B. (2008). A modified FCM algorithm for MRI brain image segmentation. *Computerized Medical Imaging and Graphics, 32*, 685–698.

Wolfram, S. (2002). A new kind of science. *Champaign, IL: Wolfram media., 5*, 130.

Yang, C., Ye, H., & Wang, G. (2002). Cellular automata modeling in edge recognition. *Proceedings of the Seventh International Symposium on Artificial Life and Robotics* , (pp. 128-132).

Zabir, I., P. S., Rayhan, M. A., Sarker, T., Fattah, S. A., & Shahnaz, C. (2015). Automatic brain tumor detection and segmentation from multi-modal MRI images based on region growing and level set evolution. *IEEE International WIE Conference on Electrical and Computer Engineering (WIECON-ECE)*, (pp. 53-506).

Zeinalkhani, L., Jamaat, A. A., & Rostami, K. (. (2018). Diagnosis of Brain Tumor Using Combination of K-Means Clustering and Genetic Algorithm. *Iranian Journal of Medical Informatics*.

Zhang, W., Li, R., Deng, H., Wang, L., Lin, W., Ji, S., & Shen, D. (2015). Deep convolutional neural networks for multi-modality isointense infant brain image segmentation. *NeuroImage, 108*, 214-224.

Zhang, Y. D., Chen, S., Wang, S. H., Yang, J. F., & Phillips, P. (2015). Magnetic resonance brain image classification based on weighted-type fractional Fourier transform and nonparallel support vector machine. *International Journal of Imaging Systems and Technology, 25*(4), 317-327.

Zucker, S. W. (1976). Region growing : Childhood and adolescence. *Computer Graphics and Image Processing, 5*(3), 382-399.